A COMPUTATIONAL INVESTIGATION OF THE EFFECT OF SPIN-CROSSING ON THE DISSOCIATION OF CHLORO- AND DICHLOROBENZENE ON THE SILICON (100) SURFACE AND THE MECHANICAL AND ELECTRONIC PROPERTIES OF COBALT DOPED ZINC OXIDE

By

ERIC DONALD BUTSON

Bachelor of Science in Chemistry
Northeastern State University
Tahlequah, Oklahoma
2012

Submitted to the Faculty of the
Graduate College of the
Oklahoma State University
in partial fulfillment of
the requirements for
the Degree of
DOCTOR OF PHILOSOPHY
July, 2017

A COMPUTATIONAL INVESTIGATION OF THE EFFECT OF SPIN-CROSSING ON THE DISSOCIATION OF CHLORO- AND DICHLOROBENZENE ON THE SILICON (100) SURFACE AND THE MECHANICAL AND ELECTRONIC PROPERTIES OF COBALT DOPED ZINC OXIDE

Dissertation Approved:

Dr. Nicholas Materer

Dissertation Adviser

Dr. Allen Apblett

Dr. Richard Bunce

Dr. Barry Lavine

Dr. Mario Borunda

.

ACKNOWLEDGEMENTS

I would like to thank my graduate advisor, Dr. Nicholas Materer, for all the support and guidance he has provided throughout my graduate career, and for pushing me to become a better scientist. I would like to thank the members of my graduate committee, Dr. Allen Apblett, Dr. Mario Borunda, Dr. Richard Bunce, and Dr. Barry Lavine. Without their guidance and words of encouragement, I would not be where I am today. I would also like to thank Dr. John Gelder for helping me become a better teacher, and for all the advice he has given me over the years. I would like to express my sincere gratitude to my friends, Robert Newman, Kendra Lizama, Anthony Wellman, Linda Falling, Darryl Falling, Alex Shumaker, Sangeetha Komanduri, Miguel Leal, Dr. Wesley Honeycutt, and my parents Don and Ruth Butson for the support they have given me throughout the years. Most of all, I would like to thank my wife, Lynse Butson, for loving and supporting me. I could ask for no better person to share my achievements with.

Dedicated to Jakub M. Wilden

1996-2017

Name: Eric Donald Butson

Date of Degree: JULY, 2017

Title of Study: A COMPUTATIONAL INVESTIGATION OF THE EFFECT OF SPIN-CROSSING ON THE DISSOCIATION OF CHLORO- AND DICHLOROBENZENE ON THE SILICON (100) SURFACE AND THE MECHANICAL AND ELECTRONIC PROPERTIES OF COBALT DOPED ZINC OXIDE

Major Field: Chemistry

The adsorption and dissociation of chlorobenzene and dichlorobenzene on the Si(100) surface was modeled using hydrogen terminated silicon clusters within the density functional theory framework. Using single dimer to much larger clusters, containing up to four surface dimers, to model multiple Si-dimer rows on the Si(100) surface, the adsorption energy and potential dissociation pathways were investigated on singlet and triplet surfaces. After a systematic study of possible chlorobenzene adsorption geometries, including analogs generated from benzene adsorption geometries, and their possible dissociation products, the 1,2-tilted, 1,4-butterfly, and row-linking butterfly structures were found to be the most energetically favorable starting structures for dissociation. Similar results were found with dichlorobenzene, with the 2,3-tilted, 1,4-butterfly and row-linking butterfly structures being the only feasible starting structures for 1,2-dichlorobenzene, and the 1,2-tilted and 1,4-butterfly structures being the only feasible starting structures for 1,4-dichlorobenzene. In all cases, the dissociation pathway required intermediates in the triplet state. The necessity of a spin-crossing event was found to have a minimal effect on the energies of the dissociation pathways. In all cases, no more than 20% of the adsorption structures lead to dissociation; these results are consistent with experimental investigations which show little to no dissociation of chlorobenzene and dichlorobenzene. In addition to this work, the effects of cobalt doping on the optical properties of zinc oxide were studied. Most work in this area has focused on the magnetic properties of Co-doped ZnO, as it is predicted to have a Curie temperature around room temperature, making it desirable for spintronics. As a first step, pseudopotentials were developed and used to calculate the bulk modulus. These results were compared to other experimental and theoretical data.

TABLE OF CONTENTS

Chapter Page

LIST OF TABLES

Table Page

Table Page

LIST OF FIGURES

Figure Page

Figure Page

CHAPTER I

Introduction to the Silicon (100) Reconstructed Surface and Zinc Oxide

The Si(100) Surface Structure

Despite the argument that silicon-based devices are reaching their physical limit and the increasing attention on the development of novel semiconducting materials, silicon remains to be the foundation of the current semiconductor industry. Silicon is a covalent solid with a face-centered cubic crystal structure (shown as a supercell in Figure I-1A so that bonding can be easily seen). The technologically important surface of silicon is the Si(100) surface, where (100) represents the plane orthogonal to the [100] Miller indices, indicated by the plane shown on the top of the bulk Si structure in Figure I-1A. When cut along the (100) plane, two bonds are broken for every Si atom resulting in two dangling bonds for every Si atom. This newly formed surface is highly unstable and in order to reduce the number of dangling bonds, and consequently the surface free energy, a reconstruction occurs. In this reconstruction, the molecular orbitals of the Si atoms on the surface are rehybridized, forming a σ-bond and a weak π-bond between pairs of Si atoms. The energy gained from rehybridization and reduction of the dangling bonds on the Si(100) surface is balanced against the increased stress on the surface, due to the mismatch of the reconstructed surface on the underlying lattice resulting in dimer rows [1-6].

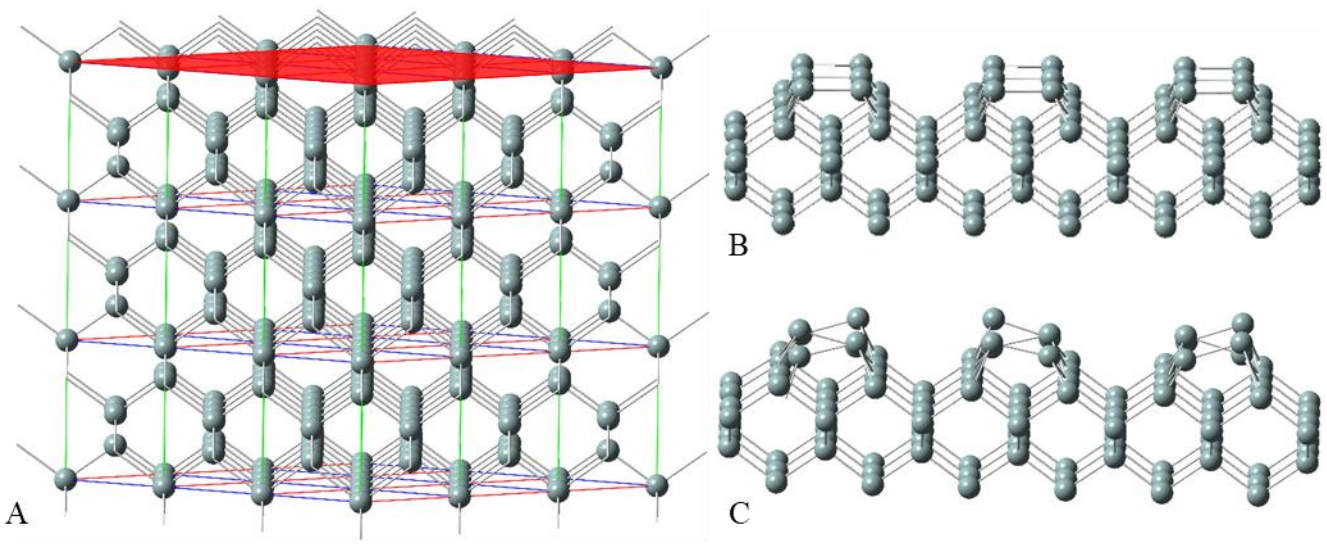

Figure I-1. Bulk silicon has a face centered cubic structure, as seen by the (A) supercell of Si unit cells. The red plane indicates the (100) Miller plane, and the most technologically important silicon surface. The Si(100) surface (B) is reconstructed to for dimer rows in a (2x1) periodicity. The true structure of this surface has a c(4x2) periodicity due to the (C) buckled surface.

Schlier and Farnsworth were the first to suggest the Si(100) surface had a symmetric (2x1) periodicity using low-energy electron diffraction (LEED) techniques [7]. Energy minimization calculations later found that the asymmetric, buckled dimer surface was the most stable reconstruction of the Si(100) surface, having either the (2x1) or c(4x2) periodicity [8]. Subsequent room temperature studies of the surface structure confirm a symmetric dimer row structure with the (2x1) periodicity, with buckled dimers observed near defect sites with the c(4x2) periodicity [9]. At low temperatures, the buckled c(4x2) periodicity is observed, with an order-disorder phase transition observed near 200K leading to the (2x1) periodicity observed above this temperature [10]. Above 200K, the random alternation between the buckling orientations is time averaged, resulting in what appears to be a (2x1) periodicity in which the dimers are not buckled with respect to one another [11]. A model of the buckled Si(100) c(4x2) surface can be seen in Figure I-1C. In the STM images obtained by Hamer, Tromp, and Demuth, symmetric dimers appear as oblong shapes, while the buckled dimers have alternating bulges [9]. This is "zig-zag" observed in the STM images of the buckled dimers is due to a charge

transfer from the “down” Si atom to the “up” Si atom [9], and contributes to the reactivity of the Si(100) surface.

A cluster model of the Si(100) surface is used for the calculations discussed in Chapters II and III. This model is ideal for calculations of adsorption and dissociation on the Si(100) surface, as the primary concern is of localized bonding, thus a slab model is not a feasible method. In the cluster model, a selection of the surface dimers and several rows of bulk Si atoms are used to represent the surface. Figures I-2A, I-2B and I-2C depict the cluster models for the single, double, and trench dimer clusters, and their location in the slab model of the Si(100) surface. For the single and double dimer cluster models, the surface dimer and an additional three layer of bulk Si atoms are used, and the bulk Si atoms are truncated with H atoms to cap the unsatisfied bonds. In the case of the trench dimer, an additional row of Si atoms is used in order to mitigate any unrealistic distortions that may arise from the curling of the two dimer rows toward one another. Without this extra layer, structures with bonding across dimer rows result in artificially low energies, resulting in stable structures that would likely be unstable in a real system. This method is used in many other cases [12], and provides good results while being computationally efficient.

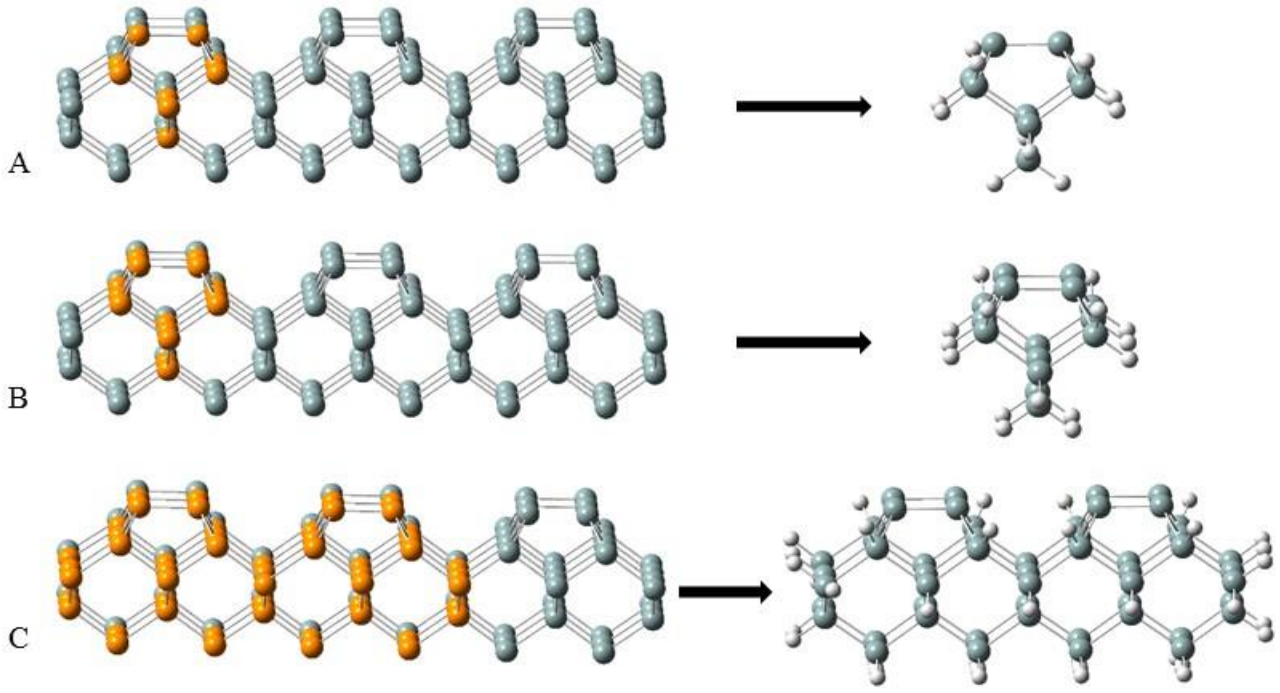

Figure I-2. The cluster model for the (A) single, (B) double, and (C) trench dimer clusters are formed from a cluster of Si atoms taken from the Si(100) surface, and the bulk Si atoms are truncated with H atoms.

Reactivity of the Si(100) Surface

Much of the interest relating to the adsorption of organic molecules on the Si(100) surface is sparked by the potential applications in chemical sensors, biological recognition, information storage, and molecular and optical electronics [13-16]. In addition to these applications, the highly ordered dimer surfaces provide a template for the ordered self-assembly of organic films and molecular wires [17-21]. Lopinski, Wolkow and coworker [18] found that self-directed growth of styrene lines could be achieved by the formation of a dangling bond on the hydrogen-terminated surface using scanning tunneling microscopy. This dangling bond is reacted with a styrene molecule and chain reaction forms long runs of styrene lines along the Si(100) dimer rows. Another study found that this method could be extended to create lines across rows using allyl mercaptan [19]. Two dimensional structures were also attempted by this group, but steric effects did not allow for the junction of cross-row lines

and lines along the rows [20]. Nevertheless, these methods prove promising for the fabrication of two dimensional structures using the Si(100) surface as a template, and using dangling bond initiated chain reactions. On clean surfaces, the buckling of the dimers in a row offer a template for the formation of heterogeneous structures as well, since the electrophilic down atoms act as a Lewis base while the nucleophilic up atom act as a Lewis acid [21]. The reaction of cyclopentene with the clean Si(100) surface has demonstrated that ordered monolayers can also be formed via reaction of the double bond with the dimer surface [17]. With the appropriate choice of adsorbate, additional functionalization of these monolayer films and molecular wires can be realized.

In order to develop methods for the adsorption of targeted functional groups on the Si(100), a fundamental understanding of these reactions with the dimer surface must be obtained. From a surface science perspective, the Si(100) surface is of particular importance because of the highly reactive silicon dimers on the surface, owing to the double bonding between dimers, and the charge transfer caused by the buckling of the dimers. Because of this double bonding, and the similarity of the surface dimers to alkenes, many reactions analogous to alkene reactions have been studied on the Si(100) surface [12, 14, 15, 17, 18, 22-36]. In particular, two interesting alkene reaction analogues that occur on the Si(100) surface are the [4+2] and [2+2] cycloaddition reactions.

In the typical [4+2] cycloaddition reaction, also known as the Diels-Alder cycloaddition reaction, two alkenes, commonly referred two as the diene and the dienophile, react with one another to form a six-membered ring with one double bond in the ring. The simplest example of this reaction is seen in Figure I-3, where ethylene, the dienophile, and 1,3-butadiene, the diene, react with one another to form cyclohexene. The nomenclature of this reaction, [4+2] indicates that four electrons in the diene two electrons in the dienophile are involved in the reaction. In this reaction, the double bonds in both

the diene and dienophile are broken and the terminal C atoms on both molecules form a single bond, while the remaining electrons form a double bond on the newly formed ring on what was previously a single bond on the diene. This reaction occurs simultaneously and yields no intermediates between the reactants and the product. According to the Woodward-Hoffman selection rules, which use frontier molecular orbital theory to examine the overlap of the highest occupied molecular orbital (HOMO) and the lowest unoccupied molecular orbital (LUMO) or reacting molecules, the HOMO and LUMO of the reacting molecules are in phase and thus the reaction is allowed. Indeed this reaction is quite common in organic chemistry and also readily occurs on the Si(100) surface despite the buckling of the surface dimers. This cycloaddition reaction has be achieved using 2,3-dimethyl-1,3-butadiene and 1,3 butadiene as the diene, and the Si(100) surface dimer as the dienophile [37, 38]. Theoretical predictions of this reaction find that the Diels-Alder adduct is more stable than the [2+2] cycloaddition adduct for both 2,3-dimethyl-1,3-butadiene and 1,3-butadiene [39].

In contrast to the [4+2] cycloaddition reaction, according to the Woodward-Hoffman selection rules, the [2+2] cycloaddition reaction is symmetry forbidden, as the HOMO and LUMO of the reacting molecules are out of phase. In the [2+2] cycloaddition reaction, the reaction of two alkenes results in the formation of a four-membered ring structure with no double bonds present. The simplest case of this reaction is between two ethylene molecules depicted in Figure I-3. In this reaction, the double bonds are broken and single bonds are formed between the terminal C atoms. Like the [4+2] cycloaddition reaction, this is a concerted reaction which does not form any intermediates. However, due to the out-of-phase overlap of the frontier molecular orbitals, the activation energy to form this structure is prohibitively high and this reaction does not occur readily. In addition to the high barrier to formation of the four-membered ring product, the strain induced by the decreased bond angles means that these products are much less stable that those of the [4+2] reactions.

Like its alkene reaction analogue, reaction of ethylene with a symmetrical surface dimer would have a similarly high activation barrier. However, due to the buckling of the surface dimers, which causes a charge transfer from the down Si atom the up Si atom, a new asymmetric reaction pathway is available on the c(4x2) or asymmetric (2x1) Si(100) surface. This pathway is a non-concerted reaction in which a dative bond is formed between the electron density of the ethylene double bond, and the electrophilic down Si atom. Two new single bonds are then formed in a step-wise reaction between the C atoms and the dimer Si atoms, forming the four-membered ring product [12, 15, 25, 26].

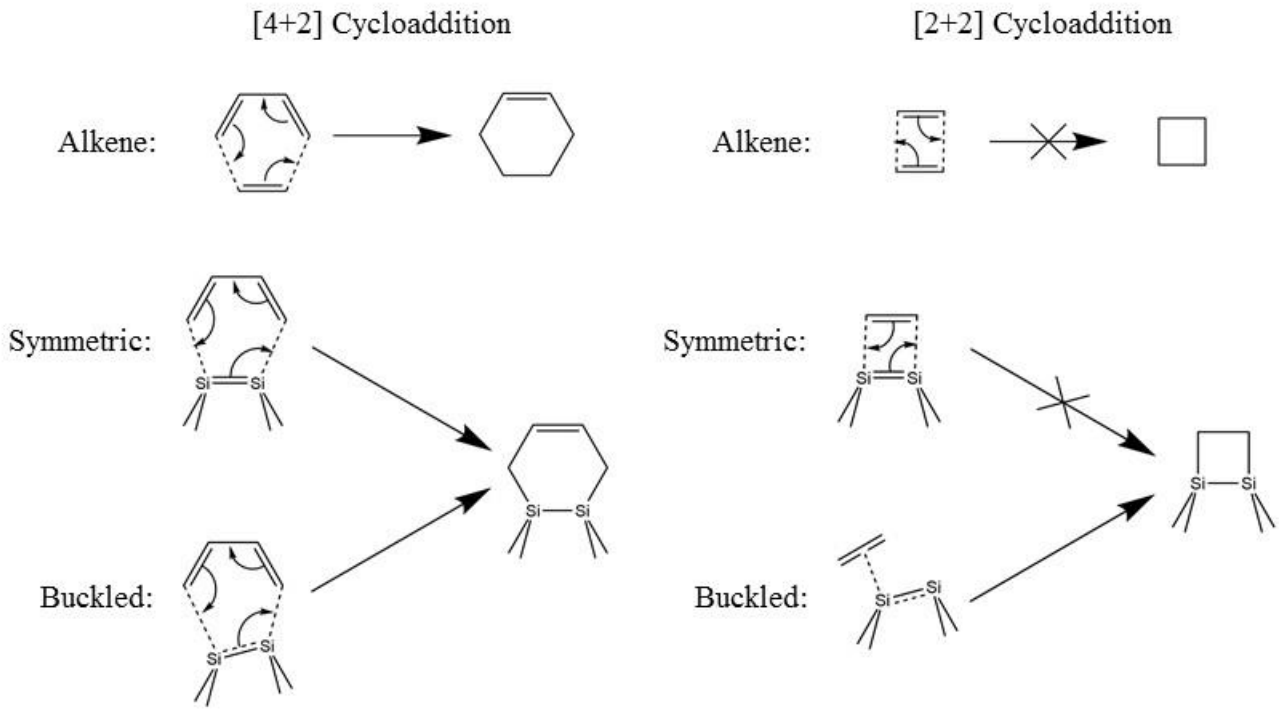

Figure I-3. Schematic representation of the [4+2] and [2+2] cycloaddition reactions and their analogous reactions on the symmetric and buckled dimer surfaces.

The reaction of organic compounds with the Si(100) surface has been the focus of many studies. A comparison of the sticking probabilities of propane and propene revealed that the C-C single bond and the C-H bonds are both inactive when reacting with this surface, while the C=C double bond was required to obtain a non-zero sticking probability [22]. Later studies by Yoshinobu and co-workers found that ethylene adsorbs to the Si(100) surface, forming a four-membered C-C-Si-Si ring, consistent with the product of the asymmetric [2+2] pathway. This product was stable up to 600K, but undergoes some desorption and decomposition at around 650K [24]. Liu and Hamers examined the stereoselectivity of 1,2-dideuteroethylene on the Si(100) surface. Their work found that the same four-membered ring structure, showing no isomerization when adsorbing to the surface [25]. However, STM results show that around 2% of trans-2-butene and cis-2-butene undergo isomerization when adsorbing to the surface. It is suspected that this isomerization is due to rotations about the C-C single bond in the intermediate of the step-wise asymmetric adsorption pathway, giving further support to this mechanism [40]. Further work by Yoshinobu and co-workers found that acetylene, when reacted on the Si(100) surface, forms a similar product to ethylene [23], suggesting a similar pathway for the adsorption of this molecule. Later, this mechanism for a stepwise adsorption reaction was confirmed by computational results for acetylene [12].

In addition to these alkene reactions several studies for various other double bonded molecules such as azo and isothiocyanate derivatives (see [15], [26], and references therein) have been conducted and found similar results. In addition, the adsorption and reactivity of simple aromatic molecules have also received much attention from the surface science community [27, 33, 34, 41-45]. The most well documented case of this is for the adsorption of benzene on the Si(100) surface. Bent and co-workers found that the reaction of benzene with the Si(100) surface at room temperature yields two products, the di-σ butterfly structure, which is bound to a single dimer with single bonds to C_1 and C_4, and the tetra-σ twisted bridge structure, which is bound to two adjacent dimers with single bonds to C_1, C_2,

C_3, and C_4. The remaining, unbound, C atoms lie over the trench between dimer rows. The butterfly structure is the predominant structure observed, however over larger time scales, more of the twisted bridge structure is seen [46]. A theoretical investigation, which utilized a slab model of the Si(100) surface to model various possible adsorption structures on the surface, confirmed the butterfly and twisted bridge structures, as well as several other possible adsorption structures [41]. In addition to the twisted bridge structure, a tight bridge structure was modeled and was found to be the most stable adsorption structure. This structure is a tetra-σ adsorption structure with C-Si bonds to C_1, C_2, C_3, and C_4, but in contrast to the twisted bridge structure, the unbound C atoms lie above the dimer row, making this structure essentially a 90° rotation of the twisted bridge structure. Another tetra-σ structure, called the pedestal, was modelled, which was bonded to two adjacent dimers by C_1, C_2, C_4, and C_5. This structure is unstable, due to the biradical character of the ring, forced by the separation of the two free C atoms. Other di-σ structures modelled were the [2+2] cycloaddition product, called the tilted structure, which has C_1 and C_2 bonded to the two Si atoms of a single dimer, the tilted bridge structure which has C_1 and C_2 bonded to Si atoms on adjacent dimers on the same side of the row, and the diagonal bridge structure, which has C_1 and C_2 bonded to Si atoms on adjacent dimers on opposite sides of the row. Their work also found that the tetra-σ structures are not formed directly from the gas phase, but instead they are formed from one of the meta-stable di-σ structures [41]. Recent STM images confirm the existence of the tilted-bridge butterfly structure on the Si(100) surface stabilized by a C-type defect [45]. Jung and Gordon later modeled the tilted, butterfly, tight bridge, twisted bridge, and pedestal structures on the cluster model of the Si(100) surface and, in contrast with previous work, found the butterfly structure to be the most stable structure. However, some agreement was found, in that the tight and twisted bridge structures were found to be formed from the isomerization of the di-σ structures. It was suggested that both structures are formed from the tilted structure [42]. Further theoretical studies on the cluster model by Zhu and Materer examined the possible dissociation mechanisms of benzene on the Si(100) surface, and determined

that the dissociation pathways required a change in spin state. While the spin-crossing is not rate limiting, the barrier to formation of the common intermediate of the pathways was too large, and the tilted structure would more readily convert to the tight bridge, while the butterfly structure is stable to isomerization. This result consistent with previous studies by Jung and Gordon [33, 42]. The lack of dissociation observed in theoretical studies is consistent with experimental STM studies [29].

Similar investigations into the reactivity of substituted benzenes with the Si(100) surface have also been conducted. One study examined the bonding configurations of toluene and xylene, and determined that, while the methyl substituents may influence the ratio of the configurations, these molecules bond to the surface forming the same adsorption structures as benzene. Additionally, evidence of an Si-H vibration indicates that an H atom from the methyl group may dissociate, a result not observed for benzene [35]. Further experimental studies have confirmed this result toluene, and found that polymerization of toluene can occur on the surface when heated to temperatures between 750K and 950K [27]. Theoretical investigations have examined possible dissociation mechanisms and found that, indeed, the favored dissociation pathway is the cleavage of a C-H methyl bond to form a Si-H bond on the surface dimer. This work also found that, due to steric effects, the methyl group will promote configurations in which it is farther from the surface. Evidence for the polymerization of toluene on the Si(100) surface was also found [28].

In addition to the methyl substituted benzenes, several studies investigate the adsorption of halogenated benzenes on Si(100). Halogenated benzenes are structurally similar to benzene, but, with the exception of fluorine, C-X bonds are weaker than C-H bonds, allowing for the possibility of dissociative adsorption. In fact, a study of the adsorption of various 1,2-dihalobenzenes found that 1,2-difluorobenzene is adsorbed molecularly, while 25% of 1,2-dichlorobenzene and 100% of 1,2-

dibromobenzene is dissociatively adsorbed to the Si(100) surface. This work also found that the location of the halogen in the various isomers of a single adstructure had little effect on the adsorption energy, and, unlike the case of the methyl substituent, this does not favor one structure over another [30]. Further studies from this group found that chlorobenzene and dichlorobenzene form similar adsorption structures to benzene, but unlike 1,2-dichlorobenzene, no dissociation is observed [31]. However, the structure of chlorobenzene on the Si(100) surface is under some debate, as STM images from Naumkin and co-workers suggest that both chlorobenzene and 1,2-dichlorobenzene do, in fact, dissociatively adsorb to the Si(100) surface [29]. Theoretical investigations of stable structures from both groups indicate that the dissociated structure is the most stable configuration, indicating that kinetics play a prominent role in these observations [31, 36]. Furthermore, Naumkin and co-workers suggest a spin-crossing must occur when forming the row-linking structure, as this is the most stable spin multiplicity due to the two unpaired electrons which remain on the surface [36]. However, a detailed mechanism is not described for any of the cases mentioned above.

Spin-Crossing on the Si(100) Surface

Spin-crossing can occur when two diabatic surfaces, potential energy surfaces which, in this work, omit spin-orbit coupling, with different spin-multiplicity (e.g. singlet and triplet) intersect along the crossing seam. A depiction of this crossing is shown in Figure I-4. The most probable geometry for crossing, the minimum energy crossing point (MECP), is found by minimizing the energy along the crossing seam. In the adiabatic potential energy surfaces, this crossing is avoided, as the spin-orbit coupling creates spin-mixed potential energy surfaces, shown in Figure I-4, that approach, but do not cross. Once the MECP is obtained, the spin-orbit coupling constant can be calculated to determine the magnitude of the separation between the two adiabatic surfaces. This spin-orbit coupling constant, along with the Frobenius norm of the energy difference gradient, is used to calculate the

crossing probability according to Equation 1. The crossing probability determines the probability that the reaction will be contained to the same adiabatic potential energy surface, and not hop to the higher energy adiabatic potential energy surface; a higher crossing probability means that the transition from the singlet to triplet is more likely. Using this probability to modify the equations of transition state theory, non-adiabatic transition state theory [47] can be used to determine the rate of this spin-crossing event using Equation 2.

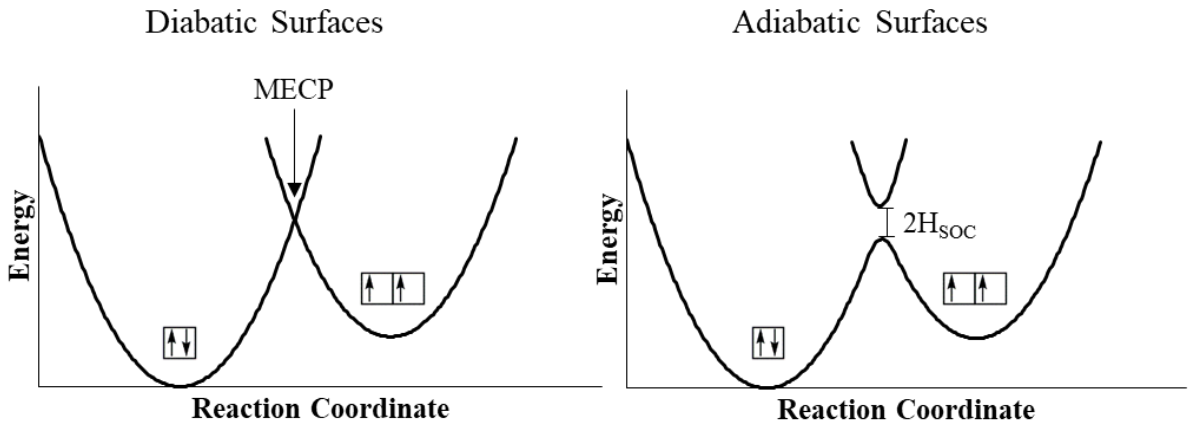

Figure I-4. This figure is a graphical depiction of the crossing of the singlet and triplet diabatic surfaces, and the avoided crossing of the adiabatic surfaces due to spin-orbit coupling. The minimum energy crossing point is found by minimizing the energy on the crossing seam (orthogonal to the page) between the two diabatic surfaces. The energy splitting due to spin-orbit coupling is twice the energy of the spin-orbit coupling constant, H_{SOC}.

Spin-crossing events, both as critical events and possibly as kinetics control, could have significance in a range of chemical processes. Traditionally, the study of surface reactions involving a change in spin often focuses on the effects of spin-crossing events for the adsorption and dissociation of oxygen, which is a triplet in the gas phase [48-52]. On Si(100), Kato *et al.* [48] and Fan *et al.* [49] demonstrated that triplet oxygen could easily adsorb to the surface, and they examined the effect of spin-crossing on the kinetics of the reaction with the surface. Further studies on this surface produced

qualitative agreement with experiments after using a non-adiabatic model for the sticking probability [50]. In another study, Bell, Head-Gordon, and co-worker found that the oxidation of methanol on VO_x/TiO_2 and VO_x/SiO_2 surfaces requires a spin crossing event [53]. Additionally, they found that the required spin-crossing event is a kinetic bottleneck for this reaction [53]. Similar results were found for hydrated vanadia [54]. Moc *et al*. [55] have shown that diatomic hydrogen will adsorb to a triplet palladium surface, then undergo a spin-crossing event to convert the system to a singlet state.

In Chapter II, the results of the DFT investigation of the adsorption and dissociation of chlorobenzene on the Si(100) surface are presented. A survey of the possible adsorption configurations is conducted to determine all possible dissociation pathways and the effect of the spin-crossing events on the dissociation pathway is discussed. In Chapter III, this work is extended to 1,2- and 1,4-dichlorobenzene, and some of the similarities and difference between dichlorobenzene and chlorobenzene are discussed in Chapter V.

Zinc Oxide

Zinc oxide is a wide band gap semiconductor and is widely used in industrial products and medicine. However, it has been largely looked over in the electronics industry due to an inability to control the doping type, as ZnO is a native n-type semiconductor [56-58]. The cause of this n-type doping has been a matter of considerable debate, and many different hypothesis have been suggested. One of the original hypotheses is that this is caused by oxygen vacancies and zinc interstitials; however, theoretical investigations do not support this [59-61]. Another possible explanation is various donor impurities such as group III elements as well as hydrogen and fluorine. While the group III elements and fluorine may or may not be present, hydrogen is present in a variety of manufacturing techniques. This n-type conductivity is also stable at elevated temperatures, and, due to high mobility, interstitial

hydrogen, while it is a donor [62-64], it is not likely the cause. However, Janotti and Van de Walle [65] have found that hydrogen can form a multicenter bond when substituted for oxygen in ZnO. This structure is stable at higher temperatures, and because hydrogen is a donor in ZnO, this is a probable explanation for the n-type conductivity. While a plausible explanation of the cause of the n-type conductivity of ZnO has been given, the issue of controlling the conductivity remains. However, ZnO has many great properties such as the availability of large single crystals with low defect concentration and a tunable band gap. Alloying ZnO with CdO and MgO allows for tuning the band gap between the theoretical limits of 1.6-4.0eV [66]. In fact, Sharma *et al.* [67] have successfully achieved a band gap of 4.0 eV in a MgO/ZnO alloy. These properties make ZnO an attractive candidate over other semiconductor materials.

Zinc oxide is a group II-VI semiconductor which crystallizes in either the rocksalt, zinc blende, or wurzite structure. While the rocksalt and zinc blende structures are achievable by formation on a particular substrate or exposure to high pressures, the wurzite structure is the most stable crystal structure under ambient conditions. It is comprised of a hexagonal close packed sublattice of Zn interlaced with a hexagonal close packed sublattice of O, such that each Zn atom surrounded by four O atoms, while each O atom is surrounded by four Zn atoms. A depiction of this structure is shown Figure I-5, with the unit cell shown in Figure I-5A and a supercell shown in Figure I-5B to display the bonding. An ideal wurzite crystal structure would have a c/a lattice constant ratio of 1.633, and a 'u' value, defined as the ratio of the bond length to c, of 0.375, however experimental results for ZnO reveal a smaller c/a ratio of ranging between 1.595-1.6035 and a slightly higher u with values ranging between 0.3817-0.3856. The experimental values of the lattice constants range between 3.2475-3.2501Å for a and 5.2042-5.2075Å for c.[68-72]

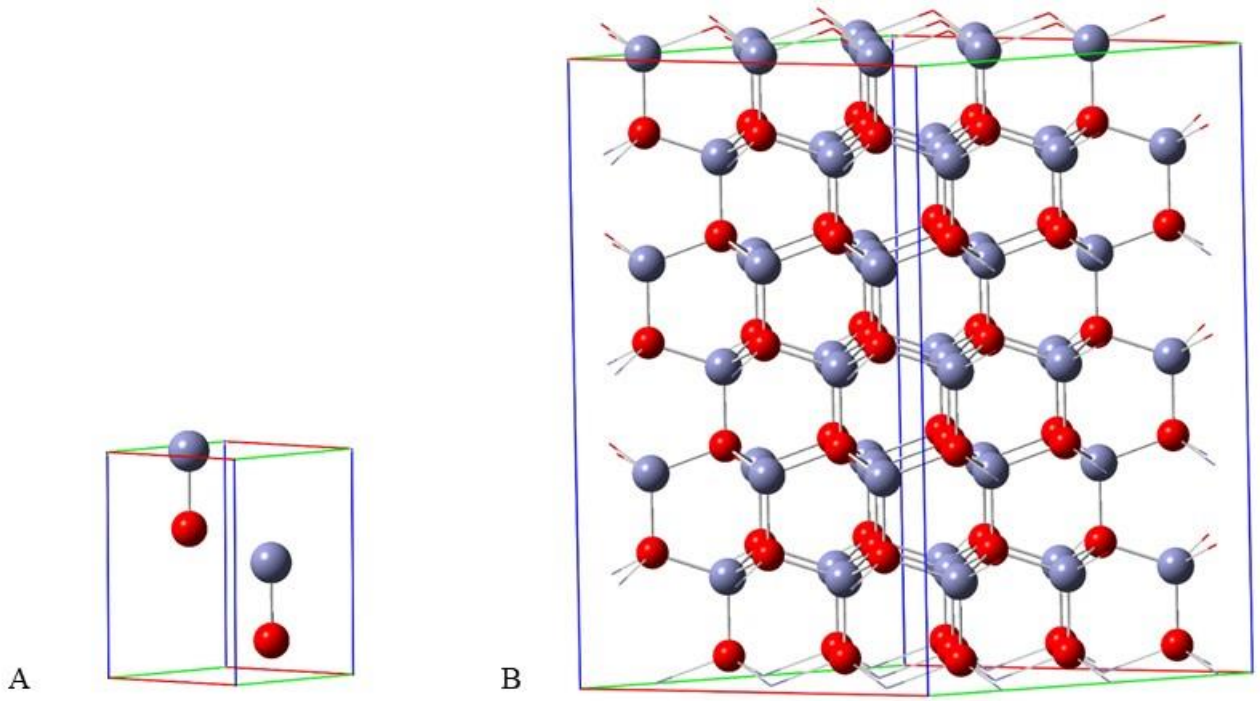

Figure I-5. The unit cell of ZnO (A) contains four atoms: two O atoms and two Zn atoms. A supercell (B) is shown to display the bonding.

The electronic band structure of ZnO can be measured experimentally using techniques such as angle resolved photoelectron spectroscopy, and spectroscopic measurements of the band gap are easily made. However, theoretical calculations of the band structure can be quite difficult. The band structure arises from the periodicity of the bulk crystal, and thus extended systems such as these are represented using periodic boundary conditions. In general, density functional theory is used with the local density approximation (LDA) of the exchange and correlation functionals. Although without some modifications, this method does a poor job of reproducing the band gap. More advanced approximations such as LDA+U or self-interaction correction [73] give results with much closer agreement to the experimental values of 3.4eV [74, 75].

In contrast to the band structure, the structural and mechanical properties of semiconductors can easily be determined using a variety of experimental and theoretical techniques. The atomic positions and lattice parameters discussed above are obtained using X-ray diffraction, and can be determined using DFT via geometry optimizations. Both the local density and generalized gradient approximations give good results for the structural properties of ZnO. Experimentally, the elastic constants of ZnO can be determined using ultrasonic techniques, and these values are used to determine the bulk modulus. Theoretical and experimental values are found in Chapter IV. The bulk modulus can also be determined by measuring the lattice parameters as a function of pressure using X-ray diffraction and fitting this data to the Murnaghan equation of state [76]. Computational determination of the bulk modulus is determined in a similar way, by fitting the total energy as a function of the volume to the Murnaghan equation of state. In general, the LDA overestimates this value, while the generalized gradient approximation (GGA) will underestimate the value [77], and thus many studies utilize both methods. Chapter IV discusses the ongoing work related to the calculation of the mechanical and electronic properties of cobalt doped zinc oxide using DFT with the LDA and GGA approximations of the exchange and correlation functionals. Some results are presented for the bulk modulus and density of states for both pure and doped ZnO in Chapter IV, and future work and modifications to the methodology are discussed in Chapter V.

CHAPTER II

Spin-Crossing and Dissociation of Chlorobenzene on Cluster Models of the Silicon (100) Surface

This chapter examines the adsorption of chlorobenzene on Si(100) surface. Previous experimental investigations of chlorobenzene show little [29] to no [31] dissociation of chlorobenzene when adsorbed onto the Si(100) surface. The experimental investigation from Zhou *et al.* [31] included a computational study which concluded that dissociation is thermodynamically favorable. Thus, the absence of dissociation products were attributed to kinetic factors [31]. A computational study by Naumkin *et al*. [36] arrived at similar conclusions, but also invoked a spin-cross argument. Such spin-crossing events are also postulated for the dissociation of chlorobenzene on Au/Pd nanoclusters [78] and nitrobenzene on Ge(100) surface [79]. However, for Si(100), the crossing probabilities and transition states along the pathway suggested by Naumkin *et al*. [36] were not investigated in detail.

This work builds on a previous publication from our laboratory in which a computational investigation of the dissociation pathway of benzene on cluster models of the Si(100) surface was conducted. This work found that benzene adsorbs onto the singlet surface, but must undergo a spin-crossing event for dissociation to occur [33]. For a Si-dimer cluster, the spin-crossing occurs easily [80], and the adsorption does not significantly affect the probability as long as a cluster

contains an unreacted Si-dimer [33]. Thus, this chapter will examine the dissociation mechanism of chlorobenzene on the Si(100) surface, explicitly taking into account the spin-crossing events.

Computational Methods

The computational methods follow those used by Zhu and Materer [33], and are briefly explained here. Using the Gaussian 09 software package [81], the geometry of all stable structures on the cluster model of Si(100) was optimized. Adsorption energies are reported in reference to the bare cluster and the chlorobenzene in the singlet electronic state. No zero point corrections were applied. Frequency calculations were performed to ensure stable structures had no imaginary frequencies, while transition states only had one imaginary frequency. Internal reaction coordinate (IRC) calculations were performed to ensure that the transition states connected to the expected stable structures. However, IRC calculations for transition states that require the large trench cluster were unobtainable, due to computational limitations. All calculations used the B3LYP hybrid functional, which consists of Becke's three parameter exchange functional[82] along with the Lee-Yang-Parr correlation functional [83]. The 6-31G(d) split valence basis set with the polarization d-function [84] on all atoms except hydrogen was utilized. This basis set is used for all computations, as computational limitations limited expanded basis set for the larger structures. To address potential issues with this basis set, single point calculations were performed on several adsorption structures, at the geometry optimized using the smaller basis set, using the 6-311++G(d,p) basis set. These computations reveal that the average change in adsorption energy due to the change in basis set is 3.0 kJ/mol, with the largest change of only 5.1 kJ/mol.

Minimum energy crossing point (MECP) geometries were calculated using a program developed by Harvey *et al*. [85], based on an algorithm developed by Bearpark *et al*. [86] Once obtained, the spin-orbit coupling (SOC) coefficients were calculated at the MECP geometry using a methodology similar to a previous publication [80]. The Breit-Pauli spin-orbit Hamiltonian, including both one and two electron terms, was used in GAMESS(US) software package [87] to compute the SOC coefficient. These computations utilize the same Gaussian-type basis set as the one used in Gaussian 09. The SOC computation procedure starts with a full second order configuration interaction calculation at the MECP geometry. Once the optimized molecular orbital coefficients are determined, they are utilized to compute the spin-orbit coupling coefficient using a complete active space self-consistent field (CASSCF) computation with an active space consisting of seven valance and seven virtual orbitals.

The Landau-Zener formula [88-90] determines the probability of a non-adiabatic crossing (Equation 1). To calculate the probability of the spin crossing event at the MECP geometry, the double pass formula described by Harvey [47], the difference being $8\pi^2$ in the exponential for a double pass versus $4\pi^2$ for the single pass formalism, was utilized (Equation 1).

$$P_{sh}(E) = 1 - \exp\left(\frac{-8\pi^2 H_{soc}^2}{h\Delta F}\left[\frac{\mu}{2E}\right]^{1/2}\right) \quad \text{(E1)}$$

In Equation 1, H_{soc} is the spin-orbit coupling coefficient, h is Planck's constant, ΔF is the Frobenius norm of the energy gradient difference, μ is the reduced mass of the system along the crossing coordinate, and E is the kinetic energy of the system. Similar to a previous publication [80], this study used the reduced mass along the crossing coordinate obtained by frequency analysis of MECP structure. Due to the complex nature of the larger trench clusters, an averaged

reduced mass from all contributing normal modes of the double-dimer structures was used for all probability calculations. Similarly, and averaged kinetic energy of those normal modes was used to determine the kinetic energy of the system. Once obtained, the crossing probability can be used to determine the rate coefficient of the spin-crossing by utilizing non-adiabatic transition state theory [47]:

$$k(T) = P_{sh}\left[\frac{k_B T}{h}\exp\left(\frac{-\Delta G}{RT}\right)\right] \qquad \text{(E2)}$$

In Equation 2, k_B is Boltzmann's constant, T is temperature, ΔG is the change in Gibb's free energy, and R is the ideal gas constant.

Since this paper studies the localized adsorption and dissociation of the chlorobenzene on the Si(100) surface, the cluster model was chosen, as opposed to the slab model, which uses periodic boundary conditions to model the surface. The general rules for the formation of cluster models is described by Evarestov *et al*. [91]. The use of clusters can be contrasted with results from the slab model. For the dissociative adsorption and desorption of hydrogen on various cluster models of the Si(100) surface, it was found that although small, single dimer clusters overestimate the reaction barriers with respect to the slab model, larger clusters, such as the triple dimer cluster, give similar results to slab computations [92]. Other studies on the desorption of hydrogen on the Si(100) surface show that a cluster containing eight surface dimers is nearly identical to the slab model, with the triple dimer cluster, with an additional layer of bulk Si atoms, being only 0.8 kcal/mol higher in energy than the cluster with eight surface dimers [93]. Thus, the advantages of treating the surface using small clusters when dealing with spin-crossing outweigh the small differences in energy between the clusters chosen for this work and much larger clusters or the slab computations. In order to account for distortions in the cluster model, a custom python script

was used to fit an ideal lattice to the bottom two layers of Si atoms for each structure in the dissociation pathways.

Results and Discussion

This study uses molecular clusters to model the localized bonding of chlorobenzene on the Si(100) surface. The hydrogen truncated single-dimer (Si_9H_{12}), double-dimer ($Si_{15}H_{16}$), triple-dimer ($Si_{21}H_{20}$), and trench-dimer ($Si_{53}H_{44}$) clusters, which consists of two fused double-dimer clusters, are utilized. For the dissociation pathway of chlorobenzene, a majority of the structures require adjacent dimers to provided by the double-dimer and trench clusters. Since trench clusters have a tendency to buckle due to the smaller number of bonds connecting the dimer rows, an extra layer of silicon atoms was added to the cross-dimer cluster to minimize buckling during optimization. A single-dimer based trench cluster was not utilized to avoid any twisting or buckling in a smaller trench cluster.

Adsorption Structures

The di-σ butterfly and tetra-σ tight bridge adsorptions structures have been proposed for non-dissociative adsorption of chlorobenzene on the Si(100) surface [31]. The di-σ adsorption structures consist of geometries with two Si-C bonds, while the tetra-σ adsorption structures have four Si-C bonds. These structures are chlorobenzene analogs of a much larger list of structures formed by benzene adsorption on the Si(100) surface [41-43]. Recent STM experiments have observed evidence for the existence of a tilted-bridge butterfly configuration near C-type Si(100) defect [45]. Also, a row-linking butterfly structure suggested by Naumkin *et al*. was included [36]. Given the wide possibilities for benzene adsorption, a thorough investigation of the possible

analogs was required for chlorobenzene. The results are summarized in Table II-1. Although larger clusters were utilized to examine cluster size effect, the reported structures are on the smallest possible clusters for the molecular adsorption, and the smallest cluster possible for dissociation. For the adsorption structures, all coordinates are fully optimized except when noted. The transition states have one imaginary frequency, and IRC calculations were performed to confirm that the transition structures indeed connect the initial and final stable structures.

Table II-1. Adsorption energies of chlorobenzene on the Si(100) surface in kJ/mol for the adsorption structures (AS) and the transition structure (TS1) from the gas phase (except as noted), all with singlet multiplicity. Adsorption and transition state energies are referenced to the isolated singlet chlorobenzene and singlet Si(100) cluster. All coordinates are fully optimized except when noted in the text. The transition states have one imaginary frequency, and IRC was performed to confirm that the transition structures connected the stable structures.

Di-σ	Cluster	TS1	AS	Tetra-σ	Cluster	TS1	AS
Tilted				*Tight-Bridge*			
1,2	Single	86.9	-27.9	1,2,3,4	Double		-57.6
	Double	82.0	-24.2		Trench		-141.8
2,3	Single	62.6	-27.7	1,2,3,6	Double		-53.7
	Trench	52.6	-32.1		Triple		-55.1
3,4	Single	65.2	-21.2	2,3,4,5	Double		-64.8
	Double	56.0	-19.8		Triple		-65.4
Butterfly				*Twisted-Bridge*			
1,4	Single	23.4	-79.9	1,2,3,4	Double	39.6[a]	-43.2
	Trench	31.0	-71.2		Triple		-42.1
2,5	Single	14.6	-89.9	1,2,3,6	Double		-33.2
	Double	10.1	-89.8		Triple		-39.9
Tilted-Bridge				2,3,4,5	Double	30.5[b]	-45.9
Butterfly					Trench		-101.1
1,4	Double	64.6	-16.0				
	Triple	64.0	-15.5				
2,5-Parallel	Double	43.2	-28.9				
2,5-Perpendicular	Double	46.1	-24.9				
	Trench	56.2	-35.2				

a) From the 1,4-Tilted-Bridge Butterfly b) From the 2,4-Tilted-Bridge Butterfly

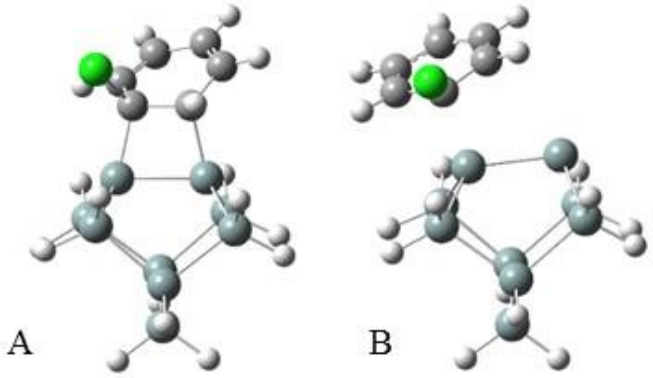

Figure II-1. Di-σ chlorobenzene adsorption structure and transition state: (A) 1,2-tilted adsorption structure on a single-dimer cluster and (B) asymmetric transition state into the adsorption structure.

Di-σ Adsorption Structures: Tilted Structures

Starting with the tilted structures, there are three possible adsorption configurations on the single-dimer cluster. These geometries are formed from a gas phase chlorobenzene molecule via an asymmetric non-concerted transition state in which the π-electrons across one of the carbon-carbon double bonds form a dative bond with the electrophilic "down" Si atom on the Si dimer. This reaction is symmetry forbidden for a typical [2+2] cycloaddition reaction, in which the C_n-C_{n+1} and Si-Si π-bonds break forming two new Si-C bonds, since two of the p-orbitals are not in phase. However, the buckled structure of the dimers reduces the symmetry of the surface, allowing the reaction to proceed along the asymmetric pathway. As this structure moves toward the tilted adsorption structure, the π-bond is broken as the chlorobenzene moves over the dimer, and two new σ-bonds are subsequently formed. The numbers, typically assigned to each carbon in the benzene ring, denoting the two carbons across which the Si-dimer adds, label the configurations. Only the cis- configurations, where both hydrogen atoms are on the same side of the aromatic ring, are reported because the trans-geometries have significantly higher energy due to twisting of the carbon ring. The 1,2-tilted structure on a single-dimer cluster is shown in

Figure II-1A and has an adsorption energy of -27.9 kJ/mol. This structure is formed from the isolated chlorobenzene through an asymmetric transition state shown in Figure II-1B. An 86.9 kJ/mol barrier is found for the formation of the 1,2-tilted structure on a single-dimer cluster. Using a larger double-dimer cluster, the barrier is decreased by 4.9 kJ/mol to 82.0 kJ/mol. On this larger cluster, the chlorine atom is positioned 4.10 Å away from the closest Si atom on the adjacent dimer. The 2,3-tilted and 3,4-tilted analogs have adsorption energies of -27.7 and -21.2 kJ/mol on single-dimer clusters, respectively. Similar to the 1,2-tilted structure, larger Si cluster models are needed to evaluate the nearest distance between Cl and Si atoms. For the 2,3-tilted structure, the minimum Cl to Si distance was evaluated using a trench cluster. The adsorption energy on this cluster is decreased by 4.4 kJ/mol to -32.1 kJ/mol, and the minimum Cl-Si distance is 4.07 Å to the Si across the trench. For the 3,4-tilted, a double-dimer was used (adsorption energy of -19.8 kJ/mol, a change of only 1.4 kJ/mol) and the distance is 4.47 Å to a Si atom of a dimer on the same row.

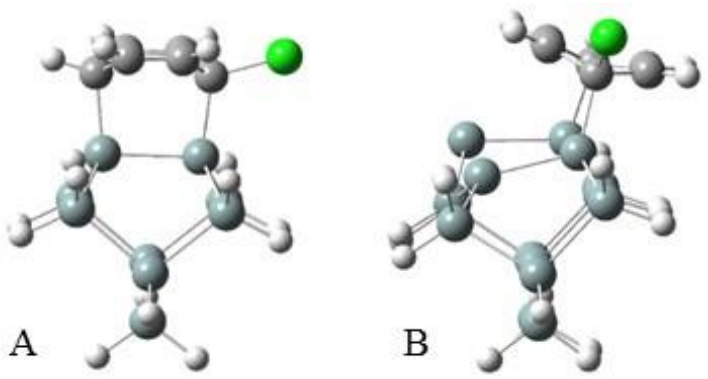

Figure II-2. Additional di-σ adsorption structures: (A) The 1,4-butterfly on a single-dimer cluster and (B) 1,4-tilted-bridge butterfly on a double-dimer cluster.

Di-σ Adsorption Structures: Butterfly Structures

The butterfly structures are formed via a [4 + 2] Diels-Alder cycloaddition reaction. In the [4 + 2] cycloaddition reaction, two of the π-bonds in the chlorobenzene ring are broken and the weak π-bond in the Si dimer is broken. The ring attaches to the dimer forming two σ-bonds at the C_n and C_{n+1} carbon atoms, and the remaining π-electrons in the ring form a new π-bond. This reaction is symmetry allowed, and, as expected, has an activation energy that is significantly lower than the asymmetric cycloaddition of the tilted structures. For butterfly structures, there are two possible configurations on the single-dimer cluster. The first (Figure II-2A) is formed by the attachment of the C_1 and C_4 atoms to a single Si dimer, resulting in a 1,4-butterfly structure with an adsorption energy of -79.9 kJ/mol and an adsorption barrier of 23.4 kJ/mol. On a trench cluster (adsorption energy of -71.2 kJ/mol), the chlorine atom protrudes into the trench region in between two Si dimer rows, making same-row dissociation unlikely due to the large distance (5.53 Å) between the chlorine atom and adjacent silicon dimer on the same row. However, the chlorine atom is only 3.91 Å from the Si dimer across a different dimer row. In addition to the 1,4-butterfly structure, the 2,5-butterfly structure can be formed by the attachment of the C_2 and C_5 atoms to the Si dimer. This structure has an adsorption energy of -89.9 kJ/mol, with an adsorption energy barrier of 14.6 kJ/mol on the single-dimer cluster. These adsorption barriers are much lower compared to the adsorption barrier of 86.9 kJ/mol to form the 1,2-titled structure. When using double-dimer clusters, the adsorption energy and adsorption barrier change to -89.8 kJ/mol and 10.1 kJ/mol respectively, and the Cl atom is slightly closer to the adjacent Si dimer (3.83 Å) on the same row than the 1,2-titled structure.

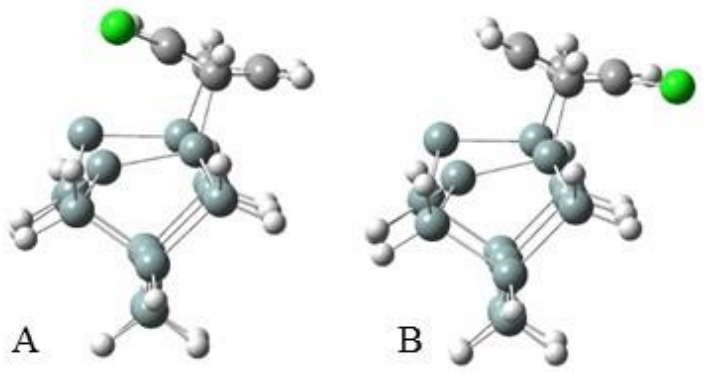

Figure II-3. Additional di-σ structures: (A) 2,5-same tilted-bridge and (B) 2,5-adjacent tilted-bridge butterfly.

On larger clusters, three more variations of the butterfly structure become available, which are referred to as the tilted-bridge butterfly (Figure II-2B), the diagonal-bridge butterfly and the row-linking butterfly. The tilted- and diagonal-bridge butterfly structures require a double-dimer cluster and impart a significant strain on the cluster. To avoid unrealistic distortions, the bottom two layers of Si atoms were frozen during optimization. On the Si(100) surface, distortions are energetically limited due to the deeper Si layers. Thus, the constrained optimization is expected to provide a more realistic representation on the Si(100) surface. The 1,4-tilted-bridge butterfly is formed when the C_1 atom bonds to a Si atom on one Si dimer, and the C_4 atom bonds to the adjacent Si dimer on the same side. This structure is essentially a 90° rotation of the butterfly structure (compare Figure II-2A with II-2B). The tilted-bridge butterfly structure is angled into the trench between two Si dimer rows, but the chlorine atom is quite close (4.16 Å) to a neighbor Si dimer within the same row. The adsorption energy of this structure is much weaker (-16.0 kJ/mol) than either the tilted or the butterfly structures due to the increased strain on the Si-dimers. There are two additional tilted-bridge butterfly structures available where the C_2 and C_5 atoms are bonded to the Si surface (see Figure II-3A and B). In the first case (2,5-Same shown in Figure II-3A), the C_l atom, which contains the C-Cl bond, is located above the same dimer row,

and the Cl atom is 3.56 Å from the nearest Si atom. This structure has an adsorption energy of -28.9 kJ/mol. The second case (2,5-Adjacent shown in Figure II-3B) has an adsorption energy of -24.9 kJ/mol. The Cl atom is pointed towards adjacent dimer row and is located in the trench region between the two dimer rows. This structure has the Cl atom 3.20 Å from a Si atom on the adjacent dimer row.

A diagonal-bridge butterfly can be formed when the C_1 atom bonds to Si atom on one Si dimer, and C_4 atom bonds to a Si atom across the diagonal direction on an adjacent Si dimer of the same row. Although the benzene analog has been found for the diagonal-bridge butterfly structure on an extended slab model [41], no stable structure for the chlorobenzene analog of the diagonal-bridge butterfly structure could be found. The tilted-bridge butterfly chlorobenzene configurations are analogs to the inter-dimer butterfly benzene on Si(100) reported in an STM study by Polanyi and coworkers [45]. The inter-dimer butterfly configuration for benzene is stabilized by the existence of C-type Si(100) defects and becomes even more stable than the conventional butterfly adsorption configuration. Although not examined here, it is possible that the tilted-bridge butterfly chlorobenzene configurations may also be favored on a Si(100) surface when certain defects exist.

Figure II-4. Row-linking butterfly di-σ adsorption structure on the trench cluster.

The final butterfly structure is the row-linking butterfly (see Figure II-4). This structure has a bond between the C_1 atom and a Si atom on a dimer on one row, while the C_4 atom is bonded to a Si atom on the adjacent row, linking the two dimer rows together. This adsorption structure has an energy barrier of 70.2 kJ/mol and an adsorption energy of 3.6 kJ/mol in the singlet state. Since this structure is slightly unstable with respect to the free reactants as a singlet, it is expected to rapidly convert to a stable triplet state. In the triplet structure, the Si-Si distance between the dimer rows is shortened to 4.88 Å from 5.27 Å on the bare cluster due to some unbuckling of the dimers, while the C_1-C_4 distance is lengthened to 2.98 Å by the loss of a π-bond. A computation with the bottom layer frozen has a similar adsorption energy (8.4 kJ/mol lower in the singlet state and 5.5 kJ/mol lower in the triplet state), indicating that small changes in the positions of the Si atoms do not significantly affect the energetics of the dissociation pathway.

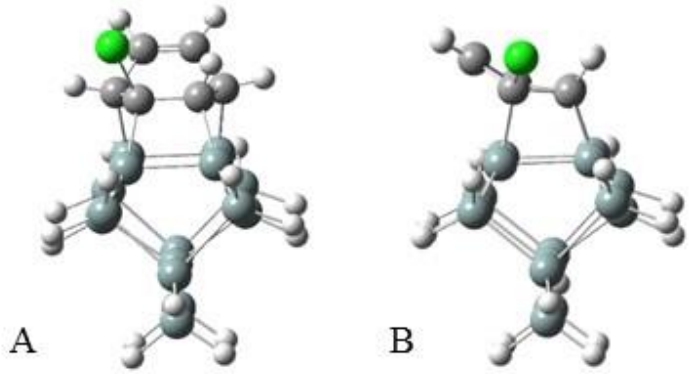

Figure II-5. Tetra-σ bonded adsorption structures: (A) tight-bridge and (B) twisted-bridge.

Tetra-σ Adsorption Structures: Pedestal, Tight-Bridge, and Twisted-Bridge

There is also a set of tetra-σ (four Si-C bonds) chlorobenzene structures that are analogs of structures found for benzene adsorption on the Si(100) surface, including the pedestal, tight bridge, and twisted-bridge [41]. These structures require clusters with a minimum of two Si-dimers. For benzene, Jung and Gordon [42] have shown, using clusters models, that the tight-bridge structure can be obtained from the tilted structure. All bridge structures require the Si atoms in the bottom two layers to be fixed during optimizations to minimize unrealistic distortions. Starting with the 1,2,3,6-tight bridge (Figure II-5A), an adsorption energy of -53.7 kJ/mol is found for a double-dimer cluster. Under full optimization, which allows unrealistic distortions of the cluster, the adsorption energy is reduced significantly to -142.1 kJ/mol. This energy is similar to -160.2 kJ/mol, found by Zhou and Leung [31]. However, in the fully optimized structure, the double-dimer cluster "curls up" to accommodate the additional C-Si bonds to the adjacent dimer. As for the butterfly configuration, some distortions are expected but would be constrained by deeper layers in an extended system. Thus, the constrained 1,2,3,6-tight bridge is more of a realistic depiction on what could occur on the Si(100) surface.

In addition to the 1,2,3,6-tight bridge, there are two additional tight bridge structures, one with the Cl atom attached to a silicon bonded carbon atom, C_3 or C_6, on the neighbor dimer, and one with the Cl atom on a non-silicon bonded carbon atom, C_4 or C_5. These geometries have similar adsorption energies to that of the 1,2,3,6-tight bridge (Table II-1). The 1,2,3,6-tight bridge has its Cl atom closer to the surface than both of the two other tight bridge structures with a distance of 5.40 Å, although it is still over 1 Å further from the surface than the tilted and the tilted-bridge butterfly structures. Unlike the work of Jung and Gordon [42], transition states into the tight-bridge structures, from either the gas phase or a di-σ tilted structure, were not obtained for either benzene or chlorobenzene. It is possible that differences in the computation approach or the degree of distortion allowed of the cluster are responsible. Thus, no tight-bridge based potential dissociative pathways were considered.

A twisted-bridge structure can be generated from the tilted-bridge butterfly structures through a reaction with the nearby bare Si atoms and is equivalent to a 90° rotation of the tight bridge structures. Again, freezing the Si atoms in the bottom two layers during the optimization is required to minimize unrealistic distortions of the cluster. Figure II-5B shows the 1,2,3,4-twisted-bridge, formed from the 1,4-tilted-bridge butterfly structure via a reaction of the C_2 and C_3 with the bare Si atoms on each dimer, with a transition barrier of 55.6 kJ/mol. This structure has an adsorption energy of -43.2 kJ/mol for the structure, and the distance between the chlorine and the surface (4.14 Å) is similar to that of the tilted structure. Similar to the 1,2,3,4-twisted-bridge, the 2,3,4,5-twisted-bridge structure can be formed from the 2,5-adjacent titled-bridge butterfly structure with the chlorine atom over the trench. The barrier to this structure is 55.5 kJ/mol, and the adsorption energy is -45.9 kJ/mol on the double-dimer cluster. Although a transition into the 1,2,3,6 structure could not be found, a stable adsorption structure was found

with an adsorption energy of -33.2 kJ/mol. It should be noted that while transitions into these structures were found on the double-dimer cluster, none were found on larger clusters.

Finally, no stable pedestal geometry could be found, in agreement with Silvestrelli *et al.* [41] and Jung and Gordon [42]. The pedestal geometry is bonded to the Si(100) surface by the C_1-Si and C_2-Si bonds on one dimer, and the C_4-Si and C_5-Si bonds on another dimer in the same row. This leaves only the C_3 and C_6 carbon atoms without bonds to the Si surface resulting in an unstable biradical carbon ring. The formation of a double bond may result in a more stable structure, however, separation of the radical carbon atoms does not allow for a double bond to be formed in the ring.

Cluster Effects

For the adsorption structures discussed above, the effect of partial optimization was already discussed with respect to modeling the extended Si(100) surface with clusters. An additional consideration is the effect of the size (see Table II-2) of the Si cluster model on calculated adsorption energy. Cluster size effects were assessed by comparing the adsorption energy for the 1,2-tilted adsorption structure on single, double, triple, and trench-dimer clusters. Although the increased delocalization provided by larger clusters can reduce the energy, the energy is also increased by additional steric interactions of the adsorbate with the cluster as additional dimers are added. The average difference in adsorption energy for the singlet is 4.3 kJ/mol with a maximum difference of 8.1 kJ/mol, while the average and maximum difference are much larger for the triplet with values of 10.3 kJ/mol and 17.6 kJ/mol, respectively. Thus, increasing the cluster size has a small, but measurable, effect on the adsorption energy. Comparison with the trench structure and the double-dimer structure reveals that increasing the size without increasing

adsorbate interaction (as additional dimers are added to an adjacent dimer row) with the cluster lowers the calculated adsorption energies. There is, however, one outlier in this trend. In the case of the adsorption structure on the single-dimer cluster in the triplet electronic state, the adsorption energy is large and positive. The unfavorable adsorption is due to the lack of a bare dimer to accommodate the unpaired electron causing the chlorobenzene to break a double bond in the triplet state, resulting in the loss of aromaticity.

In addition to the effect of cluster size, the issue of distortions in the cluster, caused by full optimizations, is also considered. Partially optimized geometries are formed by fitting the fully optimized structures to the ideal lattice positions for the lower two layers of Si atoms. The Si layers in the ideal atomic positions are held in place, while the rest of the structure is allowed to fully optimize. The adsorption energies of the partially optimized structures are calculated with respect to the partially optimized singlet bare cluster and the singlet chlorobenzene structure. These deviations from the ideal positions in the fully optimized structures result in small changes of the adsorption energy. On average, the adsorption energies for the partially optimized double dimer structures are decreased by 2.1 kJ/mol and the adsorption energies of the partially optimized trench dimer structures are decreased by 8.9 kJ/mol. The adsorption energies for each of the fully and partially optimized structures are tabulated in Table II-5.

Table II-2. The absolute value of the difference in the adsorption energy (kJ/mol) of the 1,2-tilted adsorption structure on the single, double, triple, and trench dimers. The triple dimer has two unique structures with the chlorobenzene adsorbed to the middle dimer (Triple Mid in the table) and adsorbed to the end dimer (Triple End in the table). Values are reported for both singlet and triplet spin multiplicities.

Singlet ΔE	Double	Triple Mid	Triple End	Trench
Single	3.7	8.1	6.5	1.3
Double		4.4	2.8	2.4
Triple Mid			1.6	6.9
Triple End				5.3
Average	4.3		*Maximum*	8.1

Triplet ΔE	Double	Triple Mid	Triple End	Trench
Double		9.7	9.0	7.9
Triple Mid			0.7	17.6
Triple End				16.9
Average	10.3		*Maximum*	17.6

Dissociation Structures

For the dissociation of chlorobenzene on Si(100), the transition state involves the breaking of the C-Cl bond and formation of a Si-Cl bond to the nearest Si atom for each adsorption structure. Thus, an intermediate structure with a Cl-Si bond must be found. One study, conducted by Zhou and Leung [31], used x-ray photoelectron spectroscopy to measure the ratio between C-H/C-Si bonds and C-Cl bonds and found that chlorobenzene molecularly adsorbs to the surface without any C-Cl breakage. In contrast, STM experiments done by Naumkin et al. [29] found two dissociated structures on the Si(100). Thus, a thorough examination of potential dissociated structures is required. As discussed below, many of these potential dissociated structures are not stable on the singlet surfaces, implying that any dissociation pathway will occur on the triplet surface. The feasibility of spin-crossing will be discussed later for favorable pathways. The adsorption energies and transition state energies for possible dissociation structures can be found in Tables II-3 and II-4. All reported energies are referenced to the isolated singlet chlorobenzene

and singlet Si cluster. For these structures, all coordinates are fully optimized except when noted. The transition states have one imaginary frequency, and IRC was performed to confirm that the transition structures connected the stable structures.

Table II-3. Adsorption energies for the adsorption structure (AS), the transition (TS1) into this structure from the gas phase, the first dissociation structure (DS1) and the transition (TS2) from triplet AS to triplet DS1 on the Si(100) surface are reported in kJ/mol. The AS is reported for both the singlet and triplet, while TS1 is only reported in the singlet, and TS2 and DS1 are only reported in the triplet state. Adsorption and transition state energies are referenced to the isolated singlet chlorobenzene and singlet cluster.

Model	Cluster	TS1	Singlet AS	Triplet AS	TS2	DS1
Tilted						
1,2	Double	82.0	-24.2	-0.8	30.0	-163.9
2,3	Trench	52.6	-32.1	-8.8	80.4	-12.0
3,4	Double	56.0	-19.8	5.3		
Butterfly						
1,4	Trench	31.0	-71.2	-53.1	27.3	-27.7
2,5	Double	10.1	-89.8	-60.4	51.2	-68.0
Tilted-Bridge Butterfly						
1,4	Triple	64.0	-15.5	-60.1	34.5	-139.1
2,5- Same	Double	43.2	-28.9	-66.4	67.1	-69.7
2,5- Adjacent	Trench	56.2	-35.2	-80.7	6.4	-54.3

Table II-4. Adsorption energies for the singlet and triplet dissociation structures (DS1) of the twisted-bridge structures, and the transition structures (TS2) from the adsorption structure to the dissociation structure, in kJ/mol. Adsorption and transition state energies are referenced to the isolated singlet chlorobenzene and the smallest singlet cluster that can accommodate dissociation.

Singlet	Cluster	TS2	DS1	Triplet	Cluster	TS2	DS1
Twisted-Bridge				*Twisted-Bridge*			
1,2,3,4	Triple	56.5	-71.1	1,2,3,4	Triple	81.4	-116.2
1,2,3,6	Triple		-143.5	1,2,3,6	Triple		-122.2
2,3,4,5	Trench		131.8	2,3,4,5	Trench		-83.9

In general, one expects that the singlet state will be lower in energy than the triplet state. However, the tilted-bridge butterfly and the row-linking butterfly adsorption structures (AS) are

more stable in the triplet spin state (Triplet AS) than they are in the singlet spin state (Singlet AS). In the tilted and butterfly adsorption configurations, the two unsaturated Si atoms are on the same Si-dimer and can pair with each other, but in the tilted-bridge and row-linking butterfly structures, the unsaturated Si atoms are on two separate dimers. This separation does not allow any unsaturated Si atoms to form a weak π-bond in the singlet state like the tilted and butterfly structures would. Thus, it is the formation of the Si-dimer bond in the singlet spin state that results in the singlet being more stable in the tilted and butterfly configurations, while the triplet is more stable in the tilted-bridge and row-linking butterfly configurations.

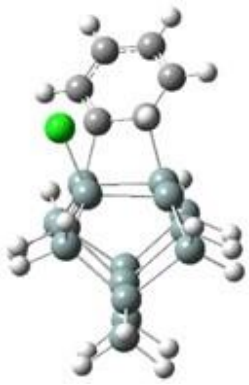

Figure II-6. The first dissociation structure (DS1) formed from the 1,2-tilted adsorption structure.

Tilted Based Dissociation Structures

Depending on the position of the nearest Si atom, the description of the dissociated structure may require a larger cluster than the initial adsorption structure. In both the 1,2-tilted and 3,4-tilted structures, the expected dissociated structure has the Cl atom bonded to a Si atom on an adjacent Si-dimer in the same row. The dissociated structure for the 1,2-tilted (Figure II-6) is not stable as a singlet but is stable in the triplet state with an adsorption energy of -163.9 kJ/mol. The energy

barrier (TS2), starting with a triplet 1,2-tilted structure and ending with the first dissociated structure (DS1), is 30.8 kJ/mol. Thus, this dissociation pathway is energetically feasible and is explored in detail in the next section. The 2,3-tilted has an expected dissociated structure with the Cl atom attached to a Si atom on an adjacent dimer row. Thus this structure requires a trench cluster. Similar to the case of the 1,2-tilted structure, no stable dissociation structures were found in the singlet electronic state. However, a dissociated structure was located on the triplet surface with an adsorption energy of -12.0 kJ/mol. The barrier to form this product from the 2,3-titled triplet adsorption structure is 89.2 kJ/mol. Given the MECP energy barrier of 24.54 kJ/mol and assuming a reasonable spin-orbit crossing probability, this barrier is higher than the desorption energy barrier on the singlet surface of 84.7 kJ/mol. The 3,4-tilted adsorption structure is energetically unfavorable in the triplet electronic state. No stable dissociation structure was found for this adsorption geometry either at singlet or triplet state.

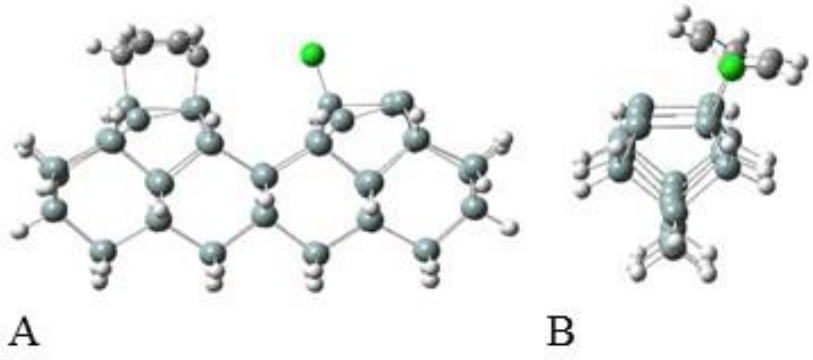

Figure II-7. The first dissociation structures (DS1) formed from (A) 1,4-butterfly and (B) 1,4-tilted-bridge butterfly.

Butterfly Based Dissociation Structures

Similar to the tilted structures, none of the butterfly structures have stable dissociation structures in the singlet state. For the 1,4-butterfly structure (Figure II-6A), the most favorable dissociation structure (DS1) has the Cl atom bonded to a Si-dimer on an adjacent dimer row. This structure has an adsorption energy of -27.7 kJ/mol in the triplet state, with a transition state barrier (TS2) 80.4 kJ/mol for the formation of DS1. This barrier is 21.8 kJ/mol less than the barrier to desorption on the singlet surface. Assuming the spin-crossing probability is reasonable and given the MECP barrier (20.7 kJ/mol) is relatively low, this pathway is considered in detail below. The 2,5-butterfly structure has a stable triplet dissociation structure with an adsorption energy of -68.0 kJ/mol on a double-dimer cluster with the Cl atom bonded to a Si atom on an adjacent Si-dimer in the same row. The transition state barrier into this structure is 111.6 kJ/mol, slightly larger than the desorption barrier of 100.0 kJ/mol on the singlet surface. Given the relatively low MECP (30.1 kJ/mol) energy barrier leading back to the singlet state, desorption is expected to be favored over dissociation.

The 1,4-tilted-bridge butterfly gives a proposed dissociation structure (Figure II-7B) with the Cl atom bonded to a Si atom on adjacent Si-dimer in the same row. This structure has an adsorption energy of -139.1 kJ/mol at the triplet configuration. However, a transition state leading to this dissociation structure was not found and this pathway is not explored further. The potential triplet dissociation structure for the 2,5-same tilted-bridge butterfly has the Cl atom bonded to the Si atom on the same dimer as the Si-C_1 bond. One the singlet double-dimer cluster, the adsorption energy is -69.7 kJ/mol, with a barrier to desorption of 72.1 kJ/mol. After spin-crossing to the triplet, the energy barrier to form the dissociated structure is 133.5 kJ/mol; thus desorption is expected. It is also possible to form a dissociation structure from the 2,5-adjacent

tilted-bridge butterfly with the Cl atom attached to a Si atom on a Si-dimer in an adjacent row. This dissociation structure has an adsorption energy of -54.3 kJ/mol on a trench cluster with a transition state barrier (TS2) of 87.1 kJ/mol to form the first dissociation structure. Using reasoning similar to that for the 1,4-tilted-bridge butterfly, it is expected that desorption will be favored over dissociation for 2,5-same-tilted-bridge butterfly structure. However, in the case of the 2,5-adjacent-tilted-bridge butterfly, the barrier to dissociation is slightly more favorable, having an energy barrier 4.3 kJ/mol lower than the barrier for desorption. Even though the barrier is slightly lower, the formation of any dissociation structure will result in a less stable ring structure that contains a dangling bond. Thus, the tilted-bridge butterfly geometries are poor candidates for the dissociation pathways and are not considered further.

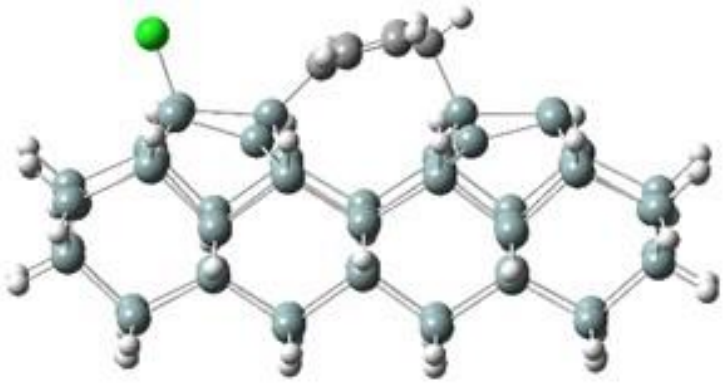

Figure II-8. Row-linking butterfly first dissociation structure on the trench cluster.

The potential first dissociation structure of the row-linking butterfly structure (Figure II-4) is shown in Figure II-8. The barrier to dissociation is 54.8 kJ/mol in the triplet state, which is 11.9 kJ/mol lower than the barrier to desorption from the singlet state of 66.6 kJ/mol. Given that the MECP energy barrier is almost non-existent and that this pathway merges with the 1,2-tilted pathway, this structure will be considered for dissociation alongside the 1,2-tilted pathway.

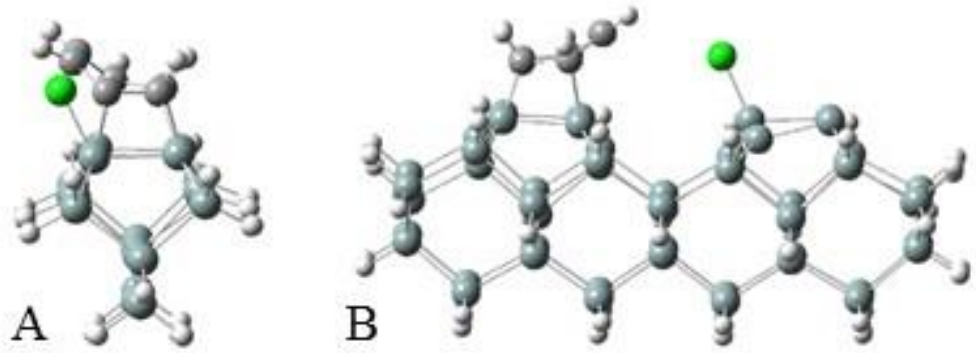

Figure II-9. Additional first dissociation structures (DS1) formed from the (A) 1,2,3,4-twisted-bridge and (B) 2,3,4,5-twisted-bridge.

Twisted-Bridge Based Dissociation Structures

Of the tetra-σ twisted-bridge structures, only the 1,2,3,4- and 2,3,4,5-twisted-bridge can be formed from a di-σ tilted-bridge butterfly intermediate. A potential dissociation structure can be formed from the 1,2,3,4-twisted-bridge (Figure II-9A) on a triple-dimer cluster by attaching the Cl atom to the adjacent Si-dimer on the same row. This structure has an adsorption energy of -71.1 kJ/mol in the singlet state and -116.2 kJ/mol in the triplet state, with transition state barriers on the singlet and triplet of 98.6 kJ/mol and 96.2, respectively. On the singlet and triplet surface, the barrier to dissociation is greater than the barrier to revert to the 1,4-tilted-bridge butterfly (approximately 80 kJ/mol), making these pathways unlikely. A possible 2,3,4,5-twisted-bridge dissociation structure is shown in Figure II-9B with the Cl atom attached to an adjacent Si-dimer row. Although this structure is unstable as a singlet (131.8 kJ/mol), it is stable as a triplet with an adsorption energy of -83.9 kJ/mol. However, no transition state into this structure from a twisted-bridge adsorption structure could be found. The lack of a transition state for the 2,3,4,5-twisted-bridge and the high barrier for dissociation of the 1,2,3,4-twisted-bridge make these pathways

improbable. As such, none of the twisted-bridge structures are treated as candidates for dissociation.

Dissociation Pathways

Of a large number of possible adsorption structures, a systematic study of potential desorption structures shows that there are only two unique dissociation pathways starting from three adsorption structures. One pathway starts with either the 1,2-tilted or the row-linking butterfly structure. The other pathway starts with 1,4-butterfly adsorption structure. Both pathways are considered in turn.

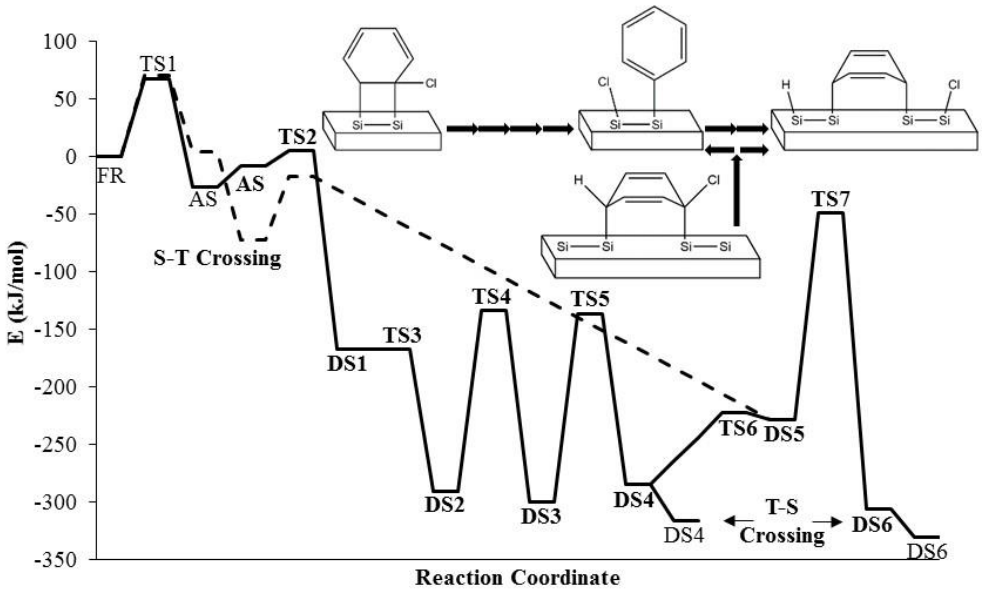

Figure II-10. This energy diagram depicts the 1,2-tilted dissociation pathway (solid) and the row-linking butterfly dissociation pathway (dotted). Bold labels indicate that the structure is optimized in the triplet state. For clarity, free reactants are labeled FR; the 1,2-tilted adsorption structure is labeled AS; transition states are labeled TS, and the dissociated structures are labeled DS. Singlet-triplet (S-T) and triplet-singlet (T-S) crossing points are also labeled. The inlay shows the adsorption structures and the two main dissociation structures DS4 and DS6, and the arrows each represent a transition into a new structure.

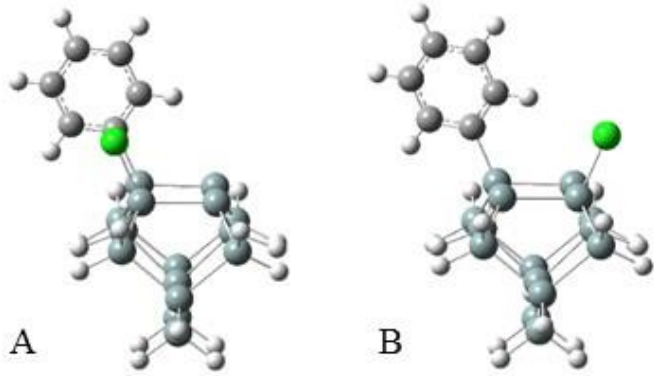

Figure II-11. Additional dissociation structures formed from the 1,2-tilted adsorption structure: (A) DS2 and (B) DS3.

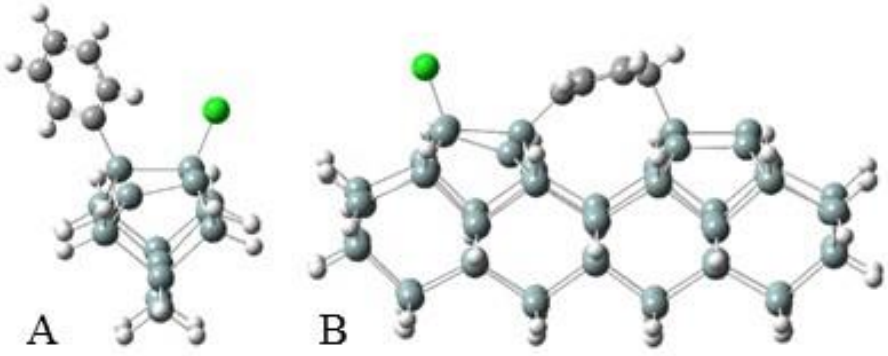

Figure II-12. Further dissociation structures along the 1,2-tilted pathway: (A) DS4 and (B) DS5.

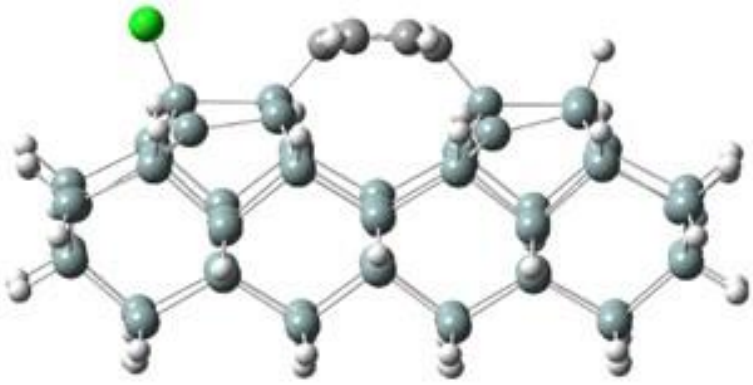

Figure II-13. Cross dimer dissociation product (DS6) for the 1,2-tilted pathway.

Dissociation Pathway for the 1,2-Tilted and Row-Linking Butterfly Adsorption Structures

The dissociation pathway starting with the 1,2-tilted adsorption geometry is shown in Figure II-10. All energies are computed on a double-dimer cluster model. Additional stable geometries are shown in Figures II-11, II-12 and II-13, and the transition state energies are summarized in Table II-5. The transition states have one imaginary frequency, and IRC confirmed that the transition structures connect the stable structures. After a change in spin state (probability considered below), the first dissociation structure (DS1), Figure II-6, can form from the adsorption structure (AS) over a 30.8 kJ/mol barrier (TS2). After which, the aromaticity of the phenyl ring can be restored by passing over a 3.9 kJ/mol barrier (TS3), which breaks the C_1-Si bond and forms a second dissociation structure (DS2), shown in Figure II-11A. This structure has an adsorption energy of -293.3 kJ/mol, significantly lower by 129.4 kJ/mol than that of the DS1 due to the restoration of aromaticity in the carbon ring. Once DS3 (Figure II-11B) is formed, the chlorine may migrate along the free Si atoms on the surface. However, the barriers to these migrations are large (163.1 kJ/mol and 191.2 kJ/mol) and do not impart a significant reduction in the adsorption energy. Of these structures, the lowest energy dissociation structure (DS4 shown in Figure II-12A) has the chlorine and phenyl group bonded to the same dimer, with an adsorption energy of -

318.4 kJ/mol in the singlet electronic state. To obtain this structure, a barrier of 191.2 kJ/mol must be overcome to form a triplet DS4, with an adsorption energy of -290.0 kJ/mol, before transitioning into the singlet state.

Table II-5. Adsorption energy in kJ/mol for stable structures and transition states along the 1,2-tilted, 1,4-butterfly and the row-linking butterfly dissociation pathways. All transition states are in the triplet state except TS1 which is in the singlet state. All stable structures are in the triplet state, except as noted. A double-dimer cluster is utilized for the 1,2-tilted pathway wherever possible. All structures following DS4 are computed on the trench cluster. Please note that the row-linking butterfly merges with the 1,2-tilted pathway at DS5, and can subsequently form either DS4 or DS6. The adsorption energy of each partially optimized structure is given in bold.

	TS1	AS Singlet	AS Triplet	TS2	DS1	TS3	DS2 Singlet	DS2 Triplet	TS4
1,2-Tilted	82.0	-24.2	-0.8	30.0	-163.9	-160.0	-293.3		-130.2
	86.4	**-21.8**	**-2.9**	**28.3**	**-165.6**	**-162.3**	**-297.5**		**-130.3**
1,4-Butterfly	31.0	-71.2	-53.1	27.3	-27.7	-87.7		-287.0	
	20.1	**-83.1**	**-70.0**	**19.6**	**-133.0**	**-105.3**		**-302.4**	
Row-Linking Butterfly	70.2	3.6	-72.3	-17.6					
	62.1	**-4.8**	**-77.8**						

	DS3	TS5	DS4 Singlet	DS4 Triplet	TS6	DS5	TS7	DS6 Singlet	DS6 Triplet
1,2-Tilted	-296.6	-105.4	-318.4	-290.0	-222.4	-227.9	-49.3	-330.2	-306.2
	-301.0	**-115.4**	**-318.6**	**-295.0**		**-232.7**	**-43.2**	**-338.1**	**-320.4**

From DS4, there is an additional dissociation pathway across Si-dimer rows. Once the triplet DS4 structure is formed, the phenyl ring may react over a barrier of 67.6 kJ/mol with a Si atom across the trench, forming DS5 (Figure II-10B) with an adsorption energy of -227.9 kJ/mol. Once DS5 has formed, the C_4-H bond may break over a 178.6 kJ/mol barrier (TS7) and create a new Si-H bond. This structure, DS6 (Figure II-11 has an adsorption energy of -306.2 kJ/mol in the triplet electronic state. In the singlet electronic state, this structure is the most stable dissociation structure with an adsorption energy of -330.2 kJ/mol.

The row-linking butterfly structure begins with the adsorption structure shown in Figure II-4. The energy diagram of this pathway is shown by the dotted line in Figure II-10. Once the more stable triplet structure is formed, the first dissociation structure (Figure II-8) can be formed. From here, an energy barrier of 54.8 kJ/mol must be overcome to form the next dissociation structure of this pathway, which is identical to DS5 of the 1,2-tilted pathway. From this structure, the single row or cross-dimer row products can be formed as they are in the 1,2-Tilted pathway.

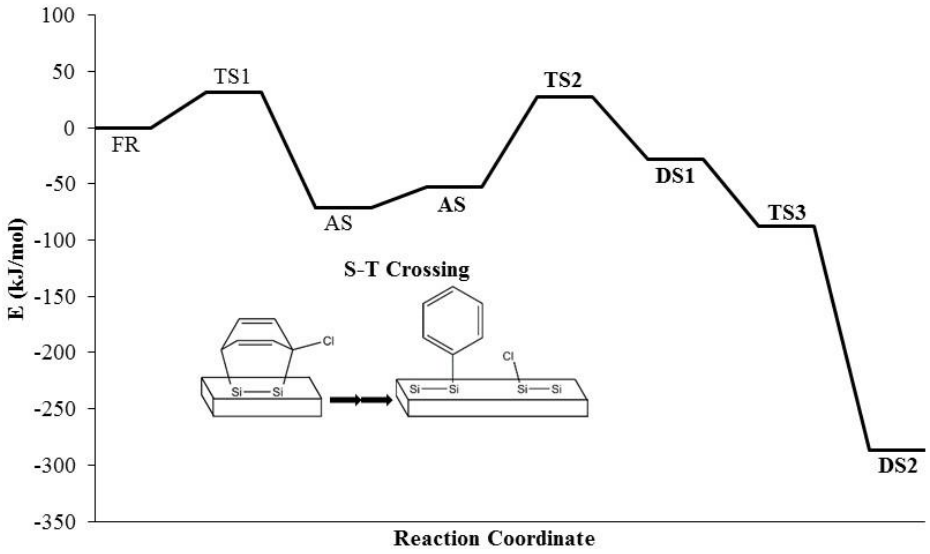

Figure II-14. The 1,4-butterfly dissociation pathway on the trench-dimer cluster. Bold labels indicate that the structure is optimized in the triplet state. For clarity, free reactants are labeled FR; the 1,4-butterfly adsorption structure is labeled AS; transition states are labeled TS, and the dissociated structures are labeled DS. The singlet to triplet (S-T) crossing is also labeled. The inlay shows the adsorption structure as well as the final dissociated structure, DS2.

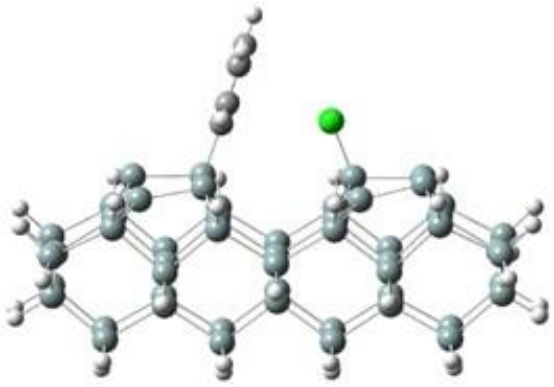

Figure II-15. Dissociation structure (DS2) from the 1,4-butterfly pathway.

Dissociation Pathway for the 1,4-Butterfly Adsorption Structure

The dissociation pathway starting with the 1,4-butterfly adsorption geometry is shown in Figure II-14. Since first dissociation structure (DS1, Figure II-7A) occurs across dimer rows, these computations require a trench-dimer cluster. The next dissociation structure (DS2) is shown in Figure II-15. After a change in spin state, discussed in the next section, DS1 is formed from the dissociation of the Cl atom from the carbon ring and the formation of a Cl-Si bond on the adjacent Si-dimer row. After which, aromaticity can be restored to the carbon ring by breaking the C_4-Si bond (DS2) (Figure II-15). By restoring aromaticity on the carbon ring, the adsorption energy of the system is significantly reduced by 259.3 kJ/mol. This structure (DS2) has an adsorption energy of -287.0 kJ/mol on the triplet surface. Since this structure has a Cl-Si bond on one row, and a C-Si bond on another with two bare dimers and two bare Si atoms, the singlet, as discussed earlier, has a significantly higher energy, making the triplet state energetically favorable. As above, it is possible that the Cl atom could migrate across the dimer surface. However, these barriers are quite large, and the reduction in energy is small.

Spin-Crossing

For these pathways to be viable, the system must undergo a spin-crossing event. As mentioned previously, the crossings occur at the MECP, where the singlet and triplet energies are identical. Selected distances and angles are shown in Table II-6 for the singlet, triplet, and MECP geometries. In addition to the crossing of the adsorption structures, the crossing of the dissociated products is also considered but not critical for the dissociation. With the only exception being the row-linking butterfly, the MECP is reached from the singlet state by the elongation of a Si-Si bond on a free Si-dimer, along with a decrease in buckling quantified by the angle between the Si-dimer bond and its projection in the plane of the Si atoms in the layer below the dimer. The geometry at the MECP is very similar to that of the triplet. Given the small MECP barrier, and reasonable crossing probability, non-adiabatic transition state theory calculations [47], reveal the rate coefficient for the 1,2-tilted and 1,4-butterfly adsorption structures are on the order of 10^5-10^6. Thus, the spin crossing events have a minimal effect on the overall pathways.

The row-linking butterfly adsorption structure is a special case because there are two unsaturated Si-atoms on opposite sides of the cluster. Since there is no possibility to form a π-bond between the two unsaturated Si-atoms on, the singlet and triplet structures are nearly identical, with the triplet, as expected from Hund's rule, being lower in energy. This assertion is further supported by spin density calculations, which show excess spin on the bare Si-atoms in the triplet, while the alpha and beta spin densities are identical on the singlet. A SOC computation was not performed on this large cluster. However, one expects that the SOC will be similar to that of other clusters, especially if one considers a larger cluster containing additional Si-dimers. Thus, the crossing is expected to occur with little difficulty.

Table II-6. Geometric information (in Å and degrees) for the singlet, the MECP, and the triplet for both the 1,2-tilted adsorption and the 1,4-butterfly adsorption structures (AS), and the two low energy dissociation structures (DS4 and DS6). The adsorption energy of the singlet, MECP, and triplet(kJ/mol), spin-orbit coupling constant (cm^{-1}), and the crossing probability are also reported. Bond lengths are the distance between the two Si atoms on the bare dimer. The buckling angles are quantified by the angle between the Si-dimer bond and its projection in the plane of the Si atoms in the layer below the dimer.

Model	Bond Length (Å)	Buckling Angle (Deg)	Adsorption Energy (kJ/mol)	SOC (cm^{-1})	Crossing Probability
1,2-Tilted					
AS	2.24/2.38/2.41	8.16/0.10/0.05	-24.2/-0.05/-0.8	13.46	2.9×10^{-3}
DS4	2.24/2.39/2.41	9.60/0.12/0.25	-318.4/-289.6/-290.0	14.91	3.5×10^{-3}
DS6	2.26/2.40/2.43	12.27/0.83/0.46	-330.2/-303.4/-306.2	10.04	1.6×10^{-3}
1,4-Butterfly					
AS	2.27/2.37/2.43	12.05/0.77/0.71	-71.2/-50.5/-53.1	8.72	1.2×10^{-3}

Conclusions

A comprehensive survey of the possible chlorobenzene adsorption and dissociation structures reveals that out of 14 adsorption structures, the 1,2-tilted, the row-linking butterfly, and the 1,4-butterfly structures are the most promising candidates for dissociation on the Si(100) surface. There are two possible final dissociation structures (DS4 and DS6) starting from the 1,2-tilted structures. One forms from dissociation on a single-dimer row, while the other forms from dissociation across adjacent dimer rows. For both pathways, the C-Cl bond first breaks and a Si-Cl bond is formed. After this, the C_2-Si bond breaks, restoring aromaticity and forming an adsorbed phenyl group. In the lowest energy single-dimer row geometry, the chlorine atom migrates further to form a Si-Cl bond on the same dimer as the phenyl group. This structure (DS4) is stable in both the singlet and triplet states, although the singlet is lower in energy. It can further react across a dimer row, with the C_4 carbon reacting across the trench forming a new C-Si bond on the adjacent row. The lowest energy structure (DS6) can form when the C_4-H bond

breaks, over a large barrier, to form a Si-H bond on the free Si atom of the same dimer. This structure (DS6) is more stable in the singlet state and is even more stable than the first structure (DS4). The row-linking butterfly structure merges with the 1,2-tilted pathway by breaking the C-Cl bond and forming a Si-Cl bond. This structure is equivalent to the DS5 structure of the 1,2-tilted pathway. In both cases, the effect of the spin-crossing events contributes little to energy barriers between the intermediates.

The 1,4-butterfly structure can dissociate across two dimer rows. The Cl atom protrudes into the trench between two rows and reacts with Si to form a Si-Cl bond on the adjacent row. Once this occurs, the C_4-Si bond breaks to restore aromaticity to the phenyl group. This dissociated structure (DS2) has dangling bonds on each of the two partially capped Si dimers, one with the Cl and one with the phenyl group. As such, it is more stable in the triplet state. Like the 1,2-tilted and row-linking butterfly pathways, the low MECP barrier and high probability of spin-crossing between singlet and triplet states of the adsorption structure mean that the spin-crossing event does not affect the viability of this pathway. A comparison to the experimental results is made in Chapter V.

CHAPTER III

Spin-Crossing and Dissociation of 1,2- and 1,4-Dichlorobenzene on Cluster Models of the Silicon (100) Surface

This chapter continues to build upon previous work from our laboratory on the adsorption and dissociation of benzene [33] and chlorobenzene (see Chapter II) on the Si(100) surface, as well as the effects of spin-crossing on these processes. This work continues that effort by examining the mechanism of the adsorption and dissociation of 1,2- and 1,4-dichlorobenzene on the Si(100) surface and the effect of spin-crossing. Previous studies have examined the extent of dissociation of dichlorobenzene on the Si(100) surface using X-ray photoelectron spectroscopy (XPS) [30] and scanning tunneling microscopy (STM) [29].

Results from the STM study suggest that 1,2- and 1,4-dichlorobenzene are molecularly adsorbed in two configurations, the butterfly and tight-bridge structures, and dissociatively adsorbed in two configurations, the displaced and linked structures [29]. According to this study, 23% of the 1,2-dichlorbenzene structures are in the displaced structure while only 8% are in the linked structure. The relative abundance of these dissociated products is reversed for 1,4-dichlorobenzene, with 7% in the displaced structure and 52% in the linked structure. XPS studies confirm that approximately 25% of the C-Cl bonds in 1,2-dichlorobenzene undergo dissociation, while also showing that the strength of the carbon halogen (F, Cl, and Br) bond correlates to the amount of dissociation on the

Si(100) surface [30]. Both studies found that the dissociated products are thermodynamically favorable, and that the kinetics of the reaction play a prominent role in their observations. Naumkin, Polanyi, and Rogers attempt to explain these results computationally, and suggest that the dissociated structures seen in the STM images can be formed starting with the butterfly structure. According to their study, this structure could then translate across the dimer rows, while simultaneously transitioning from the singlet to the triplet spin state, forming what they call the diene-L structure which has dichlorobenzene ring molecularly adsorbed across the dimer rows [36]. Alternative mechanisms are proposed, beginning with various adstructures, that could lead to the same thermodynamically favorable products. Stable structures and the transition states connecting them are calculated using DFT, and the probability of spin-crossing is determined at the appropriate structures.

Computational Details

The computational methods follow those used by Zhu and Materer [33], and are briefly explained here. Using the Gaussian 09 software package [81], the geometry of all stable structures on the cluster model of Si(100) was optimized. Partial optimizations of the dissociation pathway structures, in which the bottom two layers of Si are constrained to their ideal atomic positions, are currently underway. Adsorption energies are reported in reference to the bare cluster and the chlorobenzene in the singlet electronic state. No zero point corrections are applied. Frequency calculations were performed to ensure stable structures had no imaginary frequencies, while transition states only had one imaginary frequency. Internal reaction coordinate (IRC) calculations were performed to ensure that the transition states connected to the expected stable structures. However, IRC calculations for transition states that require the large trench cluster were unobtainable, due to computational limitations. All calculations used the B3LYP hybrid functional,

which consists of Becke's three parameter exchange functional [82] along with the Lee-Yang-Parr correlation functional [83]. The 6-31G(d) split valence basis set with the polarization d-function [84] on all atoms except hydrogen was utilized.

Minimum energy crossing point (MECP) geometries were calculated using a program developed by Harvey *et al*. [85], based on an algorithm developed by Bearpark *et al*. [86]. Once obtained, the spin-orbit coupling (SOC) coefficients were calculated at the MECP geometry using a methodology similar to a previous publication [80]. The Breit-Pauli spin-orbit Hamiltonian, including both one and two electron terms, was used in GAMESS(US) software package [87] to compute the SOC coefficient. These computations utilize the same Gaussian-type basis set as the one used in Gaussian 09. The SOC computation procedure starts with a full second order CI calculation at the MECP geometry. Once the optimized molecular orbital coefficients are determined, they are utilized to compute the spin-orbit coupling coefficient using a complete active space self-consistent field computation with an active space consisting of seven valance and seven virtual orbitals.

The Landau-Zener formula [88-90] determines the probability of a non-adiabatic crossing (Equation 1). To calculate the probability of the spin crossing event at the MECP geometry, the double pass formula described by Harvey [47], the difference being $8\pi^2$ in the exponential for a double pass versus $4\pi^2$ for the single pass formalism, was utilized (Equation 1).

$$P_{sh}(E) = 1 - \exp\left(\frac{-8\pi^2 H_{soc}^2}{h\Delta F}\left[\frac{\mu}{2E}\right]^{1/2}\right) \quad \text{(E1)}$$

In Equation 1, H_{soc} is the spin-orbit coupling coefficient, h is Planck's constant, ΔF is the Frobenius norm of the energy gradient difference, μ is the reduced mass of the system along the

crossing coordinate, and E is the kinetic energy of the system. Similar to a previous publication [80], this study used the reduced mass along the crossing coordinate obtained by frequency analysis of MECP structure. Due to the complex nature of the larger trench clusters, an averaged reduced mass from all contributing normal modes of the double-dimer structures was used for all probability calculations. Similarly, and averaged kinetic energy of those normal modes was used to determine the kinetic energy of the system. Once obtained, the crossing probability can be used to determine the rate coefficient of the spin-crossing by utilizing non-adiabatic transition state theory [47]:

$$k(T) = P_{sh}\left[\frac{k_B T}{h}\exp\left(\frac{-\Delta G}{RT}\right)\right] \qquad \text{(E2)}$$

In Equation 2, k_B is Boltzmann's constant, T is temperature, ΔG is the change in Gibb's free energy, and R is the ideal gas constant.

Results and Discussion

As in the previous study with chlorobenzene (Chapter II), this study uses a variety of different clusters including the single-dimer (Si_9H_{12}), double-dimer ($Si_{15}H_{16}$), triple-dimer ($Si_{21}H_{20}$), and the trench-dimer clusters ($Si_{53}H_{44}$). In addition, two larger dimer clusters were needed. These are the quad-dimer ($Si_{27}H_{24}$) and the triple-row trench-dimer clusters ($Si_{77}H_{60}$), which consists of three fused double-dimer clusters, one more than that of the trench-dimer cluster. Both the triple-row trench-dimer and the trench-dimer clusters have an additional row of silicon atoms on the bottom to mitigate any buckling caused by linking the two rows via adsorption of the dichlorobenzene. All dimer clusters are hydrogen truncated to satisfy the Si atoms on the bottom of the clusters and the surface dimers are left bare.

Adsorption Structures

A comprehensive study of various adsorption structures was conducted based on the structures discussed in Chapter II. These structures include the di-σ adsorption structures: tilted, butterfly, tilted-bridge butterfly, and row-linking butterfly. The diagonal-bridge butterfly was found to be unstable for chlorobenzene and is thus it is not studied. In addition to the di-σ structures, two tetra-σ structures were studied: the tight-bridge and twisted-bridge adsorption structures. The tetra-σ pedestal structure was found to be unstable for both chlorobenzene and benzene [41] due to the formation of a bi-radical carbon ring; thus, the pedestal structure is not included in this study. From these base adsorption structures, many attachments are possible and will be discussed below for both 1,2- and 1,4-dichlorobenzene. In order for dissociation to be feasible, three criteria must be met. At least one Cl atom must be adjacent to a C-Si bond in order to avoid the formation of a radical carbon ring, the Cl atom must be within reasonable proximity to a bare Si atom, and the barrier to dissociation must be lower than the barrier to desorption. In this section, the first two criteria are addressed while the final criteria is discussed in the "Dissociation Structures" section. All reported structures are modeled on the smallest possible clusters that will allow adsorption and dissociation. All structures are fully optimized except when noted, and transition states have a single imaginary frequency. Additionally, IRC calculations were performed where possible to ensure the transition structures connected the desired stable structures. The adsorption energy for the 1,2-dichlorobenzene adsorption structures and first transition state are tabulated in Table III-1, while those values for 1,4-dichlorobenzene are tabulated in Table III-2.

Table III-1. Adsorption energies of 1,2-dichlorobenzene on the Si(100) surface in kJ/mol for the adsorption structures (AS) and the transition structure (TS1) from the gas phase (except as noted), all with singlet multiplicity. Adsorption and transition state energies are referenced to the isolated singlet chlorobenzene and singlet Si(100) cluster. All coordinates are fully optimized except when noted in the text. The transition states have one imaginary frequency, and IRC was performed to confirm that the transition structures connected the stable structures on single, double, and triple-dimer clusters.

1,2-Dichlorbenzene							
Di-σ	Cluster	TS1	AS	Tetra-σ	Cluster	TS1	AS
Tilted				*Tight-Bridge*			
1,2	Single	109.7	-8.1	1,2,3,4	Double		-49.4
	Double	102.8	-0.7	1,2,3,6	Double		-34.6
2,3	Single	91.5	-34.2	2,3,4,5	Double		-57.2
	Double	84.6	-34.6	3,4,5,6	Double		-72.8
3,4	Single	68.5	-30.8	*Twisted-Bridge*			
4,5	Single	65.3	-18.7	1,2,3,4	Double		-27.6
Butterfly				1,2,3,6	Double		-12.2
1,4	Single	28.6	-76.8	2,3,4,5	Double		-45.9
	Trench	41.2	-71.9	3,4,5,6	Double		-61.0
3,6	Single	17.3	-94.8				
Tilted-Bridge Butterfly							
1,4-Same	Double	65.8	-23.0				
	Triple	77.2	-5.8				
1,4-Adjacent	Double	69.3	-17.8				
	Triple	74.8	-15.2				
3,6-same	Double	46.8	-26.7				
Row-Linking Butterfly							
1,4	Trench	72.3	-7.0				

Tilted Structures: 1,2-Dichlorobenzene

There are four possible tilted adsorption structures for 1,2-dichlorobenzene, depending on the attachment of the ring to the Si dimer. To define these structures, the carbon atoms are numbered around the ring, with C_1 and C_2 being the Cl bonded carbon atoms on 1,2-dichlorobenzene. The carbon atoms that bond to the Si dimer surface identify the structures. The first possible tilted adsorption structure discussed is the 1,2-tilted structure (Figure III-1A) which has each Cl bonded carbon atom, C_1 and C_2, bonded to each Si atom in a single Si dimer. This reaction would be symmetry forbidden in typical alkene chemistry, however, due to the buckled nature of the Si

dimer surface, this reaction can proceed via an asymmetric pathway. The transitions state for this adsorption pathway is depicted in Figure III-1B. This transition state creates an energy barrier to the formation of the 1,2-tilted structure of 109.7 kJ/mol. Once this barrier is overcome, the 1,2-tilted structure is formed and has an adsorption energy of -8.1 kJ/mol on a single-dimer cluster. On a double-dimer cluster, this barrier is decreased to 102.8 kJ/mol and the adsorption energy is increased to -0.7 kJ/mol. Using the double-dimer cluster, it was determined that the Cl atom is 3.72 Å away from the nearest bare Si atom on the adjacent dimer, while the other Cl atom is 4.59 Å away. Another tilted structure is the 2,3-tilted structure, shown in Figure III-2A, which has an adsorption energy of -34.2 kJ/mol on the single dimer cluster with a barrier to adsorption of 91.5 kJ/mol. This structure has one Cl atom pointed away from the dimer row and one Cl atom above the dimer row on the double-dimer cluster; this structure has an adsorption energy of -34.6 kJ/mol with a barrier of 84.6 kJ/mol, similar to their single-dimer counterparts. Only the Cl atom over the row is adjacent to a C-Si bond and this Cl atom is 4.20 Å from an Si atom on the adjacent dimer. The final two tilted structures are the 3,4- and 4,5-tilted adsorptions structures with energy barriers of 68.5 kJ/mol and 65.3 kJ/mol and adsorption energies of -30.8 and -18.7 kJ/mol, respectively. The 3,4-tilted structure is shown in Figure III-2B. Neither of these structures have Cl atoms adjacent to a C-Si bond and will not be studied further.

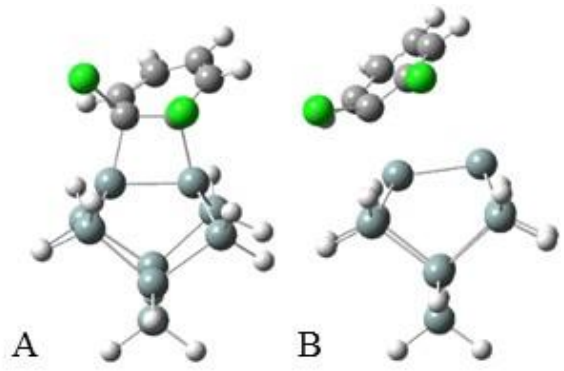

Figure III-1. Di-σ 1,2-dichlorobenzene adsorption structure and transition state: (A) 1,2-tilted adsorption structure on a single-dimer cluster and (B) asymmetric transition state into the adsorption structure.

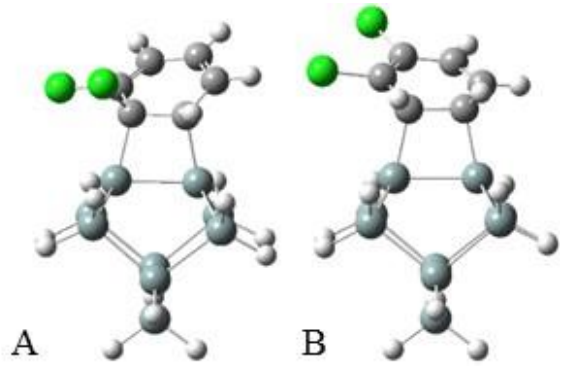

Figure III-2. Additional di-σ 1,2-dichlorobenzene adsorption structures: (A) The 2,3-tilted and (B) 3,4-tilted on a single-dimer cluster.

Table III-2. Adsorption energies of 1,4-dichlorobenzene on the Si(100) surface in kJ/mol for the adsorption structures (AS) and the transition structure (TS1) from the gas phase (except as noted), all with singlet multiplicity. Adsorption and transition state energies are referenced to the isolated singlet chlorobenzene and singlet Si(100) cluster. All coordinates are fully optimized except when noted in the text. The transition states have one imaginary frequency, and IRC was performed to confirm that the transition structures connected the stable structures on single, double, and triple-dimer clusters.

1,4-Dichlorobenzene							
Di-σ	Cluster	TS1	AS	Tetra-σ	Cluster	TS1	AS
Tilted				*Tight-Bridge*			
1,2	Single	76.6	-39.7	1,2,3,4	Double		-67.3
	Double	71.4	-35.8	1,2,3,6	Double		-71.5
2,3	Single	62.2	-46.6	*Twisted-Bridge*			
Butterfly				1,2,3,4	Double		-51.4
1,4	Single	35.2	-80.3	1,2,3,6	Double		-59.9
	Trench	27.2	-85.7				
2,5	Single	9.4	-102.1				
Tilted-Bridge Butterfly							
1,4	Quad	88.4	-17.2				
2,5	Double	36.1	-42.1				

Tilted Structures: 1,4-Dichlorobenzene

There are only two unique tilted structures formed from 1,4-dichlorobenzene: the 1,2-tilted and the 2,3-tilted structures shown in Figure III-3A and III-3B, respectively. The 1,2-tilted structure is formed over an energy barrier of 76.6 kJ/mol and has an adsorption energy of -39.7 kJ/mol on the single-dimer cluster. In order to determine the proximity of the Cl atom to the nearest bare Si atom, this adsorption structure was also modeled on the double-dimer cluster. On the double-dimer cluster this structure has an energy barrier of 71.4 kJ/mol and an adsorption energy of -35.8 kJ/mol. The Cl atom that is bonded to C_1 is 4.39 Å from the nearest Si atom on the adjacent dimer. The 2,3-tilted structure has a barrier to adsorption of 62.2 kJ/mol and an adsorption energy of -46.6 kJ/mol, making it slightly more stable than the 1,2-tilted structure. However, this structure does not have C-Si bond adjacent to either of the Cl atoms and will not be considered further.

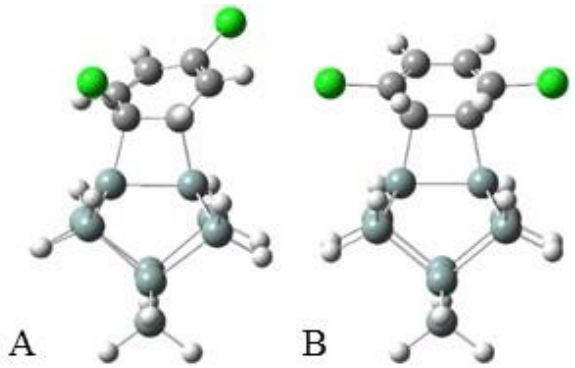

Figure III-3. Di-σ 1,4-dichlorobenzene adsorption structures: (A) The 1,2-tilted and (B) 2,3-tilted on a single-dimer cluster.

Butterfly Structures: 1,2-Dichlorobenzene

There are four types of di-σ butterfly structures: the butterfly, tilted-bridge butterfly, row-linking butterfly and the diagonal bridge butterfly. In this section, the possible butterfly, tilted-bridge butterfly, and row-linking butterfly structures of 1,2-dichlorbenzene are discussed, beginning with the butterfly. These structures are formed in a Diels-Alder like reaction, resulting in energy barriers that are much lower than the barriers for the tilted adsorption structures. There are two possible butterfly structures formed, the first of which is the 1,4-butterfly structure shown in Figure III-4A. This structure is formed from the bonding of C_1 and C_4 to the two Si atoms of a single dimer. The barrier to this structure is 28.6 kJ/mol on the single-dimer cluster and has an adsorption energy of -76.8 kJ/mol. In this structure, one of the Cl atoms is above the dimer row, while the other is above the trench, pointing toward the adjacent row, and is adjacent to the C_1-Si bond. Thus, the focus is only on the possible dissociation of the Cl atom over the trench. Since the Cl atom of interests points toward the adjacent row, the trench-dimer cluster is required to determine the proximity to the nearest bare Si atom. On the trench cluster, the energy barrier to adsorption is increased to 41.2 kJ/mol while the adsorption energy of the structure is decreased to -63.2 kJ/mol. The distance between this Cl atom and the nearest Si atom on the adjacent dimer

row is 3.87 Å on this cluster. The other possible adsorption structure is the 3,6-butterfly structure (Figure III-4B), in which each of the Cl atoms is over the dimer row. The energy barrier to the formation of this structure is 17.3 kJ/mol and the adsorption energy of the stable structure is -94.8 kJ/mol. There are no C-Si bonds adjacent to either of the Cl atoms, and this structure is not studied further.

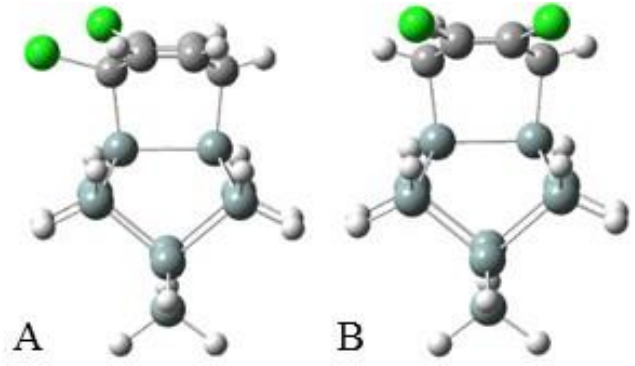

Figure III-4. Additional di-σ 1,2-dichlorobenzene adsorption structures: (A) The 1,4-butterfly and (B) 3,4-butterfly on a single-dimer cluster.

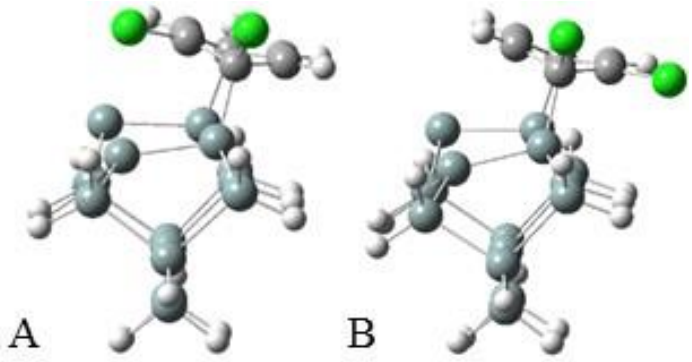

Figure III-5. Additional di-σ 1,2-dichlorobenzene adsorption structures: (A) The 1,4-same tilted-bridge butterfly and (B) 1,4-adjacent tilted-bridge butterfly on a double-dimer cluster.

In addition to the butterfly structures, there are four possible tilted-bridge butterfly structures formed from 1,2-dichlorobenzene. The tilted-bridge butterfly structures are created by the formation of C-Si bonds on two adjacent dimers of the same dimer row. This structure has one unsaturated Si atom on each dimer, resulting in higher adsorption energies compared to the butterfly structures. This is due to the ability of the butterfly structures to form a partial π-bond between the bare Si atoms on the same dimer, lowering the energy in the singlet state. The first two tilted-bridge butterfly structures are the 1,4-same tilted-bridge butterfly shown in Figure III-5A and the 1,4-adjacent tilted-bridge butterfly shown in Figure III-5B where "same" and "adjacent" identify which dimer row the Cl atom would attach to if dissociation were to occur. These structures can be visualized as a 90° rotation of the 1,4-butterfly structures. As shown in Figure III-5, both structures have a Cl atom adjacent to the C_1-Si bond. However, in the 1,4-same structure, the additional Cl atom is over the dimer row, while the Cl atom is over the trench between the two dimer rows in the 1,4-adjacent structure. The energy barrier for the formation of the 1,4-same structure on the double-dimer cluster is 65.8 kJ/mol, while a similar barrier, 69.3 kJ/mol, is found for the 1,4-adjacent structure. Adsorption energies of these structures are also similar at values of -23.0 kJ/mol and -17.8 kJ/mol for the 1,4-same and the 1,4-adjacent structures, respectively. In each case, the only interest is in the Cl atom bonded to the C_1 atom, which is bonded to an Si atom of the dimer, and the triple-dimer cluster is used to determine the proximity of the Cl atom to the nearest Si atom in a bare dimer. Both cases are similar, with a distance of 4.10 Å for the 1,4-same structure and 4.17 Å for the 1,4-adjacent structure. The energy barrier to form the 1,4-same structure of 77.2 kJ/mol and the adsorption energy of -5.8 kJ/mol on the triple-dimer cluster are both increased from the smaller cluster. The 1,4-adjacent structure has a similar increase in the energy barrier (74.8 kJ/mol), but the increase in adsorption energy (-15.2 kJ/mol) is less significant with a change of only 2.6 kJ/mol compared to a change of 17.2 kJ/mol. This difference in adsorption energy is likely due to the strain caused by the

interaction of the Cl atom with the dimer surface, which would be larger for the 1,4-same structure. The other two structures are the 3,6-same and 3,6-adjacent tilted-bridge butterfly structures, which can be visualized as 90° rotations of the 3,6-butterfly structure. The energy barrier for 3,6-same tilted-bridge butterfly is 46.8 kJ/mol and the adsorption energy of the stable structure is -26.7 kJ/mol on the double-dimer cluster. Since there is no Cl atom adjacent to either of the C-Si bonds, this structure is not discussed further. No stable structure was found for 3,6-adjacent tilted-bridge butterfly.

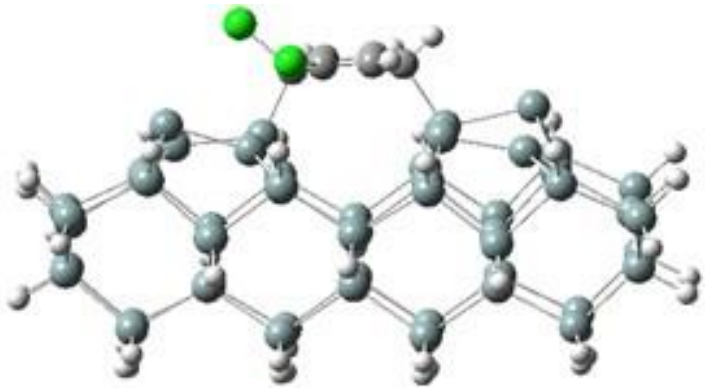

Figure III-6. Row-linking butterfly 1,2-dichlorobenzene di-σ adsorption structure on the trench cluster.

The final type of butterfly structure is the row-linking butterfly structure. This structure is created by the formation of C-Si bonds on adjacent dimers of two different dimer rows. Thus, the smallest cluster used is the trench dimer cluster. There are two possible row-linking butterfly structures formed from 1,2-dichlorobenzene, the 1,4-row-linking butterfly (Figure III-6) and the 3,6-row-linking butterfly. Like the 3,6-butterfly and the 3,6-tilted-bridge butterfly structures, the 3,6-row-linking butterfly structure will not be considered as a viable pathway for dissociation since no Cl atoms are adjacent to either of the C-Si bonds. However, the 1,4-row-linking

butterfly is considered as a possible viable dissociation pathway and has a 72.3 kJ/mol barrier to the formation of the structure and an adsorption energy of -7.0 kJ/mol. The Cl atom adjacent to the C_1-Si bond is close in proximity to the unsaturated Si atom of the same dimer, with a distance of 3.76 Å.

Butterfly Structures: 1,4-Dichlorobenzene

The reaction of 1,4-dichlorobenzene with the Si(100) surface forms two unique butterfly structures. The first is the 1,4-butterfly structure shown in Figure III-7A, which has an adsorption energy of -80.3 kJ/mol on the single dimer cluster and is formed over an energy barrier of 35.2 kJ/mol. In this structure, each of the Cl atoms is adjacent to a C-Si bond, and each sits above the trench on opposite sides of the row. Since dissociation is possible for both Cl atoms, the larger triple-row trench-dimer cluster was utilized in order to determine the distance of the Cl atom to bare Si atoms on the rows on either side of the adsorbed dichlorobenzene ring. On this larger cluster, the energy barrier is slightly decreased to 27.2 kJ/mol while the adsorption energy is slightly increased to -75.7 kJ/mol. The distance for each Cl atom to the nearest Si atom on an adjacent row is 3.95 Å for one and 4.31 Å for the other. This difference is due to the buckling angle of the bare Si dimers. The first Cl atom is near a buckled up Si atom resulting in a smaller distance than that of the Cl atom near the buckled down Si atom. The second structure is the 2,5-butterfly structure shown in Figure III-7B. Formation of the 2,5-butterfly structure occurs over a small energy barrier of 9.4 kJ/mol and forms a more stable structure, when compared with the 1,4-butterfly structure, with an adsorption energy of -102.l kJ/mol on the single dimer cluster. However, this structure is not considered further, since there is no Cl atom adjacent to a C-Si bond.

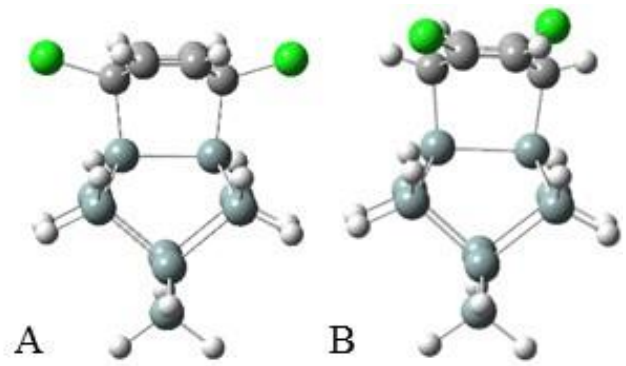

Figure III-7. Additional di-σ 1,4-dichlorobenzene adsorption structures: (A) The 1,4-butterfly and (B) 3,6-butterfly on a single-dimer cluster.

In addition to the butterfly structures, 1,4-dichlorobenzene can form two unique tilted-bridge butterfly structures. As noted in the case of 1,2-dichlorobenzene, these structures have larger energy barriers and form less stable adsorption structures compared to the butterfly structures due to the location of the unsaturated Si atoms. The 1,4-tilted-bridge butterfly structure shown in Figure III-8A is structurally equivalent to a 90° rotation of the 1,4-butterfly structure. Similar to the 1,4-butterfly structure, in the 1,4-tilted-bridge butterfly both Cl atoms are adjacent to C-Si bonds. In order to determine the distance of each of the Cl atoms from their nearest Si atoms, the quad-dimer cluster was utilized. To form this structure, an energy barrier of 88.4 kJ/mol must be overcome forming the adsorption structure with an energy of -17.2 kJ/mol on the quad-dimer cluster. No adsorption structure was found on the smaller double-dimer cluster. The Cl-Si distances are 4.09 Å and 4.25 Å between each Cl atom and the bare Si dimers on the adjacent dimers in the row. Like the 1,4-butterfly structure, this difference is due to the buckling of the dimers. The 2,5-tilted-bridge butterfly structure shown in Figure III-8B is equivalent to a 90° rotation of the 2,5-butterfly and has C-Si bonds to C_2 and C_5. The barrier to the formation of this structure is much lower (36.1 kJ/mol) than the barrier for the 1,4-tilted-bridge butterfly, and the adsorption structure is much more stable (-42.1 kJ/mol). This result is due to the increased strain

in the dichlorobenzene ring in 1,4-dichlorobenzene due to the proximity of the Cl atom to the dimer row. Since the Cl atoms in the 2,5-tilted-bridge butterfly structure are above the row and above the trench, this interaction is diminished, resulting in a more stable adsorption structure. However, since there are no Cl atoms adjacent to the C-Si bonds, this structure is not considered a viable candidate for dissociation.

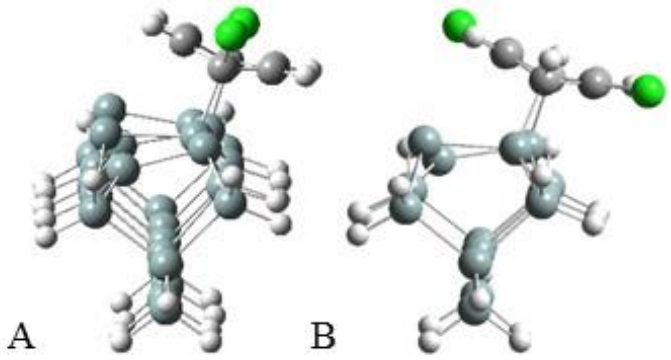

Figure III-8. Additional di-σ 1,4-dichlorobenzene adsorption structures: (A) The 1,4-tilted-bridge butterfly on the quad-dimer cluster and (B) 2,5-tilted-bridge butterfly on a double-dimer cluster.

While 1,2-dichlorobenzene yields a stable row-linking butterfly structure, geometry optimizations yield a highly unstable structure (24.9 kJ/mol) for the case of 1,4-dichlorobenzene. While the triplet state is quite stable for this structure (-58.8 kJ/mol), no transition state leading to this structure could be found in either the singlet or triplet electronic state. Thus this structure is not a viable candidate for adsorption and dissociation on the Si(100) surface.

Bridge Structures: 1,2- and 1,4-Dichlorobenzene

The final set of structures considered are the bridge structures. These are tetra-σ bonded structures which form bonds to four Si atoms in two adjacent dimers on the same row. These structures include the tight-bridge, twisted-bridge, and the pedestal structures. As previously stated, the pedestal structure is not stable for either benzene [41] or chlorobenzene (Chapter II), thus this structure is not studied. The tight-bridge structures have four consecutive C-Si bonds to the dimers on the surface leaving a single C-C double bond in the ring. This unattached portion of the ring is above the dimer row for tight-bridge structures. The twisted-bridge structures also have four consecutive carbon atoms bonded to the Si dimers, however, the remaining double bonded carbon atoms are above the trench. Previous work shows that two of the twisted bridge structures can be formed from the tilted-bridge butterfly structure on smaller clusters. Although stable bridge adsorption structures were located (See Tables III-1 and III-2 for adsorption energies), no transition states could be found for either the 1,2- or 1,4-dichlorobenzene bridge structures in either the singlet or triplet state. Because these transition states were not located, these structures are not considered further.

Dissociation Structures

In this section, the first dissociation structure of each of the adsorption structures that satisfied the criteria in the previous section are examined. These include the 1,2- and 2,3-tilted, 1,4-butterfly, 1,4-same and 1,4-adjacent tilted-bridge butterfly, and the row-linking butterfly for 1,2-dichlorobenzene, and the 1,2-tilted and 1,4 butterfly for 1,4-dichlorobenzene. This first dissociation structure is formed from the breaking of a C-Cl bond and the forming of a Cl-Si bond to the nearest bare Si atom. All potential first dissociation structures were found to be unstable in the singlet state and require a spin-crossing event. The probability of transitioning between the

singlet and triplet states will be discussed in the "Spin-Crossing" section. Unless otherwise indicated, all adsorption energies of the dissociated structures are reported in the triplet state. The final criterion for dissociation is that the barrier to dissociation is lower than the barrier to desorption; the desorption and dissociation barriers will be compared in this section. The adsorption energies and transition state energies for possible first dissociation structures can be found in Table III-3. All reported energies are referenced to the isolated singlet dichlorobenzene and singlet Si cluster. For these structures, all coordinates are fully optimized unless otherwise noted. The transition states have one imaginary frequency, and IRC was performed to confirm that the transition structures connected the stable structures wherever possible.

Table III-3. Adsorption energies for the adsorption structure (AS), the transition (TS1) into this structure from the gas phase, the first dissociation structure (DS1) and the transition (TS2) from triplet AS to triplet DS1 on the Si(100) surface are reported in kJ/mol. The AS is reported for both the singlet and triplet, while TS1 is only reported in the singlet, and TS2 and DS1 are only reported in the triplet state. Adsorption and transition state energies are referenced to the isolated singlet dichlorobenzene and singlet cluster.

Model	Cluster	TS1	Singlet AS	Triplet AS	TS2	DS1
1,2-Dichlorobenzene						
Tilted						
1,2	Double	102.8	-0.7	23.9	-	-
2,3	Double	84.6	-34.6	-6.7	25.7	-180.0
Butterfly						
1,4	Trench	41.2	-71.9	-45.7	5.8	-121.5
Tilted-Bridge Butterfly						
1,4-Same	Triple	77.2	-5.8	-55	-	-
1,4-Adjacent	Triple	74.8	-15.2	-60.8	37.9	-152.5
Row-Linking Butterfly						
1,4	Trench	72.3	-7.0	-72.4	3.9	-228.7
1,4-Dichlorobenzene						
Tilted						
1,2	Double	71.4	-35.8	-12.4	24.3	-177.6
Butterfly						
1,4	Quad	27.2	-85.7	-61.0	0.9	-126.7

Tilted Based Dissociation Structures

For the dissociation of both 1,2-dichlorobenzene tilted structures, a double-dimer structure is required. The structure formed from the dissociation of a single Cl atom (DS1) could not be found, in either the singlet or triplet state, on any cluster size. However, a dissociation structure (DS2, Figure III-9A) formed from the dissociation of both Cl atoms onto the adjacent dimer is found in the singlet state (-548.2 kJ/mol) on the double-dimer cluster. This structure is also found in the singlet and triplet states on the triple-dimer structure attached to the end dimer (-541.5 kJ/mol for the singlet and -515.0 kJ/mol for the triplet) and attached to the middle dimer (-537.4 kJ/mol for the singlet and -513.3 kJ/mol for the triplet). Due to the absence of a bare dimer for the 1,2-tilted structure on the double-dimer cluster, a double bond in the carbon ring must be broken in the triplet state, which is why no stable triplet structure could be found on the double-dimer cluster. In the first dissociation structure of the 2,3-tilted adsorption structure pathway, shown in Figure III-9B, the chlorine atom is bonded to one of the Si atoms in the adjacent dimer on the same row and has an adsorption energy of -180 kJ/mol on the double-dimer cluster. The barrier to dissociation is 32.4 kJ/mol, which is much lower than the barrier to desorption (119.2 kJ/mol), thus this pathway is discussed in the pathway section. The only tilted pathway for 1,4-dichlorobenzene that meets the first two criterion begins with the 1,2-tilted structure. This dissociation structure (Figure III-9C) is formed from the bonding of Cl to an Si atom in the adjacent dimer of the same row. This structure has an adsorption energy of -177.6 kJ/mol on the double-dimer cluster and the barrier to the formation of this dissociation structure is 36.7 kJ/mol. This is much lower than the barrier to desorption (137.2 kJ/mol) thus it is expected to dissociate.

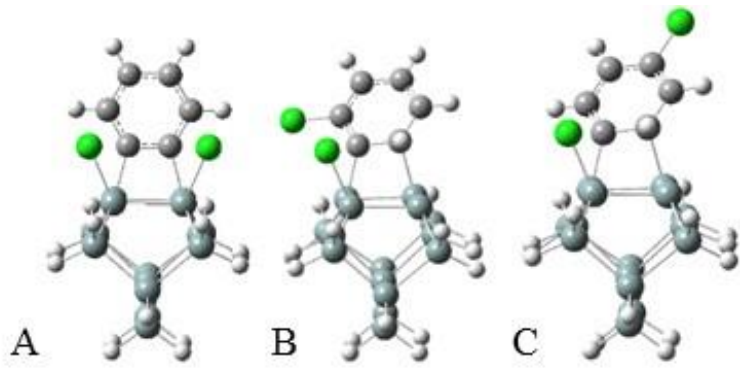

Figure III-9. The (A) second dissociation (DS2) structure of the 1,2-tilted pathway and the first dissociation structures formed from the (B) 2,3-tilted structure of 1,2-dichlorobenzene and (C) 1,2-tilted structure of 1,4-dichlorobenzene.

Butterfly Based Dissociation Structures

The pathways beginning with the 1,4-butterfly structure meet the first two criteria for both 1,2- and 1,4-dichlorobenzene. For 1,2-dichlorobenzene, the first dissociation structure, depicting in Figure III-10, is formed from the attachment of the Cl atom to the nearest Si atom across the dimer row. This structure is modeled on the trench-dimer cluster and has an adsorption energy of -121.5 kJ/mol. The barrier to the formation of this structure is 51.5 kJ/mol, which is lower than the barrier to desorption at 104.4 kJ/mol. A similar result is found for the 1,4-butterfly structure formed from 1,4-dichlorobenzene. This dissociation structure is modeled on the triple-row trench-dimer cluster and is formed by the bonding of one of the Cl atoms to the nearest Si atom in a row adjacent to the adsorbed carbon ring. This structure is shown in Figure III-11. The adsorption energy of this structure is -126.7 kJ/mol and the barrier to form this structure is lower than the desorption barrier (102.9 kJ/mol) with a value of 61.9 kJ/mol. Both of these pathways satisfy all criteria and will be considered in detail in the pathway section.

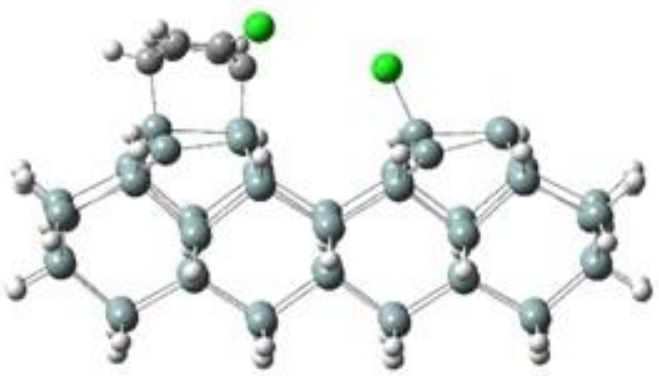

Figure III-10. The first dissociation structure (DS1) formed from the 1,4-butterfly structure of 1,2-dichlorobenzene.

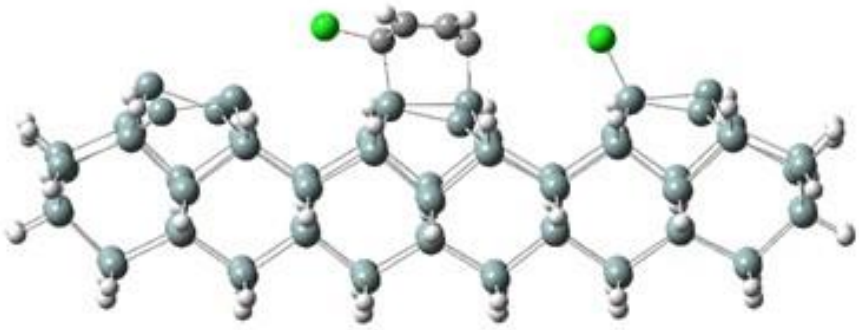

Figure III-11. The first dissociation structure (DS1) formed from the 1,4-butterfly structure of 1,4-dichlorobenzene.

There are two possible pathways beginning with tilted-bridge butterfly structures for 1,2-dichlorobenzene. These are the 1,4-same and 1,4-adjacent tilted-bridge butterfly structures. Both have similar dissociation structures formed from the breaking of the C_1-Cl bond and the formation of a Cl-Si bond on the adjacent dimer in the same row. The 1,4-same tilted-bridge structure does not have a stable dissociation structure in either the triplet or singlet state. However, the 1,4-adjacent tilted-bridge butterfly structure does have a stable dissociation structure with an adsorption energy of -152.5 kJ/mol and a 98.7 kJ/mol barrier to the formation of

this structure. This barrier is slightly higher than the barrier for desorption (90.0 kJ/mol) and is not expected to dissociate. While the 1,4-tilted bridge butterfly structure formed from 1,4-dichlorobenzene meets the first two criteria, no transition state leading to the first dissociation structure could be found. Thus the tilted-bridge butterfly pathways are not considered further.

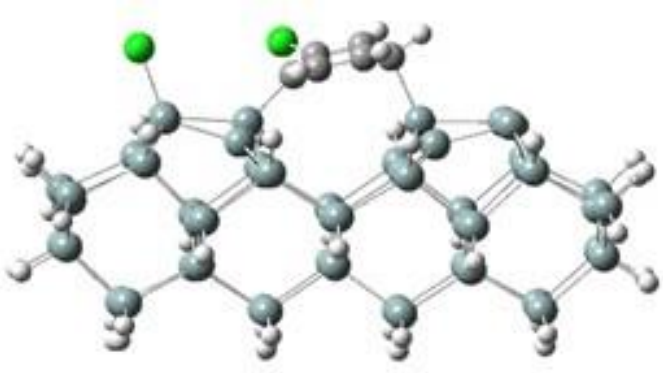

Figure III-12. The first dissociation structure of the row-linking butterfly structure of 1,2-dichlorobenzene. This structure is equivalent to the fifth dissociation structure of the 2,3-tilted pathway of 1,2-dichlorobenzene.

The final possible dissociation pathway begins with the 1,4-row-linking butterfly formed from 1,2-dichlorobenzene. This dissociated structure, shown in Figure III-12, is formed when the Cl atom bonds to the unsaturated Si atom on the same dimer as the C_1-Si bond. This structure has an adsorption energy of -228.7 kJ/mol, with a barrier of 76.3 kJ/mol. The 1,4-row-linking butterfly structure is expected to dissociate, as the barrier to desorption is slightly higher than the barrier to dissociate with a value of 79.3 kJ/mol. This pathway merges with the 2,3-tilted pathway and these pathways will be considered together in the next section.

Table III-4. Adsorption energy in kJ/mol for stable structures and transition states along the 2,3-tilted, 1,4-butterfly and the row-linking butterfly dissociation pathways for 1,2-dichlorobenzene and the 1,2-tilted and 1,4-butterfly pathways for 1,4-dichlorobenzene. All transition states are in the triplet state except TS1 which is in the singlet state. All stable structures are in the triplet state, except as noted. A double-dimer cluster is utilized for the 1,2-tilted and 2,3-tilted pathways wherever possible. All structures following DS4 are computed on the trench cluster. The 1,4-butterfly structures are calculated on the trench-dimer cluster for 1,2-dichlorobenzene and the triple-row trench-dimer for 1,4-dichlorbenzene. Please note that the row-linking butterfly merges with the 2,3-tilted pathway at DS5, and can subsequently form either DS4 or DS6.

1,2-Dichlorobenzene								
TS1	AS (singlet)	AS (triplet)	TS2	DS1	TS3	DS2	TS4	DS3
2,3-Tilted								
84.6	-34.6	-6.7	25.7	-180.0	-172.5	-305.1	-140.4	-307.8
1,4-Butterfly								
41.2	-63.2	-45.7	5.8	-121.5	-98.3	-288.2		
Row-Linking Butterfly								
72.3	-7.0	-72.4	3.9					
TS5	DS4 (triplet)	DS4 (singlet)	TS6	DS5	TS7	DS6 (triplet)	DS6 (singlet)	
2,3-tilted								
-116.8	-297.5	-325.8	-218.2	-228.7	-42.1	-304.2	-330.1	
1,4-Dichlorobenzene								
TS1	AS (singlet)	AS (triplet)	TS2	DS1	TS3	DS2	TS4	DS3
1,2-Tilted								
71.4	-35.8	-12.4	24.3	-177.6	-173.3	-306.6	-143.8	-309.6
1,4-Butterfly								
27.23	-75.71	-60.97	0.95	-126.73	-51.47	-310.47	31.42	-215.87
TS5	DS4 (triplet)	DS4 (singlet)	TS6	DS5	TS7	DS6 (triplet)	DS6 (singlet)	
1,2-tilted								
-120.1	-303.2	-331.3	-213.9	-226.1	-141.2	-454.0	-478.8	

Tilted and Row-Linking Butterfly Pathways

1,2-Dichlorobenzene: 1,2-Tilted, 2,3-Tilted, and 1,4-Row-Linking Butterfly

The adsorption energy for each of the structures discussed in this section can be found in Table III-4. The 1,2-tilted adsorption structure is unstable at 23.9 kJ/mol on the double-dimer cluster. Thus, any pathway proceeding from this initial geometry would occur only in the singlet state.

As mentioned in the previous section, no stable DS1 structure or the transition state leading to this structure could be found for the 1,2-tilted pathway. This may be due to an incredibly small barrier between DS1 and DS2, making it difficult to find a stable structure for DS1. This assertion is supported by the fact that all attempts to optimize the DS1 structure lead to the DS2 structure instead. It is unclear whether the DS2 structure is formed via a stepwise or concerted dissociation of the Cl atoms. Another pathway could occur when, after the dissociation of the first Cl atom, the C-Si bond breaks. However, if the assertion that the barrier to form the DS2 structure is small were correct, this pathway would be unlikely. Thus the very stable DS2 structure (-548.2 kJ/mol) would be formed exclusively.

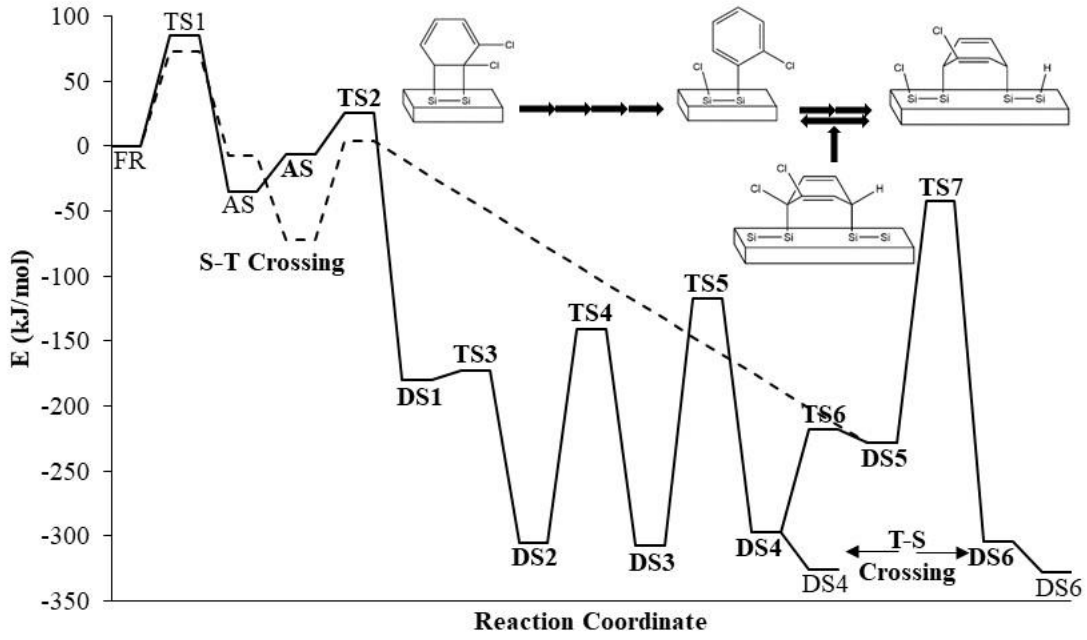

Figure III-13. This energy diagram depicts the 2,3-tilted dissociation pathway (solid) and the row-linking butterfly dissociation pathway (dotted) of 1,2-dichlorobenzene. Bold labels indicate that the structure is optimized in the triplet state. For clarity, free reactants are labeled FR; the 2,3-tilted adsorption structure is labeled AS; transition states are labeled TS, and the dissociated structures are labeled DS. Singlet-triplet (S-T) and triplet-singlet (T-S) crossing points are also labeled. The inlay shows the adsorption structures and the two main dissociation structures DS4 and DS6, and the arrows each represent a transition into a new structure.

The 2,3-tilted structure is formed over a barrier of 84.6 kJ/mol (TS1) on the double-dimer cluster, and, in order for dissociation to occur, it must then undergo a spin-crossing event, the probability of which will be discussed in the "Spin-Crossing" section, to the triplet state (-6.7 kJ/mol). This pathway, as well as the row-linking butterfly pathway, are summarized in Figure III-13. Once in the triplet state, the C-Cl bond will break, over a barrier of 32.4 kJ/mol, and form a new Cl-Si bond on the adjacent dimer in the same row creating the first dissociation structure (DS1) with an adsorption energy of -180.0 kJ/mol. Overcoming a small barrier of 7.4 kJ/mol, the second dissociation structure (DS2, Figure III-14A) is formed by breaking the C_6-Si bond, restoring aromaticity to the carbon ring and reducing the adsorption energy to -305.1 kJ/mol. Once this structure is formed, the Cl atom can migrate along the dimer surface forming the third dissociation structure (DS3, Figure III-14B), with an adsorption energy of -307.8 kJ/mol, over a barrier of 164.7 kJ/mol, then forming the most stable dissociation structure (DS4, Figure III-14C) over a barrier of 191.0 kJ/mol. This dissociation structure is stable in both the singlet and triplet states with adsorption energies of -325.8 kJ/mol and -297.5 kJ/mol respectively.

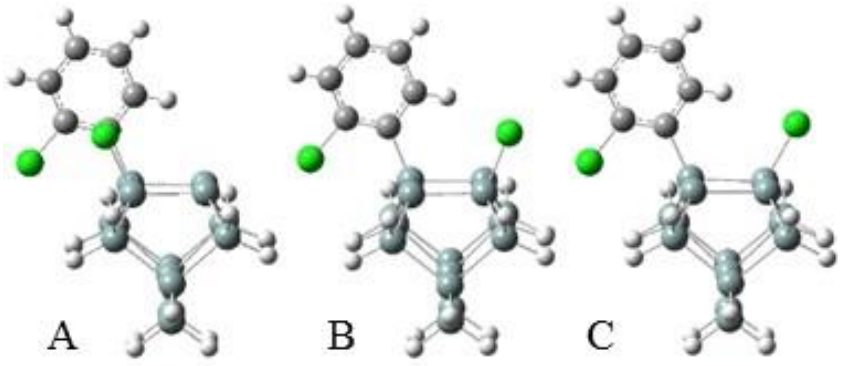

Figure III-14. Additional dissociation structures formed from the 2,3-tilted pathway of 1,2-dichlorobenzene: (A) DS2, (B) DS3, and (C) DS4.

Further dissociation of the 2,3-tilted structure can occur across dimer rows; these structures are modeled on the trench-dimer cluster. It should be noted that on the trench dimer cluster, no stable DS1 structure could be found; all attempts to find a stable DS1 structure found only the DS2 structure. This is due to the small barrier between the DS1 and DS2 structures. For this reason, modelling on the trench dimer cluster begins with the DS4 structure to explore the dissociation pathway across dimer row. On the trench dimer cluster, the triplet adsorption energy of the DS4 structure is increased slightly from -297.5 kJ/mol, on the double-dimer cluster, to -294.7 kJ/mol. Overcoming a barrier of 76.5 kJ/mol, the carbon ring can lay across the trench forming a C_4-Si bond to the dimer on the adjacent row. This dissociation structure (DS5, Figure III-12) is equivalent to the DS1 structure of the row-linking butterfly, has an adsorption energy of -228.7 kJ/mol in the triplet state, and is unstable in the singlet state. The final dissociated structure (DS6, Figure III-15) can be formed by breaking the C_4-H bond and forming a new Si-H bond on the unsaturated Si atom on the dimer. This barrier is quite large at 186.6 kJ/mol and forms a stable structure with an adsorption energy of -304.2 kJ/mol in the triplet state, and -330.2 kJ/mol in the singlet state.

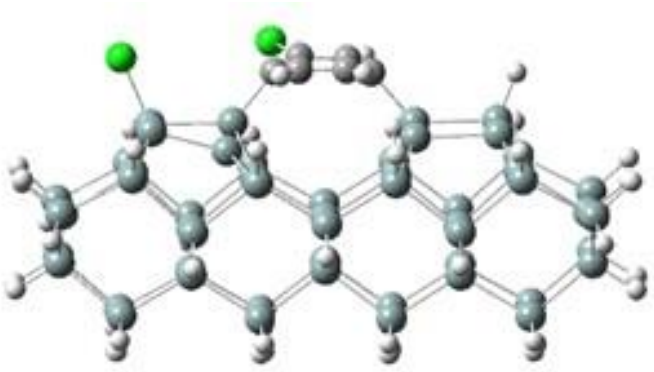

Figure III-15. Cross dimer dissociation product (DS6) for the 2,3-tilted pathway of 1,2-dichlorobenzene.

The 1,4-row-linking butterfly structure is formed over a barrier of 72.3 kJ/mol on the trench-dimer cluster and has an adsorption energy of -7.0 kJ/mol in the singlet state. This structure undergoes a spin-crossing event, forming the more stable triplet state structure with an adsorption energy of -72.4 kJ/mol. Once in the triplet state, the C_1-Cl bond is broken and a Cl-Si bond is formed on the unsaturated Si atom of the same dimer over a barrier of 3.9 kJ/mol. This forms the first dissociation structure (Figure III-12) and is equivalent to the DS5 structure of the 2,3-tilted pathway with an adsorption energy of -228.7 kJ/mol. This structure can then proceed to form either product by overcoming a barrier of 10.4 kJ/mol to form the DS4 structure or a barrier of 186.6 kJ/mol to form the DS6 structure.

1,4-Dichlorobenzene: 2,3-Tilted

The only possible tilted pathway for 1,4-dichlorobenzene begins with the 1,2-tilted structure and is similar to that of the 2,3-tilted pathway of 1,2-dichlorobenzene. This pathway is summarized in the energy diagram of Figure III-16, and the adsorption energies are tabulated in Table III-4. The adsorption structure is formed over a barrier of 71.4 kJ/mol and has an adsorption energy of -35.8 kJ/mol in the singlet state and -12.4 kJ/mol in the triplet state on the double-dimer cluster. Once the triplet structure is formed, the C_1-Cl bond is broken, a barrier of 36.7 kJ/mol, and the first dissociation structure (DS1) is formed by the creation of new Cl-Si bond on the adjacent dimer in the same row. This structure has an adsorption energy of -177.6 kJ/mol. Then, by overcoming a small barrier of 4.4 kJ/mol, aromaticity is restored to the carbon ring by breaking the C_1-Si bond forming the second dissociation structure (DS2, Figure III-17A) and significantly reducing the adsorption energy to -306.6 kJ/mol. At this stage, the Cl atom can migrate along the Si dimer surface by overcoming two large barriers, 162.9 kJ/mol and 189.6 kJ/mol, to form the DS3 (-309.6 kJ/mol) and DS4 structures, respectively. The DS3 and DS4 structures are pictured

in Figures III-17B and III-17C, respectively. The final dissociation structure on the singlet row, DS4, has an adsorption energy of -303.2 kJ/mol in the triplet state but is more stable in the singlet state with an adsorption energy of -331.3 kJ/mol.

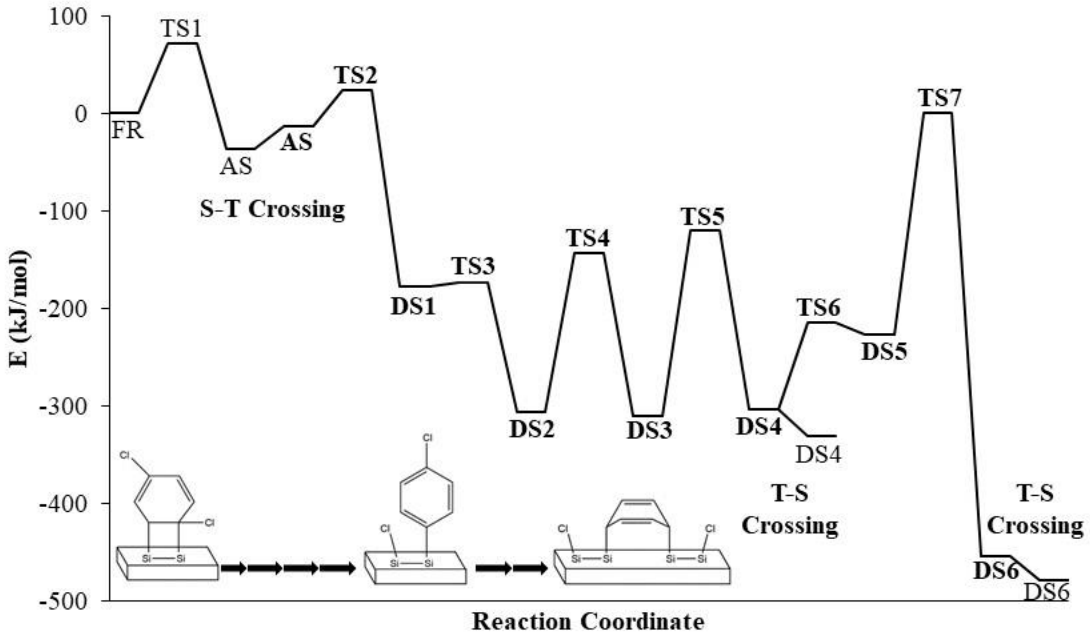

Figure III-16. This energy diagram depicts the 1,2-tilted dissociation pathway of 1,4-dichlorobenzene. Bold labels indicate that the structure is optimized in the triplet state. For clarity, free reactants are labeled FR; the 1,2-tilted adsorption structure is labeled AS; transition states are labeled TS, and the dissociated structures are labeled DS. Singlet-triplet (S-T) and triplet-singlet (T-S) crossing points are also labeled. The inlay shows the adsorption structures and the two main dissociation structures DS4 and DS6, and the arrows each represent a transition into a new structure.

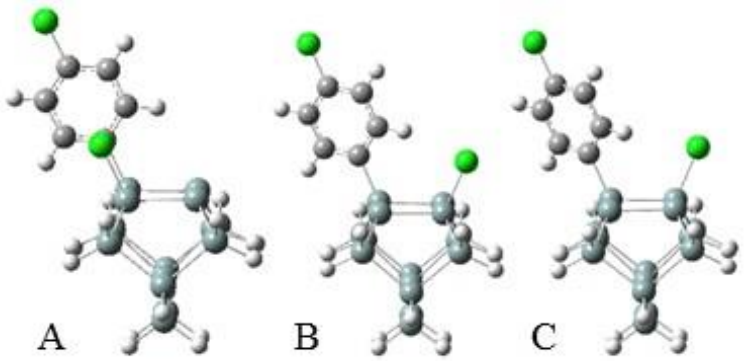

Figure III-17. Additional dissociation structures formed from the 1,2-tilted pathway of 1,4-dichlorobenzene: (A) DS2, (B) DS3, and (C) DS4.

This tilted dissociation pathway can also proceed across dimer row. As in the case of 1,2-dichlorobenzene, a stable DS1 structure was not found on the trench-dimer cluster due to the extremely low barrier to form the DS2 structure (4.4 kJ/mol on the double-dimer cluster). Thus modelling on the trench-dimer cluster will start with the triplet DS4 structure, which has an adsorption energy (-306.5 kJ/mol) that is only 3.2 kJ/mol lower than that structure on the double-dimer cluster. The fifth dissociation structure (DS5), shown in Figure III-18A, is formed when the carbon ring lays across the trench to form the C_4-Si bond to the adjacent dimer row over an energy barrier of 92.5 kJ/mol. In order to form the final dissociation structure (DS6, Figure III-18B), the C_4-Cl atom must break and form a new Cl-Si bond with the unsaturated Si atom of the same dimer. In contrast to the 1,2-dichlorobenzene case, the C-Cl bond is much weaker and results in a much lower energy barrier of 84.9 kJ/mol, a difference of 101.7 kJ/mol. The final structure is much more stable than the DS4 structure with an adsorption energy of -478.8 kJ/mol in the singlet state and -454.0 kJ/mol in the triplet state.

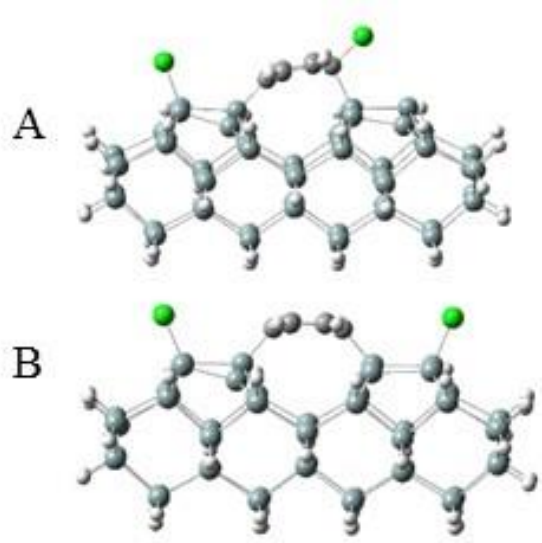

Figure III-18. Further dissociation structures along the 1,2-tilted pathway of 1,4-dichlorobenzene: (A) DS5 and (B) DS6.

Butterfly Pathways

1,2-Dichlorobenzene: 1,4-Butterfly

The 1,4-butterfly pathway is summarized in Figure III-19 and Table III-4. The adsorption structure is formed over a low barrier of 41.2 kJ/mol and has an adsorption energy of -63.2 kJ/mol in the singlet state and -45.7 kJ/mol in the triplet state. The formation of the first dissociation structure (-121.5 kJ/mol) occurs when the C_1-Cl bond breaks, over a barrier of 51.5 kJ/mol, and the Cl atom bonds to the Si atom in the adjacent row. The final dissociation (DS2, Figure III-20) structure is then formed by restoring aromaticity to the carbon ring by breaking the C_4-Si bond. The barrier to the formation of this dissociation structure is 23.2 kJ/mol and forms a very stable structure at -288.2 kJ/mol in the triplet state. This structure is less stable in the singlet state (-249.6 kJ/mol) due to the two unsaturated Si atoms on separate dimers. This configuration does not allow the formation of a partial π-bond in the singlet state, as it would if both unsaturated Si atoms were on the same dimer, making the triplet state the lower energy state.

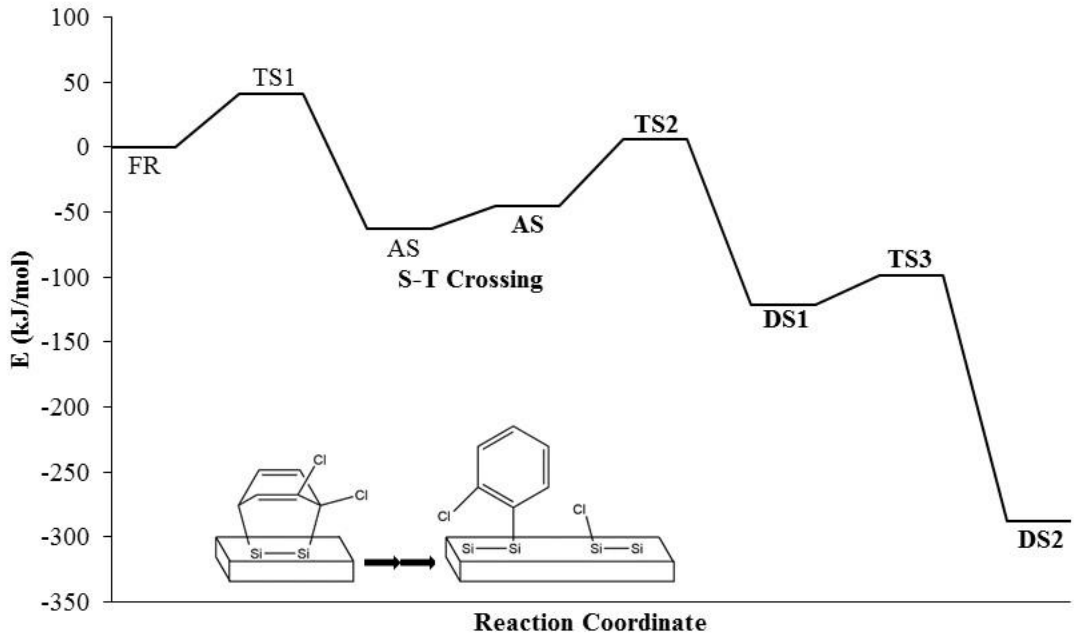

Figure III-19. The 1,4-butterfly dissociation pathway of 1,2-dichlorobenzene on the trench-dimer cluster. Bold labels indicate that the structure is optimized in the triplet state. For clarity, free reactants are labeled FR; the 1,4-butterfly adsorption structure is labeled AS; transition states are labeled TS, and the dissociated structures are labeled DS. The singlet to triplet (S-T) crossing is also labeled. The inlay shows the adsorption structure as well as the final dissociated structure, DS2, and the arrows each represent a transition into a new structure.

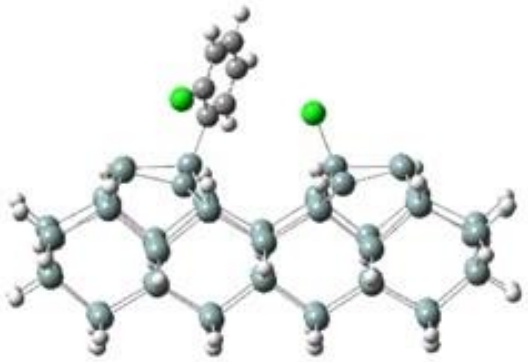

Figure III-20. The final dissociation product (DS2) of the 1,4-butterfly pathway of 1,2-dichlorobenzene.

1,4-Dichlorobenzene: 1,4-Butterfly

The 1,4-butterfly structure of 1,4-dichlorobenzene is formed over a barrier of 27.2 kJ/mol on the triple-row trench-dimer cluster and has an adsorption energy of -75.7 kJ/mol in the singlet state and -61.0 kJ/mol in the triplet state. This large cluster is needed since one of the possible dissociation structures takes place across three rows. The energetics of this pathway is summarized in Figure III-21, and the adsorption energies are tabulated in Table III-4. Similar to 1,2-dichlorobenzene, this 1,4-dichlorobenzene structure can form the first dissociation structure by breaking the C_1-Cl bond and forming a Si-C bond on the nearest bare Si atom on the adjacent row. The barrier to this structure is 61.9 kJ/mol and has an adsorption energy of -126.7 kJ/mol. This structure may then follow one of two possible pathways. The first possible pathway restores aromaticity to the carbon ring by breaking the C_4-Si bond over a barrier of 75.3 kJ/mol to form one of the stable dissociation structure (DS2, Figure III-22A) with an adsorption energy of -310.5 kJ/mol in the triplet state. Alternatively, the second C-Cl bond can break and form a Si-Cl bond on the opposite dimer row by overcoming a barrier of 158.2 kJ/mol, forming a less stable dissociation (DS3, Figure III-22B) structure at -215.9 kJ/mol in the triplet state. Both of these structures are more stable in the triplet state due to the location of the unsaturated Si atoms as described in the previous section.

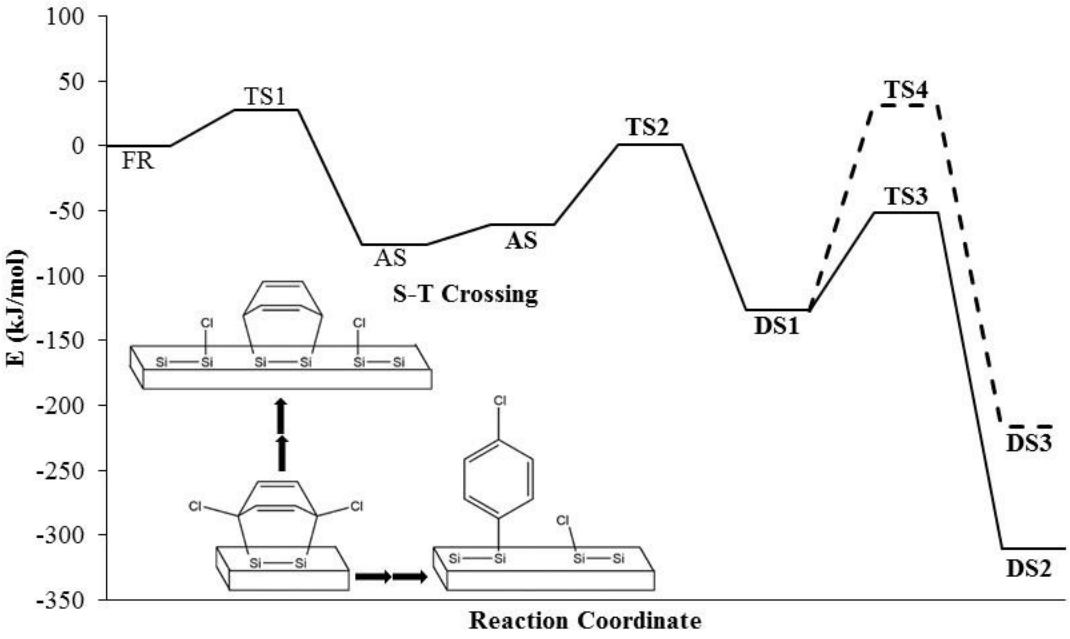

Figure III-21. The 1,4-butterfly dissociation pathway of 1,4-dichlorobenzene on the trench-dimer cluster. Bold labels indicate that the structure is optimized in the triplet state. The solid line represents the pathway to the most stable dissociation product, DS2, and the dotted line represents the pathway to the alternate product, DS3. For clarity, free reactants are labeled FR; the 1,4-butterfly adsorption structure is labeled AS; transition states are labeled TS, and the dissociated structures are labeled DS. The singlet to triplet (S-T) crossing is also labeled. The inlay shows the adsorption structure (center) as well as the final dissociated structures, DS2 (right) and DS3 (top), and the arrows each represent a transition into a new structure.

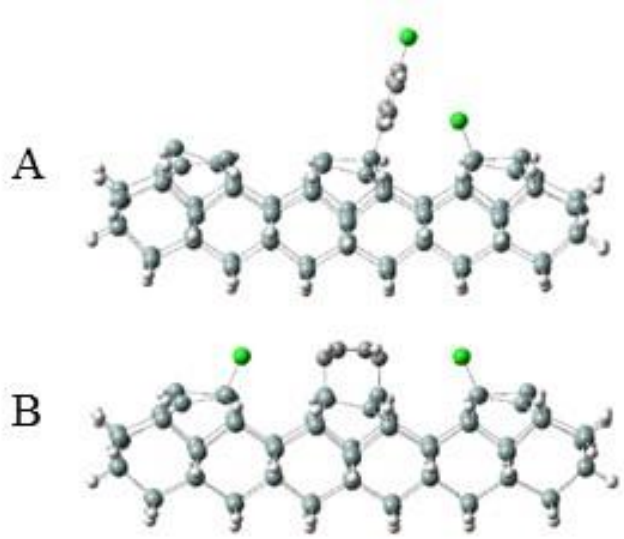

Figure III-22. The final two possible dissociation structures for the 1,4-butterfly pathway of 1,4-dichlorobenzene: (A) the lower energy DS2 and (B) the higher energy DS3.

Spin-Crossing

In order for dissociation to occur, the adsorption structures must undergo a spin-crossing event. As stated in Chapter II, the minimum energy crossing point (MECP) must first be determined. This is the structure of lowest energy along the crossing seam between the singlet and triplet potential energy surfaces. Once the MECP is determined, the spin-orbit coupling constant and the Frobenius norm of the energy difference gradient between the two potential energy surfaces are calculated and utilized to determine the crossing probability using Equation 1. The crossing probability is then used to determine the rate coefficient for the spin-crossing even using Equation 2. Relevant geometric data is summarized in Table III-5 along with the singlet, triplet, and MECP energies, the spin-orbit coupling constant, and the crossing probability. All values are calculated on the smallest possible cluster size.

Table III-5. Geometric information (in Å and degrees) for the singlet, the MECP, and the triplet for all structures that undergo a spin-crossing event, with the exception of the row-linking butterfly structure of 1,2-dichlorobenzene. The adsorption energy of the singlet, MECP, and triplet(kJ/mol), spin-orbit coupling constant (cm^{-1}), and the crossing probability are also reported. The spin-orbit coupling constant for the 1,4-dichlorobenzene 1,4-butterfly structure was not calculated due to the size of the system. Bond lengths are the distance between the two Si atoms on the bare dimer. The buckling angles are quantified by the angle between the Si-dimer bond and its projection in the plane of the Si atoms in the layer below the dimer.

1,2-Dichlorobenzene					
Model	Bond Length (Å)	Buckling Angle (Deg)	Adsorption Energy (kJ/mol)	SOC (cm^{-1})	Crossing Probability
2,3-Tilted					
AS	2.26/2.38/2.41	10.68/0.11/0.01	-34.6/-5.9/-6.7	12.87	2.50×10^{-3}
DS4	2.24/2.39/2.41	9.94/0.32/0.30	-325.8/-297.1/-297.5	12.51	2.40×10^{-3}
DS6	2.26/2.40/2.43	12.25/0.91/0.85	-330.2/-303.6/-304.2	9.37	1.40×10^{-3}
1,4-Butterfly					
AS	2.28/2.39/2.43	11.98/0.52/0.26	-71.9/-44.4/-45.7	9.26	1.30×10^{-3}
1,4-Dichlorobenzene					
Model	Bond Length (Å)	Buckling Angle (Deg)	Adsorption Energy (kJ/mol)	SOC (cm^{-1})	Crossing Probability
1,2-Tilted					
AS	2.24/2.38/2.41	8.26/0.00/0.09	-35.8/-11.7/-12.4	13.15	2.60×10^{-3}
DS4	2.24/2.39/2.41	9.51/0.28/0.28	-331.3/-302.9/-303.2	11.48	2.00×10^{-3}
DS6	2.26/2.39/2.43	12.14/0.64/0.60	-478.8/-453.2/-454.0	9.32	1.30×10^{-3}
1,4-Butterfly					
AS	2.29/2.37/2.43	13.92/0.83/0.31	-85.7/-58.8/-61.0	-	-

Comparison of the 1,2- and 1,4-dichlorbenzene analogs reveals that the bond lengths and buckling angles are nearly identical. This suggests that the placement of the additional Cl atom does not have a significant effect on the geometry of the stable structures or the MECP. Comparison with chlorobenzene analogs supports this assertion, as the geometric parameters are similar. In addition, the structures modeled on the double dimer cluster all have similar spin-orbit coupling constants, while the structures modeled on the trench dimer cluster are slightly lower; this trend is also observed in the chlorobenzene analogs. This suggests the addition and placement of the additional Cl atom has little to no effect on the spin-orbit coupling while the size of the cluster has a small effect resulting in an even smaller change in the crossing probability and rate constant.

Like the case of chlorobenzene, it has been determined that a spin-crossing event is required in order for dissociation of these structures to occur, however the kinetics of the spin-crossing events of the adsorption structures are not rate limiting. Although the spin-crossing events of dissociated structures are not required for dissociation to occur, these crossing events are also analyzed. Like those of the adsorptions structures, these rate constants are large, due to the small barriers and reasonable crossing probabilities.

Conclusions

This work finds 18 stable adsorption structures for 1,2-dichlorbenzene on the Si(100) surface and 10 stable adsorption structure for 1,4-dichlorobenzene. Of these structures, only 4 viable pathways are found for 1,2-dichlorobenzene, and only 2 are found of 1,4-dichlorobenzene. These pathways all meet the criteria that a Cl atom is in close proximity to a surface Si atom, the Cl atom is adjacent to a C-Si bond, and the energy barrier to dissociation is lower than that of desorption. Pathways were also disregarded if no transition state could be found, as in the case of the tight-bridge and twisted-bridge structures, or if the pathway was interrupted by a lack of intermediate stable structures.

Of the 1,2-dichlorobenzene structures, the viable pathways discussed began with the 1,2-tilted, 2,3-tilted, 1,4-butterfly, and the row-linking butterfly structures. While no stable first dissociation structure, in which one Cl atom dissociates, was found for the 1,2-tilted pathway, a highly stable dissociation product was found which has both Cl atoms attached to the adjacent Si dimer, while the phenyl ring is attached to the first dimer at the C_1 and C_2 atoms. The lack of first

dissociation structure is likely due to an incredibly small barrier to the dissociation of the second Cl atom, making optimization of this intermediate structure difficult. This pathway likely occurs only in the singlet state, as the triplet adsorption structure is highly unstable.

The 2,3-tilted pathway of 1,2-dichlorbenzene and the 1,2-tilted pathway of 1,4-dichlorobenzene follow the same reaction mechanism. Dichlorobenzene is adsorbed to the surface via an asymmetric pathway by first forming a dative bond with the down Si atom before forming two Si-C bonds to the same dimer. After a spin-crossing event, the Cl atom closest to the surface dissociates in the triplet state. At this point, the C-Si bond that was adjacent to the now dissociated Cl atom is broken, restoring aromaticity to the ring and significantly lowering the adsorption energy. The Cl atom may then migrate along the Si dimer surface until the DS4 structure, the lowest energy structure on a single row, is formed. At this point, another spin-crossing event may occur, forming the more stable singlet structure. Alternatively, the ring may lay across the dimer rows and form a new C-Si bond to the adjacent dimer on the other dimer row. The DS6 structure may then be formed by dissociation of the H atom or the Cl atom for 1,2- and 1,4-dichlorobenzene, respectively.

The row-linking butterfly pathway is found to be a viable pathway only for 1,2-dichlorobenzene, since the 1,4-dichlorobenzene analog of the adsorption structure is highly unstable in the singlet state, and no transition state could be found in the triplet state. This structure is bound to the Si atom of one dimer by the C_1-Si bond, and to the other Si atom of the dimer in the adjacent row by the C_4-Si bond. This structure is formed in the singlet state, but quickly undergoes a spin-crossing event to form the more stable triplet structure. The C_1-Cl bond is then broken and a new Si-Cl bond is formed to the unsaturated Si atom on the same dimer as the C_1-Si bond, merging

with the 2,3-tilted pathway by forming the DS5 structure of the 2,3-tilted pathway. From this structure, either the DS4 or DS6 structure may be formed, with the DS4 structure being more likely due to the lower barrier to formation.

Both 1,2- and 1,4-dichlorobenzene have viable pathways beginning with the 1,4-butterfly structure, and both follow similar pathways with an additional possible dissociation structure for 1,4-dichlorobenzene. In both cases, the 1,4-butterfly structure is formed when the C_1-Si and C_4-Si bonds are formed on the two Si atoms of the same dimer. Once formed, a spin-crossing event occurs, then the Cl atom adjacent to the C_1-Si bond may dissociate and form a Si-Cl bond with the Si atom of a dimer on the adjacent row. The C_4-Si bond is then broken, restoring aromaticity to the ring and forming a very stable dissociation structure. Because the Si-Cl and Si-C bonds are on different dimers, each of these dimers has an unsaturated Si atom, which makes this structure more stable in the triplet state. Because of this, spin-crossing back to the singlet state is not expected to occur. In the case or 1,4-dichlorobenzene, after the first Cl atom is dissociated, the second Cl atom may then dissociate forming a Si-Cl atom on a dimer in the row on the opposite side of the ring. This pathway is only possible for 1,4-dichlorobenzene, as the C-H bond of 1,2-dichlorobenzene is shorter and stronger, leading to a much larger energy barrier. Like the other dissociation structure, the two unsaturated Si atoms are on separate dimers, thus this structure is more stable in the triplet state. Comparison to experimental results and the results of Chapter II are discussed in Chapter V.

CHAPTER IV

Mechanical and Electronic Properties of Cobalt Doped Zinc Oxide

Zinc oxide is used in a variety of commercial products such as UV-protecting lotions, food additives, and rubber. However, in recent years it has gained significant attention in the semiconductor electronics field, due to its use as a transparent light emitting diode [94-96]. Cobalt doped zinc oxide in particular has been studied recently due to its potential uses in spintronics [97-99]. It is predicted that cobalt doped zinc oxide could have a relatively high curie temperature, allowing for easy transition between the ferromagnetic and anti-ferromagnetic states, which would have great use in the development of spintronic devices. In fact, many of the studies related to cobalt doped zinc oxide focus primarily on their magnetic properties [100-104], while a full characterization of this material is still needed. In this chapter, the ongoing work determining the mechanical and electronic properties of cobalt doped zinc oxide is discussed. The bulk modulus of pure ZnO is determined and compared to the literature as validation for the methodology. The bulk modulus of cobalt doped zinc oxide is calculated and compared to that of the pure ZnO, and the band gap is determined. The shortcomings of the methodology and future modifications are discussed in Chapter V.

Computational Methods

All calculations in this work are performed using the SIESTA code [105]. A k-grid cutoff value of 40 Bohr was used for all calculations, while a real space mesh of 260 Rydbergs was used for all generalized gradient approximation (GGA) calculations and a real space mesh of 500 Rydbergs was used for all local density approximation (LDA) calculations. These values were determined by calculating the energy of a 3x3x3 supercell of the ZnO wurzite structure, with a single Co atom replacing a Zn atom in the structure, and determining the values in which the change in energy is minimized. The GGA calculations use the Perdew-Burke-Ernzerhof [106] parameterization of the exchange-correlation functional and the LDA calculations use the Ceperley-Alder [107] parameterization. The maximum difference in the elements of the density matrix must be below $1x10^{-3}$ in order for convergence to be achieved. The norm-conserving Troullier-Martins pseudopotentials are used without modification from the SIESTA package for zinc, cobalt, and oxygen [108].

The atomic coordinates and lattice of each crystal structure is first optimized using the conjugate gradients method. This optimized structure is then used as the reference structure to determine the bulk modulus of the crystal. The lattice constant is scaled linearly, keeping the fractional coordinates of the atoms the same, while determining the total energy of the system at each point. This is then fit to the Murnaghan equation of state [76] to determine the bulk modulus. The formalization of the Murnaghan equation of state used is given in Equation 1.

$$E(V) = E_0 + \frac{B_0 V}{B'}\left(\frac{(V/V_0)^{B'}}{B'-1} + 1\right) - \frac{B_0 V_0}{B'-1} \quad \text{(E1)}$$

In this equation, the calculated total energy is determined as a function of volume, E(V), the minimum energy of the structure, E_0, the volume of the unit cell, V, the volume of the unit cell at

the minimum energy, V_0, and the derivative of the bulk modulus with respect to pressure, B', to determine the bulk modulus, B. These values are compared to the literature, to assess the validity of the methodology. This method is then used to determine the density of states and bandgap, as well as the bulk modulus of ZnO structure with various concentrations of cobalt doping.

Results and Discussion

In order to assess the methodology, the bulk modulus of ZnO was calculated by fitting the Murnaghan equation of state (Equation 1). This was accomplished by first optimizing the structure by allowing the relaxation of atomic coordinates as well as the lattice. The lattice constant was then scaled in increments of 0.5%, keeping the atomic coordinates the same, and calculating the total energy at each point. The bulk modulus was calculated for pure ZnO and for $Zn_{0.9815}Co_{0.0185}O$ using both the LDA and GGA.

Bulk Modulus of ZnO

The conjugate gradients optimization of the ZnO wurzite structure is done using a single unit cell with periodic boundary conditions. Experimental measurements have determined the lattice constants of a=b=3.249Å and c=5.205Å for a hexagonal crystal structure [68]. Optimization using GGA finds a slight elongation of both parameters with a=b=3.311Å and c=5.363Å, while fractional atomic coordinates are not significantly shifted from their ideal positions. This results in an increase from the ideal Zn-O bond length of 1.80Å to 2.02Å. Optimization using LDA results in a contraction of a and b and an elongation of c with values of a=b=3.222Å and c=5.257Å. The fractional atomic coordinates are not significantly different from their ideal positions, thus the shift in lattice constants results in an increase in the Zn-O bond length (similar to the GGA calculation), with a calculated bond length of 2.00Å. Fits to the Murnaghan equation of state were accomplished by varying the bulk modulus and its derivative, while minimizing the

sum of the square of the difference in the calculated energy and the fit of each point. The fit to the Murnaghan equation of state can be seen in Figure IV-1. Using this method, GGA gives a bulk modulus of 159 GPa while LDA gives a bulk modulus of 197 GPa. Since LDA tends to overestimate the bulk modulus, while GGA underestimates it, the average value of 178 GPa was utilized. The results are approximately 20-25% larger than those found in the computational literature. However, while conflicting results have been found for the bulk modulus of ZnO, close agreement was found with the value of 183 GPa reported by Karzel *et al*. [68]. Additionally, the average of the lattice constants calculated by both GGA and LDA is 3.27Å, which is in close agreement with the experimental value of 3.249 Å [68]; these values are consistent with the computational literature [77]. The results are compared to the literature in Table IV-1.

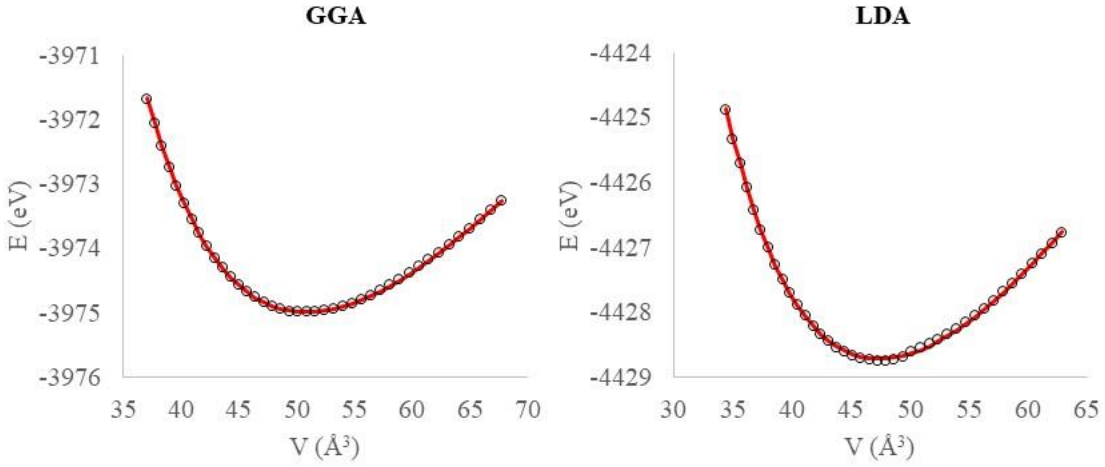

Figure IV-1. A fit of the GGA and LDA results of ZnO to the Murnaghan equation of state. Data points are represented by the black circles, and the fit is indicated by the line.

Table IV-1. Summary of the bulk modulus calculated by fitting to the Murnaghan equation of state for both GGA and LGA, and similar result from the literature.

	Current work		Literature	
	B (Gpa)	a (Å)	B (Gpa)	a (Å)
LDA	197	3.22	161, 157, 156	3.18
GGA	159	3.31	130, 132, 127	3.28
Average	178	3.27	-	-
Experimental	-	-	183, 144	3.25

Bulk Modulus of $Zn_{0.9815}Co_{0.0185}O$

In order to obtain a doping concentration of 1.85%, a 3x3x3 supercell is used to determine the geometry. This geometry is then used in the calculation of the bulk modulus of the $Zn_{0.9815}Co_{0.0185}O$ structure. The results of the optimization of the doped crystal structure reveal very small changes in the lattice parameters for both GGA and LDA, with changes less than 1%. The GGA optimization for the undoped crystal structure gives lattice constants of a=b=3.322Å and c=5.355Å, while the LDA optimization gives lattice constants of a=b=3.218Å and c=5.270Å. Fitting the results of the total energy of the structure versus the volume of the supercell gives results of 160GPa for the GGA and 198GPa for the LDA. The fit of this data to the Murnaghan equation is shown in Figure IV-2, however, the volume and total energy used in the plot have been divided by 27 for clarity of comparison to the ZnO results. This was done to account for the fact that the supercells used for these calculations were made up of 27 unit cells of ZnO. These results are not significantly different from the ZnO results, differing by less than 1% in both cases. It is unlikely that any reasonable doping concentration would significantly affect the bulk modulus, though more work is required to support this hypothesis.

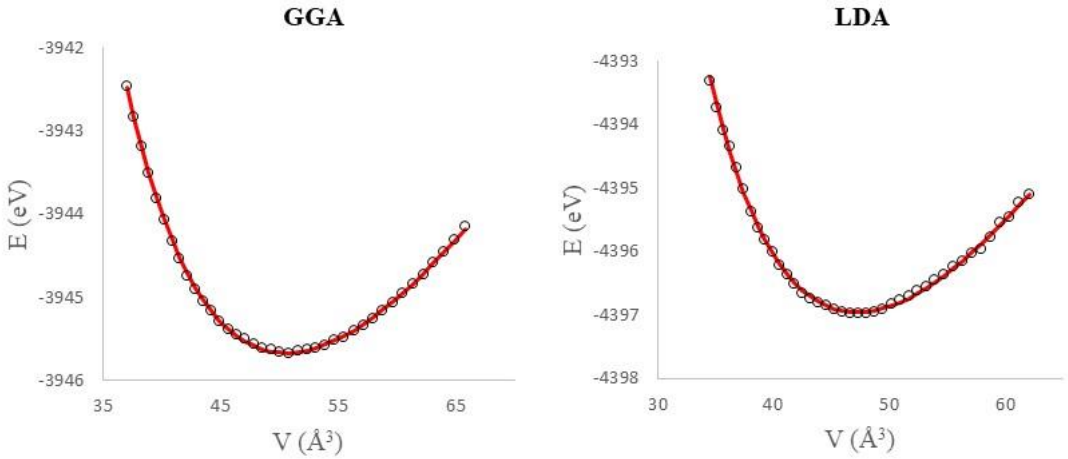

Figure IV-2. A fit of the GGA and LDA results of $Zn_{0.9815}Co_{0.0185}O$ to the Murnaghan equation of state. Data points are represented by the black circles, and the fit is indicated by the line.

Deformation of $Zn_{0.9815}Co_{0.0185}O$

Insertion of the Co atom results in a deformation of the crystal lattice due to the smaller Co-O bond length. In this section, the extent of this deformation, as calculated using both the GGA and LDA approximations, is analyzed. As shown in Figure IV-3, there are two layers, differing by the positions of the Zn and O atoms, and each layer is labelled either A or B, depending on type of layer, and each is given a number corresponding to the distance from the layer containing the Co atom. The bond lengths between the layers defined in Figure IV-3 are analyzed, then the bonding within the layers is analyzed.

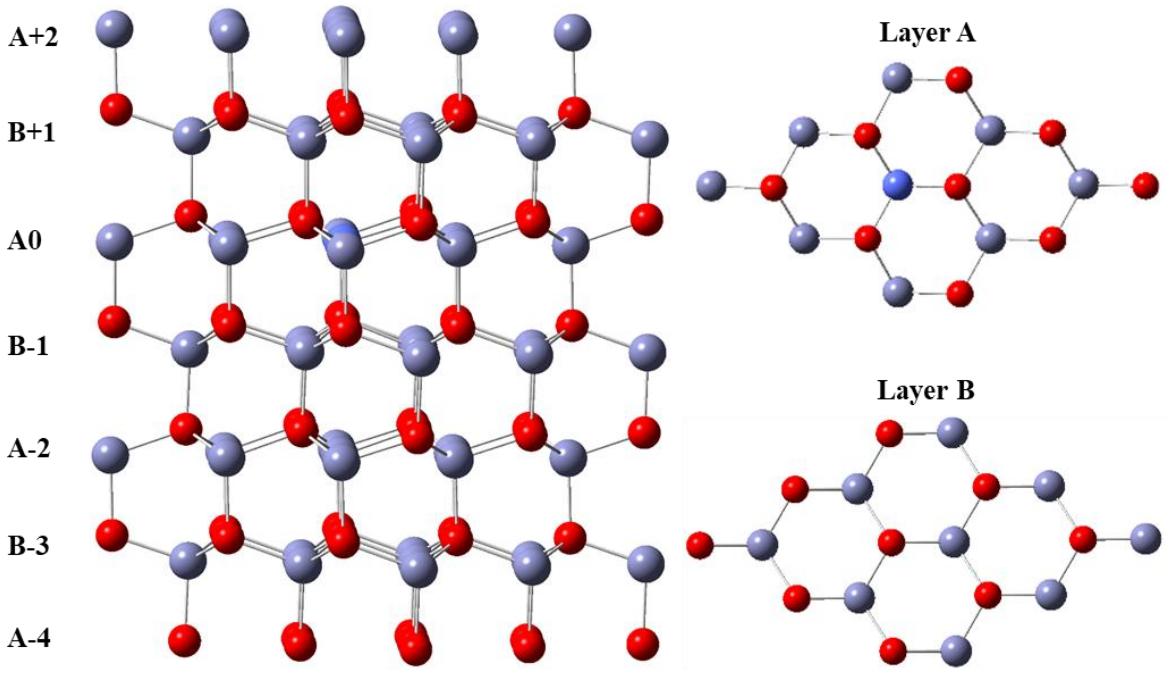

Figure IV-3. The image on the left shows the supercell used for modelling $Zn_{0.9815}Co_{0.0185}O$, with the alternating layers, shown as Layer A and Layer B, labelled by the layer type (A or B) and the distance from the layer containing the Co dopant atom, A0, for clarity.

Analysis of the bond lengths between layer A0 and the layer below it, B-1, calculated using the GGA, reveals a Co-O bond length of 1.92Å, which is 0.10Å shorter than the Zn-O bond in the undoped structure. All Zn atoms in layer A0 have a bond length of 2.02Å to the O in the B-1 layer. In the next layers, the Zn atoms in layer B+1, sharing an O atom with the Co atom in layer A0 have Zn-O bond lengths of 2.06Å, while the remaining Zn atoms have Zn-O bonds have bond lengths of 2.02Å. This variation in the bond lengths between the layers above is compensated for in the layers below the Co dopant atom. The Zn atoms sharing the O atom with Co, in layer B-1, have Zn-O bond lengths of 2.01Å, while the remaining Zn atoms have slightly larger Zn-O bond lengths of 2.02Å to the A-2 layer, which is the same as the bond lengths between B+1 and A0 layers that are farther from the Co atom. The bond lengths between layers A+2 and B+1 are quite uniform with bond lengths of 2.03Å, with the exception of the Zn-O bond directly above the Co dopant atom, which has a slightly longer bond length of 2.04Å. A similar result is found in the

bonding between layers A-2 and B-3, with uniform bond lengths of 2.02Å on all but the Zn-O bond directly below the Co atom, which has a shorter bond length of 2.01Å to compensate for the longer bond between the layers above. However, the bonding between the lowest layers, B-3 and A-4, shows no deformation near the Co atom with nearly all bond lengths being 2.02Å. There is one bond at the edge of the supercell with a bond length of 2.03Å. This deviation is due to the periodic boundary conditions, which make this bond within the "sphere of influence" of a dopant atom in an adjacent supercell.

Within the A0 layer, the Co-O bonding is slightly longer than the bond between layers, with all bond length being 1.94Å. The surrounding Zn-O bonds that share an O atom with Co are 2.05Å while the remaining bonds are between 2.01-2.03Å. These large bond lengths near the Co atom compensate for the contraction of the Co-O bond with respect to the undoped structure. Additionally, a larger deviation in bond lengths in this layer is expected, as the periodic boundary conditions will simulate further dopant atoms in this layer, resulting in more unpredictable deviations as the "sphere of influence" of each dopant may overlap. In layer B+1, the variation in bond lengths do not indicate any influence from the Co atom below, and have bond lengths between 2.01-2.02Å. Unlike the layer above A0, in the B-1 layer shows significant influence from the Co atom above due to the direct bonding between one of the O atoms and the Co atom in layer A0. Bonds between the Zn atoms and the O atom that is shared with the Co atom have bond lengths of 2.05Å, while the remaining bonds have bond lengths of 2.01Å and 2.02Å. Finally, the remaining layers, have bond lengths of 2.02 and 2.03, with seemingly no significant influence from the Co atom.

Calculations using LDA result in a Co-O bond length of 1.90Å, which is only slightly smaller than the bond length calculated using the GGA, and 0.10Å shorter than the Zn-O bond length found in the undoped structure optimized using LDA. The bonds between Zn atoms in layer A0

and the O atoms in layer B-1 are all very similar, ranging between 1.96-1.97Å. The Zn-O bonds between layer B+1 and A0 are slightly longer, ranging between 1.99-2.03Å, while those bonds sharing and O atom with the Co atom are 2.04Å. The Zn-O bonds between the B-1 and A-2 layers are mostly between 2.00-2.02Å, however, those bonds directly below the 2.04Å long bonds between B+1 and A0 are 1.97Å long. Moving farther from the A0 layer, Zn-O bonds between layers A+2 and B+1, as well as those between A-2 and B-3, all have bonds ranging between 1.96-1.97Å, with no apparent influence from the Co dopant atom. Finally, bonds between atoms in B-3 and A-4 all have bond lengths of 2.00Å.

Within the A0 layer, the Co-O bonds are slightly longer than along the z-axis, with bond lengths between 1.91-1.92Å. The Zn-O bond lengths in this layer range between 1.96-2.00Å. The bond lengths in the B+1 layers range between 1.96Å and 2.01Å. In the B+1 layer, there does not appear to be any influence, however, like the case of the GGA calculations, the lower B-1 layer, which contains an O atom directly bonded to the Co atom in the layer above, shows evidence of influence. In this layer, the bonds emanating from the O atom bonded to the Co atom above, have bond lengths of 2.01Å, while their adjacent bonds have bond lengths of 1.96Å. The remaining Zn-O bonds in this layer range from 1.97-1.99Å. The bonds in layer A-2 range between 1.95-1.98Å, with the bonds between the Zn atom directly below Co and the O atoms surrounding it, as well as the bonds emanating from those O atoms, exclusively occupying the high end of this range between 1.97-1.98Å. All bonds farther removed than this have bond lengths between 1.95-1.96Å. In row B-3, it seems all influence from the Co atom is gone, and the bond lengths range between 1.98-1.99Å, with no noticeable variation due to proximity to the Co atom.

An overall comparison of the results of the optimization of the crystal structure using LDA and GGA finds similar results. Both methods find Co-O bond lengths to be around 1.90Å, resulting in a distortion in the surrounding lattice. All Zn-O bond lengths lie within a range of 1.95-2.06Å, with variations dependent on the proximity to the dopant Co atom. A comparison of bond lengths between layers shows that the influence of the Co atom extends up to two layers above and below it. Within the A0 layer, this influence seems to extend to within two bond lengths of the Co atom, where the variation becomes much less significant. In the B-1 layer, the bond lengths to the O atom connected to the Co atom is elongated. Calculations using GGA do not show any evidence for extended influence beyond those bonds, however LDA suggests that these bonds may be contracted. GGA calculations show more uniformity and tighter groupings of the bond lengths, and this contraction seen in the LDA calculations may be due to the larger variations common throughout the various layers. This evidence suggests that as the O atoms are pulled toward the Co atom, resulting in elongated bonds within the layers. Additionally, the Co atom is pulled slightly below the A0 layer, resulting in elongated bonds between the A0 and the B+1 layers, and contracted bond lengths between the A0 and the B-1 layers. To compensate, the lattice is deformed, and this deformation extends to two or three atomic shells around the Co atom.

Band Structure of ZnO and $Zn_{0.9815}Co_{0.0185}O$

The band structure and density of states has been calculated for both the 3x3x3 supercell of pure ZnO and for $Zn_{0.9815}Co_{0.0185}O$, which is modeled by the 3x3x3 supercell of ZnO, with a single Co atom substituting a Zn atom in the lattice. A comparison of the density of states of pure ZnO to $Zn_{0.9815}Co_{0.0185}O$ for both LDA and GGA is shown in Figure IV-4. In Figure IV-4, the energy is offset in such a way that 0 eV corresponds to the Fermi energy. In each case, the Fermi energy is increased from pure ZnO to $Zn_{0.9815}Co_{0.0185}O$. This increase in Fermi energy is reflected by the

downward shift in the density of states between ZnO and $Zn_{0.9815}Co_{0.0185}O$, and this shift has a magnitude of 0.91 eV for the LDA and 0.98 eV for the GGA calculations. Initially, in the pure ZnO, the Fermi energy lies within the band gap, as expected for a semiconductor, and after doping, the Fermi energy lies within the new states created by doping ZnO with cobalt. These two new bands are comprised almost entirely of Co states, and the appearance of these states lowers the band gap significantly. For the LDA calculations, the band gap is lowered from 2.12 eV to 0.09 eV, and this shift is similar for the GGA, which is lowered from 2.15 eV to 0.12 eV. This is an underestimation of the true band gap, as DFT is not well suited for this type of calculation, however it is sufficient for a qualitative investigation of the changes in the band gap. While this shift is very similar for both the GGA and the LDA, the splitting between the two new states arising from the Co dopant are significantly different, with GGA giving a larger splitting than LDA.

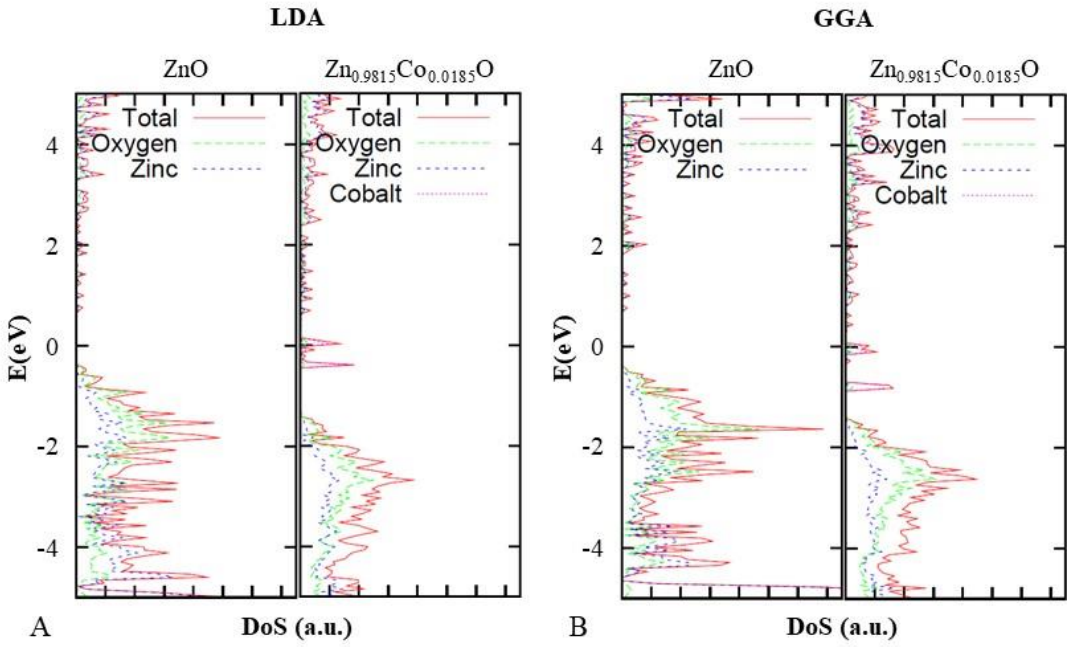

Figure IV-4. The density of states calculated using LDA (A) and GGA (B) for both the undoped 3x3x3 supercell of ZnO and the 3x3x3 supercell with a single Co dopant atom substituting a Zn atom. In these plots, the energy is shifted such that the Fermi energy is at 0eV.

Conclusions

This chapter has examined the bulk modulus of ZnO and $Zn_{0.9815}Co_{0.0185}O$ by fitting the results of GGA and LDA results to the Murnaghan equation of state. GGA tends to overestimate the bulk modulus while LDA underestimates it; thus, an average value of the GGA and LDA results is utilized. The average of these calculated values is 178 GPa for ZnO. While the GGA and LDA results are significantly larger than the values reported in previous computational work, the average value is similar to an experimental value of 188 GPa [68]. Addition of the dopant atom in $Zn_{0.9815}Co_{0.0185}O$ only raises this bulk modulus by 1 GPa, for an average of 179 GPa between the two methods. Further work is required to determine if any significant change in the bulk modulus arises from higher doping concentrations. In addition to the bulk modulus, this method does well replicating the lattice constants. The lattice constants calculated using both GGA and

LDA are identical to previous computational studies, and the average of the two calculated lattice constants, 3.27Å, agrees well with the experimental lattice constant of 3.25Å [68]. While DFT does a quantitatively poor job of determining the band gap, the qualitative results show a decrease in the band gap, calculated using both GGA and LDA, due to the appearance of new Co states within the band gap.

Due to the contraction of the Co-O bonds with respect to the undoped structure, a deformation of the lattice occurs around the dopant Co atom. The bonds between the Zn atoms and the O atoms that are bonded to the Co atom in the same layer are elongated to compensate for the contraction of the Co-O bonds within the layer. In addition, bonds within the layer below the Co atom are also deformed. The Co atom pulls the O atom in the layer below slightly upward, resulting in an elongation of the Zn-O bonds to this O atom. Bonds to the layer above the Co atom are also elongated, while the bonds directly below these elongated bonds are contracted. These results points to a structure in which the Co atom is pulled below the Zn atoms in the layer, while the O atom in the layer below is pulled slightly above the other O atoms in the layer. The Co-O bonds within the layer are contracted, and the adjacent bonds within the layer are elongated to compensate for this, while atoms further from the dopant atom remain unaltered from their positions in the undoped structure.

CHAPTER V

Conclusions

Chlorobenzene

An extensive study of the possible molecular adsorption structures has been conducted, and dissociation pathways have been proposed for chlorobenzene. The tetra-σ structures, the 1,2,3,4- and 2,3,4,5-twisted-bridge, are found to revert to the tilted-bridge structures, rather than dissociate. The dissociation barrier for the majority of di-σ adsorption configurations is large enough to favor desorption rather than dissociation. Only the 1,2-tilted, 1,4-butterfly, row-linking butterfly, and the 2,5-adjacent tilted-bridge butterfly structures have an intermediate on the triplet surface with a transition state barrier low enough to favor dissociation. However, the tilted-bridge butterfly structure leads to a less stable structure with a dangling bond on the carbon ring. Thus only the 1,2-tilted, 1,4-butterfly and row-linking butterfly structures are considered viable pathways. Dissociation mechanisms beginning with these structures were discussed in detail in Chapter II.

The results of Chapter II are consistent with experimental observations. Both X-ray photoelectron spectroscopy (XPS) [31] and scanning tunneling microscopy (STM) [29] experiments showed little to no dissociation of chlorobenzene. This result is consistent with only

three of the 15 adsorption structures being able to dissociate on the surface to form the expected lower energy dissociation structures. Thus, the kinetic barrier is a combination of both the need to form appropriate initial adsorption structures and the subsequent energy barriers along the dissociation pathways. Naumkin *et al*. [29] found a significant amount of molecular adsorption for the butterfly and tight bridge structures (50% and 25% respectively), of which, according to this study, the butterfly structure will form dissociated species on this surface. 16% of the adsorption structures of Naumkin *et al*. [29] have features that could be assigned to the DS4 dissociation structure which may be formed from either the 1,2-tilted pathway or the row-linking butterfly pathway. In addition, the DS2 structure resulting from the 1,4-butterfly could also look similar to DS4 in an STM experiment. Finally, 9% of the features assigned in the STM study [29] are equivalent to the DS6 structure, of the 1,2-tilted and row-linking butterfly pathways. Thus, the small amount of dissociation pathways and the final structures found in this study are consistent with experimental studies.

Dichlorobenzene

Of the adsorption structures discussed in Chapter III, the 1,2-dichlorobenzene analogs of the 1,2-tilted, 2,3-tilted, 1,4-butterfly, and the row-linking butterfly structures will undergo dissociation as well as the 1,4-dichlorbenzene analogs of 1,2-tilted and 1,4-butterfly structures. These results are similar to that of the chlorobenzene analogs discussed in Chapter II. In fact, for the tilted structures, except the 1,2-dichlorbenzene analog of the 1,2-tilted structure as discussed in Chapter III, the adsorption energies and energy barriers are similar for 1,2-dichlorobenzene, 1,4-dichlorobenzene, and chlorobenzene up to the DS5 structure of each pathway. While 1,2-dichlorobenzene and chlorobenzene have similar barriers and adsorption energies for the formation of the DS6 structure, 1,4-dichlorobenzene has a much smaller barrier and a much more

stable dissociation product. This is result is expected as it is correlated to the relative bond energies of the C-H and C-Cl bonds. Thus, the addition and placement of the Cl atom has little effect on the energetics of the pathways until it is directly interacting with the surface, as is the case for the 1,4-dichlorobenzene structure.

According to STM results for 1,2-dichlorobenzene, 23% of the observed structures are in the displaced geometry, DS4 in this work, while 8% are in the linked geometry, DS6 in this work [29]. The relative proportion of dissociated structures is confirmed by XPS studies showing that 25% of 1,2-dichlorobenzene is dissociatively adsorbed to the Si(100) surface. According to this work, two of the dissociation structures may resemble the displaced structure reported in the STM results, the DS4 structure of the 2,3-tilted pathway, and the DS2 structure of the 1,4-butterfly pathway, both having an Si-Cl bond and Si-Ph bond. Conversely, there is only one structure formed from 1,2-dichlorobenzene that would resemble the linked structure, the DS6 structure formed from the 2,3-tilted pathway. Additionally, the large barrier to formation of the DS6 structure, due to the strength of the C-H bond, also restricts the formation of this structure. These findings support the claim that the displaced feature in the STM should be more prevalent than the linked feature. Although the large number of possible adsorption structures conflicts with their findings of only two adsorption structures, it supports the relative abundance of molecularly adsorbed structures to the dissociated structure.

In the case of 1,4-dichlorobenzene, the authors of the STM work found that 7% of the features were the displaced structure, while 52% were the linked structure. Like 1,2-dichlorobenzene, 1,4-dichlorobenzene forms two structures that may resemble the displaced structure and only one that resembles the linked structure. While the 1,4-butterfly pathway may form another dissociation product, this has a higher energy barrier and is thus less likely to be formed. Since the C-Cl bond

is much weaker than the C-H bond, more of the DS6, or linked, structure compared to 1,2-dichlorobenzene is expected. However, one would expect to see more features in an STM experiment that resemble the displaced structure than the linked structure for 1,4-dichlorobenzene. In addition, one would expect to see more molecularly adsorbed structures than dissociated structures.

Zinc Oxide

The results discussed in Chapter IV indicate that the methodology used is adequate for the calculation of the geometrical and mechanical properties of $Zn_{1-x}Co_xO$, however this methodology underestimates the band gap of this structure. The results of the local density approximation (LDA) and generalized gradient approximation (GGA) calculations give similar results for the band gap with values for ZnO of 2.12 eV and 2.15 eV from LDA and GGA calculations, respectively. The calculated band gap for Co doped ZnO, $Zn_{0.9815}Co_{0.0185}O$, is 0.09 eV and 0.12 eV from LDA and GGA calculations, respectively. However, the experimentally determined band gap for ZnO is 3.4 eV [74, 75]. Despite this, qualitative relationships between the band gap and the doping concentration can be derived using this methodology. The LDA and GGA calculations also find similar results for the positions of the new Co states within the band gap upon doping, however GGA finds a larger splitting between the two states. Regardless, the tops of these new states are similarly positioned, resulting in similar reductions of the band gap.

Future Work

This work is currently ongoing and will include additional doping concentrations and address the issues described in this chapter. Calculations for Co doping concentrations of 3.7%, 6.25%,

12.5%, 18.5% and 25% are currently underway. The 3.7% model is made by replacing two Zn atoms with Co in a 3x3x3 supercell, while the remaining concentrations are modelled by replacing one, two, three and four Zn atoms in a 2x2x2 supercell for 6.25%, 12.5%, 18.5% and 25% doping, respectively. These calculations have proven to be quite difficult, due to the large number of unique combinations of positions in which multiple Co atoms can be placed. In the cases of 1.85% and 6.25%, only one Co dopant atom is placed in the supercell and the placement of the Co atom does not matter, as all positions are equivalent to translations in the crystal structure. However, in all other cases, where multiple Co atoms are required, all unique configurations of the Co atoms in the supercell must be considered. Because of the "sphere of influence" around the Co atom, in which the Zn-O bonds in close proximity to the dopant atom are distorted from their ideal values, multiple dopant atoms in close proximity to one another may cause unique distortions of the lattice in comparison to more, spaced out, homogeneous configurations. Calculated properties will be determined by taking an average of the values determined for the various configurations.

In addition to further doping concentrations, issues in the methodology are currently being addressed. Because the geometry of undoped ZnO is used as an initial guess for the crystal structure, the introduction of additional dopant atoms causes this guess to be farther and farther off due to the distortions caused by each new Co atom. This means more computational effort is expended in determining the optimized structure, and, with the current methodology, optimizing the structure of higher concentrations is not feasible. For these larger concentrations, a higher tolerance on the difference in total energy between the steps of the conjugate gradients optimization will be used, until the forces on the atoms are minimized. Once the forces are minimized, the total energy difference tolerance can be lowered to maintain the accuracy achieved by the current methodology.

Another issue that is currently being addressed is the calculation of the band structure. The band structure is generated by plotting the energy as a function of momentum between various high symmetry points. This plot is done only in the first Brillouin zone (FBZ), the primitive cell in reciprocal space, since the bands beyond the FBZ are not unique. Because of the larger supercells required to achieve the doping concentrations in this work, the full FBZ is not utilized and instead the band plot is "folded", resulting in a larger number of bands. In order to generate a proper band plot, the plot must be unfolded. However, even though this folding creates additional bands rather than forming continuous bands, these energy states are still represented, and thus the density of states remains unaffected by this. This allows us to analyze the bandgap, as well as the contributions of each of the species in the structure to the total density of states. However, DFT calculations are known to poorly represent experimental band gaps, and this is reflected by the difference in the data presented in Chapter IV and experimental values. In order to obtain quantitatively accurate results, another method must be used. This issue may be addressed with various methodologies, including time-dependent density functional theory or LDA+U methods [109]. The results show that the current methodology is adequate for representing structural and mechanical properties of the structure, and future methodology will use the results of these calculations as a starting point for more accurate calculations pertaining to the band structure and density of states.

REFERENCES

[1] O.L. Alerhand, D. Vanderbilt, R.D. Meade, J.D. Joannopoulos, Spontaneous Formation of Stress Domains on Crystal Surfaces, Phys. Rev. Lett., 61 (1988) 1973-1976.

[2] D. Vanderbilt, Elastic stress domains on the Si(100) surface, Journal of Vacuum Science & Technology B: Microelectronics and Nanometer Structures, 7 (1989) 1013.

[3] O.L. Alerhand, A.N. Berker, J.D. Joannopoulos, D. Vanderbilt, R.J. Hamers, J.E. Demuth, Finite-Temperature Phase Diagram of Vicinal Si(100) Surfaces, Phys. Rev. Lett., 64 (1990) 2406-2409.

[4] J.J. Boland, The Importance of Structure and Bonding in Semiconductor Surface Chemistry: Hydrogen on the Si(111)-7 X 7 Surface, Surf Sci, 244 (1991) 1-14.

[5] C.B. Duke, Semiconductor Surface Reconstruction: The Structural Chemistry of Two-Dimensional Surface Compounds, Chem. Rev., 96 (1996) 1237-1259.

[6] H.N. Waltenburg, J.T. Yates, Surface Chemistry of Silicon, Chem. Rev., 95 (1995) 1589-1673.

[7] R.E. Schlier, H.E. Farnsworth, Structure and Adsorption Characteristics of Clean Surfaces of Germanium and Silicon, The Journal of Chemical Physics, 30 (1959) 917-926.

[8] D.J. Chadi, Atomic and Electronic Structures of Reconstructed Si(100) Surfaces, Physical Review Letters, 43 (1979) 43-47.

[9] R.J. Hamers, R.M. Tromp, J.E. Demuth, Electronic and Geometric Structure of Si(111)-(7 x 7) and Si(001) Surfaces, Surf Sci, 181 (1987) 364-355.

[10] T. Tabata, T. Aruga, M. Yoshitada, Order-Disorder Transition on Si(001) c(4×2) to (2×1), Surf. Sci. Lett., 179 (1987) L63-L70.

[11] R.J. Hamers, R.M. Tromp, J.E. Demuth, Scanning tunneling microscopy of Si(001), Physical Review B, 34 (1986) 5343-5357.

[12] Q. Liu, R. Hoffmann, The Bare and Acetylene Chemisorbed Si(001) Surface, and the Mechanism of Acetylene Chemisorption, J. Am. Chem. Soc., 117 (1995) 4082-4092.

[13] J.T. Yates, A New Opportunity in Silicon-Based Microelectronics, Science, 279 (1998) 335-336.

[14] R.A. Wolkow, Controlled Molecular Adsorption on Silicon: Laying a Foundation for Molecular Devices, Annu. Rev. Phys. Chem., 50 (1999) 413-441.

[15] S.F. Bent, Organic Functionalization of Group IV Semiconductor Surfaces: Principles, Examples, Applications, and Prospects, Surf Sci, 500 (2002) 879-903.

[16] K.M. Roth, A.A. Yasseri, Z. Liu, R.B. Dabke, V. Malinovskii, K.-H. Schweikart, L. Yu, H. Tiznado, F. Zaera, J.S. Lindsey, W.G. Kuhr, D.F. Bocian, Measurements of Electron-Transfer Rates of Charge-Storage Molecular Monolayers on Si(100). Toward Hybrid Molecular/Semiconductor Information Storage Devices, J. Am. Chem. Soc., 125 (2003) 505-517.

[17] R.J. Hamers, J.S. Hovis, S. Lee, H.B. Liu, J. Shan, Formation of Ordered, Anisotropic Organic Monolayers on the Si(001) Surface, The journal of physical chemistry. B, 101 (1997) 1489-1492.

[18] G.P. Lopinski, D.D. Wayner, R.A. Wolkow, Self-Directed Growth of Molecular Nanostructures on Silicon, Nature, 406 (2000) 48-51.

[19] Md. Zakir Hossain, H.S. Kato, M. Kawai, Controlled Fabrication of 1D Molecular Lines Across the Dimer Rows on the

Si(100)-(2 × 1)-H Surface through the Radical Chain Reaction, J. Am. Chem. Soc., 127 (2005) 15030-15031.

[20] M.Z. Hossain, H.S. Kato, M. Kawai, Fabrication of Interconnected 1D Molecular Lines along and across the Dimer Rows on the

Si(100)-(2 × 1)-H Surface through the Radical Chain Reaction, The journal of physical chemistry. B, 109 (2005) 23129-23133.

[21] J.-H. Choi, J.-H. Cho, Theoretical Prediction of Heterogeneous Molecular Wires on the Si(001)

Surface, J. Am. Chem. Soc., 128 (2006) 3890-3891.

[22] M.J. Bozack, P.A. Taylor, W.J. Choyke, J. J. T. Yates, Chemical Activity of the C=C Double Bond on Silicon Surfaces, Surf. Sci. Lett., 177 (1986) L933-L937.

[23] M. Nishijima, J. Yoshinobu, H. Tsuda, M. Onchi, The Adsorption and Thermal Decomposition of Acetylene on Si(100) and Vicinal Si(100), Surf Sci, 192 (1987) 383-397.

[24] J. Yoshinobu, H. Tsuda, M. Onchi, M. Nishijima, The Adsorbed States of Ethylene on Si(100)c(4×2), Si(100)(2×1), and Vicinal Si(100) 9°: Electron Energy Loss Spectroscopy and Low-Energy Electron Diffraction Studies, J. Chem. Phys., 87 (1987) 7332.

[25] R.J. Hamers, H. Liu, Stereoselectivity in Molecule-Surace Reactions: Adsorption of Ethylene on the Silicon(001) Surface, J. Am. Chem. Soc., 119 (1997) 7593-7594.

[26] R.J. Hamers, S.K. Coulter, M.D. Ellison, J.S. Hovis, D.F. Padowitz, M.P. Schwartz, Cycloaddition Chemistry of Organic Molecules with Semiconductor Surfaces, Acc. Chem. Res., 33 (2000) 617-624.

[27] Q. Li, K.T. Leung, Thermal Chemistry of Toluene and Benzene on Si(100)2 X 1 and Modified Surfaces, Surf Sci, 479 (2001) 69-82.

[28] F. Costanzo, C. Sbraccia, P.L. Silvestrelli, F. Ancilotto, Theoretical Study of Toluene Chemisorption on Si(100), The journal of physical chemistry. B, 107 (2003) 10209-10215.

[29] F.Y. Naumkin, J.C. Polanyi, D. Rogers, W. Hofer, A. Fisher, Electron-Induced Attachment of Chlorinated Benzenes to Si(100)2×1, Surf Sci, 547 (2003) 324-334.

[30] X.J. Zhou, K.T. Leung, Competition between Associative and Dissociative Adsorption of 1,2-Dihalogenated Benzenes on Si(100)2×1: Formation of Dihalocyclohexadiene, Halophenyl and Phenylene Adstructures, Surf Sci, 600 (2006) 3285-3296.

[31] X.J. Zhou, K.T. Leung, Surface Chemistry of Monochlorinated and Dichlorinated Benzenes on Si(100)2X1: Comparison Study of Chlorine Content and Isomeric Effects, The journal of physical chemistry. B, 110 (2006) 9601-9607.

[32] T. Leftwich, A. Teplyakov, Chemical Manipulation of Multifunctional Hydrocarbons on Silicon Surfaces, Surf. Sci. Rep., (2007).

[33] Q. Zhu, N.F. Materer, Feasibility of Benzene Dissociation on the Singlet and Triplet Electronic States of Selected Cluster Models for the Si(100) Surface, J. Phys. Chem. C, 115 (2011) 13377-13385.

[34] H.-J. Kim, A. Tkatchenko, J.-H. Cho, M. Scheffler, Benzene Adsorbed on Si(001): The Role of Electron Correlation and Finite Temperature, Phys. Rev. B, 85 (2012).

[35] S.K. Coulter, J.S. Hovis, M.D. Ellison, R.J. Hamers, Reactions of Substituted Aromatic Hydrocarbons with the Si(001) Surface, J. Vac. Sci. Technol., A, 18 (2000) 1965.

[36] F.Y. Naumkin, J.C. Polanyi, D. Rogers, Reaction of Chlorinated Benzenes with Si(100)2X1: A Theoretical Study, Surf Sci, 547 (2003) 335-348.

[37] A.V. Teplyakov, M.J. Kong, S.F. Bent, Vibrational Spectroscopic Studies of Diels-Alder Reactions with the Si(100)-2x1 Surface as a Dienophile, J. Am. Chem. Soc., 119 (1997) 11100-11101.

[38] A.V. Teplyakov, M.J. Kong, S.F. Bent, Diels–Alder reactions of butadienes with the Si(100)-2×1 surface as a dienophile: Vibrational spectroscopy, thermal desorption and near edge x-ray absorption fine structure studies, The Journal of Chemical Physics, 108 (1998) 4599-4606.

[39] R. Konecny, D.J. Doren, Cycloaddition Reactions of Unsaturated Hydrocarbons on the Si(100)-(2x1) Surface: Theoretical Predictions, Surf Sci, 417 (1998) 169-188.

[40] G.P. Lopinski, D.J. Moffatt, D.D.M. Wayner, R.A. Wolkow, How Stereoselective Are Alkene Addition Reactions on Si(100)?, J. Am. Chem. Soc., 122 (2000) 3548-3549.

[41] P.L. Silvestrelli, F. Ancilotto, F. Toigo, Adsorption of benzene on Si(100) from first principles, Physical Review B, 62 (2000) 1596-1599.

[42] Y. Jung, M.S. Gordon, Cycloaddition of benzene on Si(100) and its surface conversions, J Am Chem Soc, 127 (2005) 3131-3139.

[43] F. Nunzi, A. Sgamellotti, N. Re, Density functional study of the dissociative adsorption of aromatic molecules on the Si(100) surface: On the way from benzene to larger polycyclic hydrocarbons, J Phys Chem C, 111 (2007) 1392-1401.

[44] K.R. Harikumar, J.C. Polanyi, A. Zabet-Khosousi, Directed Long-Range Migratory Reaction of Benzene on Si(100), J. Phys. Chem. C, 115 (2011) 22409-22414.

[45] K.R. Harikumar, J.C. Polanyi, A. Zabet-Khosousi, A New Strongly-Bound Chemisorption Structure of Benzene on Si(100), Surf Sci, 606 (2012) 1431-1434.

[46] M.J. Kong, A.V. Teplyakov, J.G. Lyubovitsky, S.F. Bent, NEXAFS Studies of Adsorption of Benzene on Si(100)-2x1, Surf Sci, 411 (1998) 286-293.

[47] J.N. Harvey, Understanding the Kinetics of Spin-Forbidden Chemical Reactions, Phys. Chem. Chem. Phys., 9 (2007) 331-343.

[48] K. Kato, T. Uda, K. Terakura, Backbond Oxidation of the Si(001) Surface: Narrow Channel of Barrierless Oxidation, Phys. Rev. Lett., 80 (1998) 2000-2003.

[49] X. Fan, Y. Zhang, W. Lau, Z. Liu, Adsorption of Triplet O2 on Si(100): The Crucial Step in the Initial Oxidation of a Silicon Surface, Phys. Rev. Lett., 94 (2005).

[50] A. Hellman, Initial Adsorption of O2 on Si(100): Non-Adiabaticity Originating both from a Discrete and a Continuous Set of Electronic Excitations, Surf Sci, 603 (2009) 173-177.

[51] G. Geneste, J. Morillo, F. Finocchi, Adsorption and diffusion of Mg, O, and O2 on the MgO(001) flat surface, J Chem Phys, 122 (2005) 174707.

[52] D.A. Pichugina, Y.G. Polynskaya, N.E. Kuz'menko, Spin and structural features of oxygen dissociation on tetrahedral Ag20 and Ag19Au clusters, Physical chemistry chemical physics : PCCP, 18 (2016) 18033-18044.

[53] A.B. Goodrow, A. T.; Head-Gordon, M., Are Spin-Forbidden Crossings a Bottleneck in Methanol Oxidation?, The Journal of Physical Chemistry C, 113 (2009) 19361-19364.

[54] P. Gonzalez-Navarrete, L. Gracia, M. Calatayud, J. Andres, Density functional theory study of the oxidation of methanol to formaldehyde on a hydrated vanadia cluster, J Comput Chem, 31 (2010) 2493-2501.

[55] J.M. Moc, D. G.; Morokuma, K., Activation and Adsorption of Multiple H2 Molecules on a Pd5 Cluster: A Density Functional Study, Journal of Physical Chemistry A, 107 (2003) 4929-4939.

[56] D.C. Look, Recent advances in ZnO materials and devices, Materials Science and Engineering: B, 80 (2001) 383-387.

[57] U. Ozgur, Y.I. Alivov, C. Liu, A Comprehensive Review of ZnO Materials and Devices, J. Appl. Phys., 98 (2005).

[58] A. Janotti, C.G. Van de Walle, Fundamentals of Zinc Oxide as a Semiconductor, Rep. Prog. Phys., 72 (2009) 126501-126529.

[59] C.G. Van de Walle, Defect analysis and engineering in ZnO, Physica B, (2001) 899-903.

[60] A. Janotti, C.G. Van de Walle, Oxygen vacancies in ZnO, Applied Physics Letters, 87 (2005) 122102.

[61] A. Janotti, C.G. Van de Walle, New insights into the role of native point defects in ZnO, Journal of Crystal Growth, 287 (2006) 58-65.

[62] C.G. Van de Walle, Hydrogen as a Cause of Doping in Zinc Oxide, Physical Review Letters, 85 (2000) 1012-1015.

[63] S.F.J. Cox, E.A. Davis, S.P. Cottrell, P.J.C. King, J.S. Lord, J.M. Gil, H.V. Alberto, R.C. Vilão, J. Piroto Duarte, N. Ayres de Campos, A. Weidinger, R.L. Lichti, S.J.C. Irvine, Experimental Confirmation of the Predicted Shallow Donor Hydrogen State in Zinc Oxide, Physical Review Letters, 86 (2001) 2601-2604.

[64] D.M. Hofmann, A. Hofstaetter, F. Leiter, H. Zhou, F. Henecker, B.K. Meyer, S.B. Orlinskii, J. Schmidt, P.G. Baranov, Hydrogen: A Relevant Shallow Donor in Zinc Oxide, Physical Review Letters, 88 (2002) 045504.

[65] A. Janotti, C.G. Van de Walle, Hydrogen multicentre bonds, Nat Mater, 6 (2007) 44-47.

[66] Y.Z. Zhu, G.D. Chen, H. Ye, A. Walsh, C.Y. Moon, S.-H. Wei, Electronic structure and phase stability of MgO, ZnO, CdO, and related ternary alloys, Physical Review B, 77 (2008) 245209.

[67] A.K. Sharma, J. Narayan, J.F. Muth, C.W. Teng, C. Jin, A. Kvit, R.M. Kolbas, O.W. Holland, Optical and structural properties of epitaxial MgxZn1−xO alloys, Applied Physics Letters, 75 (1999) 3327-3329.

[68] H. Karzel, W. Potzel, M. Kofferlein, W. Schiessl, M. Steiner, U. Hiller, G.M. Kalvius, D.W. Mitchell, T.P. Das, P. Blaha, K. Schwarz, M.P. Pasternak, Lattice dynamics and hyperfine interactions in ZnO and ZnSe at high external pressures, Physical Review B, 53 (1996) 11425-11438.

[69] S. Desgreniers, High-density phases of ZnO: Structural and compressive parameters, Physical Review B, 58 (1998) 14102-14105.

[70] R.R. Reeber, Lattice parameters of ZnO from 4.2° to 296°K, Journal of Applied Physics, 41 (1970) 5063-5066.

[71] L. Gerward, J.S. Olsen, The High-Pressure Phase of Zincite, Journal of Synchrotron Radiation 0909-0495, 2 (1995) 233-235.

[72] E.H. Kisi, M.M. Elcombe, u parameters for the wurtzite structure of ZnS and ZnO using powder neutron diffraction, Acta Crystallographica Section C 0108-2701, 45 (1989) 1867-1870.

[73] D. Vogel, P. Krüger, J. Pollmann, Ab initio, Physical Review B, 52 (1995) R14316-R14319.

[74] D.C. Reynolds, D.C. Look, B. Jogai, C.W. Litton, G. Cantwell, W.C. Harsch, Valence-band ordering in ZnO, Physical Review B, 60 (1999) 2340-2344.

[75] A. Mang, K. Reimann, S. Rübenacke, Band gaps, crystal-field splitting, spin-orbit coupling, and exciton binding energies in ZnO under hydrostatic pressure, Solid State Communications, 94 (1995) 251-254.

[76] F.D. Murnaghan, The Compressibility of Media under Extreme Pressures, Proc Natl Acad Sci U S A, 30 (1944) 244-247.

[77] C. Fan, Q. Wang, L. Li, S. Zhang, Y. Zhu, X. Zhang, M. Ma, R. Liu, W. Wang, Bulk moduli of wurtzite, zinc-blende, and rocksalt phases of ZnO from chemical bond method and density functional theory, Applied Physics Letters, 92 (2008) 101917.

[78] B. Boekfa, E. Pahl, N. Gaston, H. Sakurai, J. Limtrakul, M. Ehara, C–Cl Bond Activation on Au/Pd Bimetallic Nanocatalysts Studied by Density Functional Theory and Genetic Algorithm Calculations, The Journal of Physical Chemistry C, 118 (2014) 22188-22196.

[79] B. Shong, S.F. Bent, Thermally Activated Reactions of Nitrobenzene at the Ge(100)-2 × 1 Surface, J. Phys. Chem. C, 118 (2014) 29224-29233.

[80] Q. Zhu, N.F. Materer, Singlet–Triplet Spin–Orbit Coupling and Crossing Probability for the Single-Dimer Cluster Model of a Si(100) Surface, Chem Phys Lett, 496 (2010) 270-275.

[81] M.J. Frisch, G.W. Trucks, H.B. Schlegel, G.E. Scuseria, M.A. Robb, J.R. Cheeseman, G. Scalmani, V. Barone, B. Mennucci, G.A. Petersson, H. Nakatsuji, M. Caricato, X. Li, H.P. Hratchian, A.F. Izmaylov, J. Bloino, G. Zheng, J.L. Sonnenberg, M. Hada, M. Ehara, K. Toyota, R. Fukuda, J. Hasegawa, M. Ishida, T. Nakajima, Y. Honda, O. Kitao, H. Nakai, T. Vreven, J.A. Montgomery, J.E.P. Jr., F. Ogliaro, M. Bearpark, J.J. Heyd, E. Brothers, K.N. Kudin, V.N. Staroverov, R. Kobayashi, J. Normand, K. Raghavachari, A. Rendell, J.C. Burant, S.S. Iyengar, J. Tomasi, M. Cossi, N. Rega, J.M. Millam, M. Klene, J.E. Knox, J.B. Cross, V. Bakken, C. Adamo, J. Jaramillo, R. Gomperts, R.E. Stratmann, O. Yazyev, A.J. Austin, R. Cammi, C. Pomelli, J.W. Ochterski, R.L. Martin, K. Morokuma, V.G. Zakrzewski, G.A. Voth, P. Salvador, J.J. Dannenberg, S. Dapprich, A.D. Daniels, Ö. Farkas, J.B. Foresman, J.V. Ortiz, J. Cioslowski, D. J. Fox, Gaussian 09, Revision D.01, in, Gaussian, Inc., Wallingford, CT, 2009.

[82] A.D. Becke, Density-functional thermochemistry. III. The role of exact exchange, The Journal of Chemical Physics, 98 (1993) 5648.

[83] C. Lee, W. Yang, R.G. Parr, Development of the Colle-Salvetti correlation-energy formula into a functional of the electron density, Physical Review B, 37 (1988) 785-789.

[84] M.M. Francl, Self-consistent molecular orbital methods. XXIII. A polarization-type basis set for second-row elements, The Journal of Chemical Physics, 77 (1982) 3654.

[85] J.N. Harvey, M. Aschi, H. Schwarz, W. Koch, The Singlet and Triplet States of Phenyl Cation. A Hybrid Approach for Locating Minimum Energy Crossing Points between Non-Interacting Potential Energy Surfaces, Theor. Chem. Acc., 99 (1998) 95-99.

[86] M.J. Bearpark, M.A. Robb, H.B. Schlegel, A Direct Method for the Location of the Lowest Energy Point on a Potential Surface Crossing, Chem Phys Lett, 223 (1994) 269-274.

[87] M.W. Schmidt, K.K. Baldridge, J.A. Boatz, S.T. Elbert, M.S. Gordon, J.H. Jensen, S. Koseki, N. Matsunaga, K.A. Nguyen, S. Su, T.L. Windus, M. Dupuis, J.A. Montgomery, General Atomic and Molecular Electronic Structure System, Journal of Computational Chemistry, 14 (1993) 1347-1363.

[88] L.D. Landau, On the Theory of the Energy Transfer, Phisikal. Z. Sovietiinion, 2 (1932) 46.

[89] E.C.G. Stueckelberg, Theorie der Unelastischen Stosse Zwischen Atomen, Helv. Phys. Acta., 5 (1932) 370.

[90] C. Zener, Non-Adiabatic Crossing of Energy Levels, Proc. R. Soc. A, 137 (1932) 696-702.

[91] R.A. Evarestov, T. Bredow, K. Jug, Connection between slab and cluster models for crystalline surfaces, Phys Solid State+, 43 (2001) 1774-1782.

[92] E. Penev, P. Kratzer, M. Scheffler, Effect of the Cluster Size in Modeling the H_2 Desorption and Dissociative Adsorption on Si(001), J. Chem. Phys., 110 (1999) 3986-3994.

[93] J.A. Steckel, T. Phung, K.D. Jordan, P. Nachtigall, Concerted use of slab and cluster models in an ab initio study of hydrogen desorption from the Si(100) surface, J Phys Chem B, 105 (2001) 4031-4038.

[94] A. Tsukazaki, A. Ohtomo, T. Onuma, M. Ohtani, T. Makino, M. Sumiya, K. Ohtani, S.F. Chichibu, S. Fuke, Y. Segawa, H. Ohno, H. Koinuma, M. Kawasaki, Repeated temperature modulation epitaxy for p-type doping and light-emitting diode based on ZnO, Nat Mater, 4 (2005) 42-46.

[95] W.Z. Xu, Z.Z. Ye, Y.J. Zeng, L.P. Zhu, B.H. Zhao, L. Jiang, J.G. Lu, H.P. He, S.B. Zhang, ZnO light-emitting diode grown by plasma-assisted metal organic chemical vapor deposition, Applied Physics Letters, 88 (2006) 173506.

[96] J.H. Lim, C.K. Kang, K.K. Kim, I.K. Park, D.K. Hwang, S.J. Park, UV Electroluminescence Emission from ZnO Light-Emitting Diodes Grown by High-Temperature Radiofrequency Sputtering, Advanced Materials, 18 (2006) 2720-2724.

[97] H. Ohno, Making Nonmagnetic Semiconductors Ferromagnetic, Science, 281 (1998) 951.

[98] Y. Ohno, D.K. Young, B. Beschoten, F. Matsukura, H. Ohno, D.D. Awschalom, Electrical spin injection in a ferromagnetic semiconductor heterostructure, Nature, 402 (1999) 790-792.

[99] S.A. Wolf, D.D. Awschalom, R.A. Buhrman, J.M. Daughton, S. von Molnár, M.L. Roukes, A.Y. Chtchelkanova, D.M. Treger, Spintronics: A Spin-Based Electronics Vision for the Future, Science, 294 (2001) 1488.

[100] E.-J. Kan, L.-F. Yuan, J. Yang, Electron-induced ferromagnetic ordering of Co-doped ZnO, Journal of Applied Physics, 102 (2007) 033915.

[101] E.-C. Lee, K.J. Chang, Ferromagnetic versus antiferromagnetic interaction in Co-doped ZnO, Physical Review B, 69 (2004).

[102] N.A. Spaldin, Search for ferromagnetism in transition-metal-doped piezoelectric ZnO, Physical Review B, 69 (2004).

[103] M.H. Sluiter, Y. Kawazoe, P. Sharma, A. Inoue, A.R. Raju, C. Rout, U.V. Waghmare, First principles based design and experimental evidence for a ZnO-based ferromagnet at room temperature, Phys Rev Lett, 94 (2005) 187204.

[104] A.S. Risbud, N.A. Spaldin, Z.Q. Chen, S. Stemmer, R. Seshadri, Magnetism in polycrystalline cobalt-substituted zinc oxide, Physical Review B, 68 (2003).

[105] M.S. José, A. Emilio, D.G. Julian, G. Alberto, J. Javier, O. Pablo, S.-P. Daniel, The SIESTA method for ab initio order- N materials simulation, Journal of Physics: Condensed Matter, 14 (2002) 2745.

[106] J.P. Perdew, K. Burke, M. Ernzerhof, Generalized gradient approximation made simple, Physical Review Letters, 77 (1996) 3865-3868.

[107] J.P. Perdew, A. Zunger, Self-interaction correction to density-functional approximations for many-electron systems, Physical Review B, 23 (1981) 5048-5079.

[108] N. Troullier, J.L. Martins, Efficient pseudopotentials for plane-wave calculations, AM. Phys. Soc., 43 (1991) 1993-2006.

[109] I.A. Vladimir, F. Aryasetiawan, A.I. Lichtenstein, First-principles calculations of the electronic structure and spectra of strongly correlated systems: the LDA + U method, Journal of Physics: Condensed Matter, 9 (1997) 767.

VITA

Eric Donald Butson

Candidate for the Degree of

Doctor of Philosophy

Thesis: A COMPUTATIONAL INVESTIGATION OF THE EFFECT OF SPIN-CROSSING ON THE DISSOCIATION OF CHLORO- AND DICHLOROBENZENE ON THE SILICON (100) SURFACE AND THE MECHANICAL AND ELECTRONIC PROPERTIES OF COBALT DOPED ZINC OXIDE

Major Field: Chemistry

Biographical:

Date and place of birth:

April 20, 1990 in San Diego, California

Education:

Completed the requirements for the Doctor of Philosophy in chemistry at Oklahoma State University, Stillwater, Oklahoma in July, 2017.

Completed the requirements for the Bachelor of Science in chemistry at Northeastern State University, Tahlequah, Oklahoma in 2012.

Experience:

Teaching and research assistant in the Department of Chemistry at Oklahoma State University in Stillwater, OK

Adjunct professor at Southern Nazarene University in Bethany, OK.

Undergraduate research and laboratory assistant at Northeastern State University in Tahlequah, OK.

Professional Memberships:

American Chemical Society